University of Alberta

LONG-TERM STRUCTURAL HEALTH MONITORING OF THE CROWCHILD TRAIL BRIDGE

by

Timothy Russell Van Zwol

A thesis submitted to the Faculty of Graduate Studies and Research in partial fulfillment of the requirements for the degree of Master of Science

in

Structural Engineering

Department of Civil and Environmental Engineering

Edmonton, Alberta

Spring 2005

0-494-08164-3

Library and Archives Canada
Published Heritage Branch
395 Wellington Street
Ottawa ON K1A 0N4
Canada

Bibliothèque et Archives Canada
Direction du Patrimoine de l'édition
395, rue Wellington
Ottawa ON K1A 0N4
Canada

Your file Votre référence
ISBN:
Our file Notre reference
ISBN:

NOTICE:
The author has granted a non-exclusive license allowing Library and Archives Canada to reproduce, publish, archive, preserve, conserve, communicate to the public by telecommunication or on the Internet, loan, distribute and sell theses worldwide, for commercial or non-commercial purposes, in microform, paper, electronic and/or any other formats.

The author retains copyright ownership and moral rights in this thesis. Neither the thesis nor substantial extracts from it may be printed or otherwise reproduced without the author's permission.

AVIS:
L'auteur a accordé une licence non exclusive permettant à la Bibliothèque et Archives Canada de reproduire, publier, archiver, sauvegarder, conserver, transmettre au public par télécommunication ou par l'Internet, prêter, distribuer et vendre des thèses partout dans le monde, à des fins commerciales ou autres, sur support microforme, papier, électronique et/ou autres formats.

L'auteur conserve la propriété du droit d'auteur et des droits moraux qui protège cette thèse. Ni la thèse ni des extraits substantiels de celle-ci ne doivent être imprimés ou autrement reproduits sans son autorisation.

In compliance with the Canadian Privacy Act some supporting forms may have been removed from this thesis.

While these forms may be included in the document page count, their removal does not represent any loss of content from the thesis.

Conformément à la loi canadienne sur la protection de la vie privée, quelques formulaires secondaires ont été enlevés de cette thèse.

Bien que ces formulaires aient inclus dans la pagination, il n'y aura aucun contenu manquant.

Canada

ABSTRACT

Steel-free bridge deck designs address corrosion and maintenance issues that plague the majority of the highway bridges built in Canada. Several steel-free deck bridges constructed in Canada exhibited satisfactory behaviour immediately after their construction, however, the long-term health and structural performance of many of these structures have not been researched. Structural health monitoring data was obtained from the steel-free Crowchild Trail Bridge in Calgary, Alberta during June 2004 and was compared to previous monitoring test results. Despite deck and barrier concrete cracks, the Crowchild Trail Bridge overall behaviour in 2004 was very similar to when it was first constructed. Measured field and numerical modelling results showed that temperature, support boundary conditions, and material stiffness were found to be the most influential factors affecting bridge behaviour during the first seven years in service. Future steel-free deck designs should consider improved fatigue resistance in order to meet serviceability requirements.

ACKNOWLEDGMENT

This research was conducted under the supervision of Dr. J.J. Roger Cheng. His patience, guidance, and support were greatly appreciated. This study was conducted with the financial assistance of the Natural Sciences and Engineering Research Council of Canada and the Informatics Circle of Research Excellence.

The testing of the Crowchild Trail Bridge was made possible through the field support and permission provided by Jadwiga Kroman, Gord Eveson, and employees from the City of Calgary. I would specially like to thank Nadeem Khattak from Colt Engineering for his tremendous friendship, support, and expertise throughout this research. Shahab Afhami from UMA Engineering provided insight into the instrumentation and test set-up. The excellent assistance of Ved Sharma, Mohammed Behbahanifard, Zoulong Chou, and Theresa Casey was also very instrumental in the success of the Crowchild Bridge testing.

I would also like to express my appreciation to the University of Alberta Department of Civil Engineering staff: Larry Burden, Richard Helfrich, Dale Lathe, and Bob Warrender for their technical assistance and cooperation during the field test preparations.

I would like to thank my parents for my upbringing and their support; their influence was instrumental in where I am today. I would especially like to thank my fiancée Carolyn for her patience, support, and encouragement.

Finally, I would like to thank God for all of His blessings and gifts that enabled me to accomplish this work.

TABLE OF CONTENTS

1.0 INTRODUCTION 1

1.1 Background 1

1.2 Need for Research 2

1.3 Objectives and Scope 3

1.4 Layout of Thesis 4

2.0 LITERATURE REVIEW 5

2.1 Introduction 5

2.2 Steel-Free Bridge Deck Research 5

2.2.1 Background 5

2.2.2 Typical Steel-Free Deck Layout and Arching Action Behaviour 6

2.2.3 Steel-Free Deck Research Prior to Construction of Crowchild Trail Bridge 7

2.2.3.1 Composite Girder and Reinforced Concrete Deck Bridges 7

2.2.3.2 Pioneering Steel-Free Deck Research – Simple Span Bridges 8

2.2.3.3 Steel-Free Deck Research - Continuous Span Bridges 10

2.2.4 Steel-Free Deck Research After Construction of Crowchild Trial Bridge 11

2.2.4.1 Canadian Highway Bridge Design Code Provisions 11

2.2.4.2 Transverse Confinement Systems 13

2.2.4.3 Precast Concrete Steel-Free Decks 14

2.2.4.4 Serviceability Issues: Fatigue and Cracking Behaviour 15

2.2.4.5 Second Generation Steel-Free Decks 18

2.2.5 Steel-Free Bridge Decks: Field Projects 19

2.2.5.1 Salmon River Bridge 19

2.2.5.2 Kent County Road Bridge 21

2.2.5.3 Crowchild Trail Bridge 22

2.2.5.4 Waterloo Creek Bridge 22

2.2.5.5 Lindquist Creek Bridge 23

2.2.5.6 Trout River Bridge 23
2.2.5.7 Red River Bridge 24
2.3 Conclusions from Literature Review 26

3.0 DESIGN, CONSTRUCTION, AND INSTRUMENTATION OF CROWCHILD TRAIL BRIDGE 29
3.1 Introduction 29
3.2 Background of Original Crowchild Trial Bridge Structure 29
3.3 Materials and Design Considerations of Crowchild Trail Bridge 30
3.3.1 Bridge Layout and Construction Costs 30
3.3.2 Concrete Deck 30
3.3.3 GFRP Deck Reinforcement 32
3.3.4 Steel-Plate Girders 33
3.3.5 Steel Straps 34
3.3.6 Bridge Barriers 34
3.4 Crowchild Trail Bridge Instrumentation and Test Equipment 35
3.4.1 Introduction 35
3.4.2 Strain Gauges 35
3.4.3 Deflection Equipment 37
3.4.4 Ambient Vibration Test Equipment 38
3.4.5 Load Test Data Collection Equipment 39
3.4.6 Loading Trucks 42

4.0 EXPERIMENTAL PROCEDURES AND RESULTS 45
4.1 Outline of Crowchild Trail Bridge Testing 1997-2004 45
4.2 Summary of 1997 Bridge Tests 48
4.2.1 1997 Ambient Vibration Test Results 48
4.2.2 1997 Static Load Test Results 49
4.2.3 1997 Dynamic Load Test Results 50
4.2.4 1997 Crack Mapping 51
4.2.5 1997 Temperature Tests 51
4.3 Summary of 1998 Bridge Tests 52

4.3.1 1998 Ambient Vibration Test Results 52
4.3.2 1998 Static Load Test Results 53
4.3.3 1998 Dynamic Load Test Results 54
4.3.4 1998 Crack Mapping 55
4.4 Results of 2004 Tests 56
4.4.1 Introduction 56
4.4.2 2004 Preliminary Bridge Tests 57
4.4.2.1 Preliminary Test Methodology 57
4.4.2.2 Preliminary Test Results 60
4.4.3 2004 Ambient Vibration Tests 64
4.4.3.1 Ambient Vibration Test Methodology 64
4.4.3.2 Natural Frequency Results 67
4.4.3.3 Mode Shape Results 71
4.4.4 2004 Static and Dynamic Load Tests 75
4.4.4.1 Loading Test Methodology 75
4.4.4.2 Static Test Results 81
4.4.4.3 Dynamic Test Results 89
4.4.5 2004 Bridge Visual Inspection 92
4.4.5.1 Bridge Deck Crack Mapping 92
4.4.5.2 Bridge Deck Leakage 92
4.4.5.3 Bridge Barrier Cracks 96

5.0 ANALYSIS AND COMPARISON OF RESULTS 98
5.1 Introduction 98
5.2 Comparison of Preliminary, Static, and Dynamic 2004 Test Results 98
5.3 Comparison of Ambient Vibration Results 101
5.3.1 Ambient Vibration Test Overview 101
5.3.2 Comparison of Natural Frequencies 101
5.3.3 Comparison of Mode Shapes 102
5.3.4 Discussion of Ambient Vibration Results 107
5.4 Comparison of Static Loading Results 108

5.4.1 Comparison of Maximum Static Strain Readings 108
5.4.2 Comparison of Deflections and Girder Load Sharing 110
5.4.3 Comparison of Strain Distributions and Neutral Axis Location 112
5.5 Crack Mapping Analysis Over Service Life 115
5.5.1 Introduction 115
5.5.2 South Span: Crack Mapping 119
5.5.3 Middle Span: Crack Mapping 119
5.5.4 North Span: Crack Mapping 120
5.5.5 Crack Mapping Summary 120

6.0 NUMERICAL MODELS OF CROWCHILD TRAIL BRIDGE 123
6.1 Introduction 123
6.2 UBC Dynamic Computer Models 124
6.2.1 UBC Dynamic Model Description 124
6.2.2 UBC Computer Model Results and Conclusions 125
6.3 Carleton University Damage Identification Models 126
6.3.1 Carleton University Model Descriptions 126
6.3.2 Model Calibration with Field Results 127
6.3.3 Vibration Based Damage Identification Testing and Results 128
6.4 U of A S-Frame Finite Element Model 129
6.4.1 U of A FEM Description 129
6.4.2 Differences in 1997, 1998, 2004 Model Construction 132
6.4.3 U of A FEM Natural Frequency Results 134
6.4.4 U of A FEM Deflection Results 136
6.5 Numerical Modeling Conclusions 137

7.0 SUMMARY, CONCLUSIONS, AND RECOMMENDATIONS 138
7.1 Summary 138
7.2 Conclusions 140
7.3 Recommendations 144

REFERENCES 146

APPENDIX A – LOCATION OF BRIDGE INSTRUMENTATION 152

APPENDIX B – 2004 STATIC LOAD TEST RAW DATA 159

LIST OF TABLES

Table		Page
Table 3.1	Crowchild Trail Bridge Instrumentation List	36
Table 3.2	Loading Truck Axle Weights	42
Table 4.1	Summary of Crowchild Trail Bridge Field Tests	47
Table 4.2	1997 Natural Frequencies and Mode Shapes	49
Table 4.3	1998 Natural Frequencies and Mode Shapes	53
Table 4.4	Summary of 2004 Crowchild Trail Bridge Tests	56
Table 4.5	Strain Gauge List for Preliminary Test	58
Table 4.6	Recorded Temperature During 2004 Preliminary Load Tests	60
Table 4.7	Preliminary Test Maximum Strain Results	60
Table 4.8	Recorded Temperature During 2004 Vibration Tests	66
Table 4.9	2004 Crowchild Trail Bridge Natural Frequencies	67
Table 4.10	List of Strain Gauges for Load Tests	79
Table 4.11	Recorded Temperature During 2004 Load Tests	80
Table 4.12	Static Test Maximum Strain Results	81
Table 4.13	Maximum Measured Deflections From Static Tests	87
Table 4.14	Maximum Strains from Dynamic Test Results	89
Table 4.15	Measured Deflections from Dynamic Tests	91
Table 5.1	Comparison of 2004 Preliminary, Static, and Dynamic Test Strains	99
Table 5.2	Comparison of 2004 Maximum Deflections	100
Table 5.3	Crowchild Trail Bridge Natural Frequencies	102
Table 5.4	Absolute Maximum Measured Static Strains	109
Table 6.1	UBC Models: Material Characteristic Assumptions	124
Table 6.2	Carleton University Results: Natural Frequencies	128
Table 6.3	S-Frame FEM Steel Section Properties	132
Table 6.4	S-Frame FEM and Measured Natural Frequencies	134
Table 6.5	S-Frame FEM and Measured Deflections	136

LIST OF FIGURES

Figure		Page
Figure 1.1	Crowchild Trail Bridge	2
Figure 2.1	Bridge Arching Action Model	7
Figure 3.1	West Elevation of Crowchild Trail Bridge	30
Figure 3.2	Crowchild Trail Bridge Deck Cross-Section	31
Figure 3.3	Steel Girder Strain Gauge Configurations	37
Figure 3.4	2004 Cable Transducer Layout	38
Figure 3.5	2004 Ambient Vibration Equipment	39
Figure 3.6	Strain Gauge Connector Junction Box	40
Figure 3.7	2004 Data Acquisition Equipment	41
Figure 3.8	2004 Load Test Truck	42
Figure 3.9	1997 Truck Loading	43
Figure 3.10	1998 Truck Loading	43
Figure 3.11	2004 Truck Loading	43
Figure 4.1	Preliminary Tests: Typical Truck Loading	59
Figure 4.2	Bridge Dynamic Behaviour: SET A Girder Strain Gauges	62
Figure 4.3	2004 Preliminary Tests: Strain Distribution in Positive Moment Region	63
Figure 4.4	2004 Ambient Vibration Tests: Accelerometer Locations	65
Figure 4.5	Power Spectrum Results: 2004 Crowchild Trail Bridge Natural Frequencies	68
Figure 4.6	North Span: Sum of 8306 Accelerometer Power Spectrums	69
Figure 4.7	Middle Span: Sum of 8306 Accelerometer Power Spectrums	70
Figure 4.8	South Span: Sum of 8306 Accelerometer Power Spectrums	70
Figure 4.9	First Vertical and Torsional Mode Shapes	73
Figure 4.10	Second Vertical and Torsional Mode Shapes	73
Figure 4.11	Third Vertical and Torsional Mode Shapes	74
Figure 4.12	Fourth Vertical and Torsional Mode Shapes	74
Figure 4.13	Static Load Point Location Markings	75
Figure 4.14	2004 Static Loading Point Locations	77

Figure 4.15	Static Response: Influence Lines of Girder Strains	82
Figure 4.16	2004 Positive Moment Region Strain Distribution	84
Figure 4.17	2004 Negative Moment Region Strain Distribution	85
Figure 4.18	Load Sharing Indicated By Girder Stains	86
Figure 4.19	Girder Deflection Influence Line	88
Figure 4.20	Dynamic Response of Girder Strain Gauges	90
Figure 4.21	Bridge Deck Leakage Near Strap	93
Figure 4.22	Bridge Deck Leakage at Deck Haunch	93
Figure 4.23	Bridge Deck Leak Locations	95
Figure 4.24	Cracking in the Concrete Bridge Barriers (Interior)	96
Figure 4.25	Cracking in the Concrete Bridge Barriers (Exterior)	96
Figure 5.1	1st Vertical Mode Shape: Comparison of 1998 and 2004 Results	103
Figure 5.2	1st Torsional Mode Shape: Comparison of 1998 and 2004 Results	103
Figure 5.3	2nd Vertical Mode Shape: Comparison of 1998 and 2004 Results	104
Figure 5.4	2nd Torsional Mode Shape: Comparison of 1998 and 2004 Results	104
Figure 5.5	3rd Vertical Mode Shape: Comparison of 1998 and 2004 Results	105
Figure 5.6	3rd Torsional Mode Shape: Comparison of 1998 and 2004 Results	105
Figure 5.7	4th Vertical Mode Shape: Comparison of 1998 and 2004 Results	106
Figure 5.8	4th Torsional Mode Shape: Comparison of 1998 and 2004 Results	106
Figure 5.9	Girder Deflection Comparisons	111
Figure 5.10	1998 vs. 2004 Positive Strain Region Comparison	112
Figure 5.11	1998 vs. 2004 Negative Strain Region Comparison	113
Figure 5.12	South Span Crack Pattern	116
Figure 5.13	Middle Span Crack Pattern	117
Figure 5.14	North Span Crack Pattern	118
Figure 5.15	Rate of Longitudinal Crack Formation	121
Figure 5.16	Rate of Transverse Crack Formation	122
Figure 6.1	FEM Modal Shapes of First Six Natural Frequencies	135

Figure A.1	Overall Instrumentation Layout	153
Figure A.2	NEFMAC Bridge Barrier Gauges	154
Figure A.3	Location of Reinforcement Bar Gauges	155
Figure A.4	Tension Strap Gauges	156
Figure A.5	Shear Stud Gauges	156
Figure A.6	Cross-Frame Gauges	157
Figure A.7	Embedded Concrete Gauges	158
Figure A.8	Embedded Thermistors	158
Figure B.1	Static Load Raw Data: G1-G3, G32-G34	160
Figure B.2	Static Load Raw Data: G4-G6	160
Figure B.3	Static Load Raw Data: G7-G9	161
Figure B.4	Static Load Raw Data: G10-G11	161
Figure B.5	Static Load Raw Data: G23-G24	162
Figure B.6	Static Load Raw Data: G25-G27	162
Figure B.7	Static Load Raw Data: G28-G30	163
Figure B.8	Static Load Raw Data: G12	163
Figure B.9	Static Load Raw Data: G13-G15	164
Figure B.10	Static Load Raw Data: G16-G18	164
Figure B.11	Static Load Raw Data: G19-G21	165
Figure B.12	Static Load Raw Data: RC1-RC2	165
Figure B.13	Static Load Raw Data: T1-T3,T7,T9-T11	166
Figure B.14	Static Load Raw Data: T2-T6	166
Figure B.15	Static Load Raw Data: S1-S6	167
Figure B.16	Static Load Raw Data: C1-C4	167
Figure B.17	Static Load Raw Data: RS1-RS3	168
Figure B.18	Static Load Raw Data: E3, E5	168
Figure B.19	Static Load Raw Data: E7-E10	169
Figure B.20	Static Load Raw Data: E11-E13	169

1.0 INTRODUCTION

1.1 Background

Bridge structures built within Canada are subject to some of the harshest environmental and load conditions in the world. Typical ambient temperatures range between +30°C in the summer and –30°C in the winter. Freezing and thawing cycles may occur daily within the presence of moisture. Although de-icing salts are used to prevent the formation of ice on roadway surfaces, they are very harmful to the long-term performance of reinforced concrete bridge decks. Current bridge designs are also required to accommodate increasingly heavier truckloads. Due to tighter government budgets and limited resources, bridge designs are required to have longer design lives with minimal maintenance. Therefore, Canadian bridge designs must give special consideration to the factors listed above.

A large majority of Canadian bridge infrastructure consists of bridges with reinforced concrete decks. Due to the detrimental conditions listed in the previous paragraph, however, the internal reinforcing steel within these types of bridge decks is subject to corrosion. Corrosion of internal steel reinforcement leads to a variety of other maintenance issues including the deterioration of the surrounding deck concrete. As a result, many of the reinforced concrete decks currently in service in Canada require extensive repairs or, in some cases, complete replacement.

In the last 10-15 years, alternatives to typical reinforced concrete deck construction have been studied. Steel-free deck designs incorporating innovative materials are one solution that eliminates the possibility of internal steel corrosion. Steel straps, that resist tensile forces in the transverse direction, are placed below the concrete deck. Several steel-free deck bridges were built in Canada during the mid-1990s and are still in service today. The Crowchild Trail Bridge in Calgary, Figure 1.1, was the first continuous steel-free deck in the world when constructed in 1997. Despite some serviceability issues over the last seven years, the Crowchild Trail Bridge is still in service today and safely supports the traffic loads of thousands of vehicles every day.

Figure 1.1 – Crowchild Trail Bridge

1.2 Need for Research

One of the goals of bridge construction is to implement a design that requires minimal maintenance and has a longer design life. The majority of new bridge decks constructed today continue to incorporate a reinforced concrete deck design even though short-term health monitoring has shown steel-free bridge decks to be a reliable construction alternative. Also, new reinforced concrete bridge decks are constructed at the same time when similar deck designs are showing significant deterioration. Currently, there are less than ten steel-free decks and thousands of reinforced concrete decks in service across Canada.

Previous research has shown that steel-free decks are capable of supporting larger wheel loads compared to reinforced concrete bridges. Steel-free deck designs also avoid the problems associated with internal steel reinforcement corrosion. Overall, the satisfactory short-term behaviour of steel-free decks has been well established with the exception of cracking limits. However, before this type of design gains wider acceptance by bridge

owners, significant research needs to be completed to establish the long-term performance.

Bridges tend to show signs of deterioration during their lifetime as a result of materials ageing, excessive use, overloading, climatic conditions, and lack of maintenance or inspection. Bridge deterioration may not be evident within the first couple years of service. Instead, problems may only start to arise after five or ten years of service. This implies that regular long-term monitoring is necessary to evaluate the structural health condition of bridges. Increased confidence in steel-free deck designs will only result once their long-term behaviour has been proven satisfactory. Insight gained from the long-term performance of the current steel-free bridges will lead to improved, less conservative, and more cost-effective designs. As contractors become more familiar with this type of construction, steel-free decks will also become cheaper to build.

1.3 Objectives and Scope

When the structural health monitoring program of the Crowchild Trail Bridge was established, the main research objectives were to determine the bridge deck performance under serviceability conditions, change of major bridge characteristics with time, and its long-term durability. The main objective of this research builds on this by determining the long-term performance of the Crowchild Trail Bridge after seven years of service. In order to fulfill these objectives, static and dynamic load tests completed in 2004 will be compared to previous load tests completed when the bridge was first constructed. In addition ambient vibration test results, consisting of natural frequencies and mode shapes, will be compared to the baseline vibration behaviour. Crack mapping completed at five stages during its service life will also be used to determine the long-term durability of the bridge deck. A finite element model will be used to determine possible causes of the stiffness changes in the bridge that have occurred over time.

1.4 Layout of Thesis

Chapter 2 provides a detailed literature review of steel-free bridge decks and a summary of the objectives of structural health monitoring. A brief summary of the application of steel-free decks to simple and continuous spans is presented. This is followed by a more detailed review of steel-free deck research that occurred after the construction of the Crowchild Trail Bridge. The current state of all the steel-free decks constructed in Canada is analyzed. Finally, an overview of structural health monitoring is presented with specific applications to steel-free bridge decks.

Chapter 3 presents a detailed description of the Crowchild Trail Bridge design and construction. All of the materials, structural components, and instrumentation used in the bridge construction are summarized.

Chapter 4 summarizes all of the Crowchild Trail Bridge tests and results completed immediately after construction in 1997, after one year of service in 1998, and after seven years of service in 2004. Results from static load tests, dynamic load tests, ambient vibration tests, crack mapping, and visual observations are presented.

Chapter 5 compares the results from the 1997, 1998, and 2004 tests. Comparisons of truck loadings, maximum strains, maximum deflections, natural frequencies and mode shapes, load sharing, neutral axis locations, and crack propagation are presented.

Chapter 6 summarizes the various Crowchild Trail Bridge numerical models that have been constructed. The contribution of models constructed at the University of British Columbia and Carleton University will be examined. An S-Frame finite element model constructed at the University of Alberta will be described in more detail. Results from this model will be used to explain any differences in the 1998 and 2004 field test results.

Finally, Chapter 7 provides the summary, conclusions, and recommendations.

2.0 LITERATURE REVIEW

2.1 Introduction

A complete overview of previous and current steel-free deck research will be presented in this section. Initial steel-free deck research that began in the early 1990s will be summarized and will cover the application of steel-free decks in the positive and negative moment regions. Next, guidelines for steel-free deck design in the Canadian Highway Bridge Design Code (2000) will be summarized. Various types of transverse confinement systems will be presented in addition to steel-free precast bridge decks. Current research dealing with fatigue behaviour, cracking resistance, and the evolution of second-generation steel-free decks will be presented in more detail. Finally, the design and current condition of several steel-free bridge decks constructed in Canada will be considered.

Numerical models and several laboratory tests contributed to the development of steel-free decks. The progression of these studies and significant research results will be discussed. With the construction of steel-free bridge decks, Structural Health Monitoring (SHM) tools were required to determine the field performance of these structures under real-life service conditions. SHM processes and current technology will be summarized. Although periodical visual inspections have been completed for most of the innovative steel-free bridge projects since they were first constructed, the importance of thorough long-term health monitoring will be emphasized and the benefits discussed.

2.2 Steel-Free Bridge Deck Research

2.2.1 Background

Part of the deterioration of Canada's infrastructure can be attributed to the corrosion of internal steel reinforcement typically used in the construction of reinforced concrete structures. Internal steel corrosion may arise from a variety of factors. For example, harmful electrochemical reactions may occur between the concrete and reinforcing steel when the pH or alkalinity of the concrete is reduced. If water and oxygen are also

present, corrosion may be initiated. The penetration of chlorides from seawater or de-icing salts may further increase the rate of internal steel corrosion. When reinforcing steel corrodes in these scenarios, it will expand in volume, causing the surrounding concrete to crack and spall. These processes are evident by rust strains on concrete surfaces or concrete disintegration within the tension region below the reinforcing steel. Far worse than the visible effects, however, is the reduction in structural capacity of the reinforced concrete members.

Innovative structural solutions are required to avoid the onset of internal reinforcing steel corrosion. Numerous methods have attempted to alleviate this problem. These methods include epoxy-coated reinforcing steel, increased concrete cover, and denser concrete mixes. However, these options are typically costly and only delay the onset of steel corrosion. The need to eliminate concrete damage caused by the corrosion of internal reinforcement steel has led to the development of steel-free decks over the last 10-15 years. Steel-free deck designs do not rely on any internal steel reinforcement for bridge deck strength. With all of the internal reinforcement removed, a lighter, more economical structure is constructed. Since the possibility of internal steel corrosion is removed, there are significant improvements in long-term durability.

2.2.2 Typical Steel-Free Deck Layout and Arching Action Behaviour

In steel-free decks, the reinforcement required to support transverse tension stresses, is placed externally below concrete members. Steel straps placed below the concrete deck are used as the transverse steel reinforcement. As a result, the steel straps are not directly exposed to chlorides within the concrete. This arrangement avoids many of the problems associated with the corrosion and deterioration of internal steel reinforcement. Corroded or damaged external steel straps are easily visible and are much more feasible to maintain or repair. Concrete compressive and steel tensile characteristics are also utilized more effectively.

Instead of pure bending, arching action within steel-free decks enable the structure to carry traffic loads. Figure 2.1 shows the basic method for internal arching. A typical

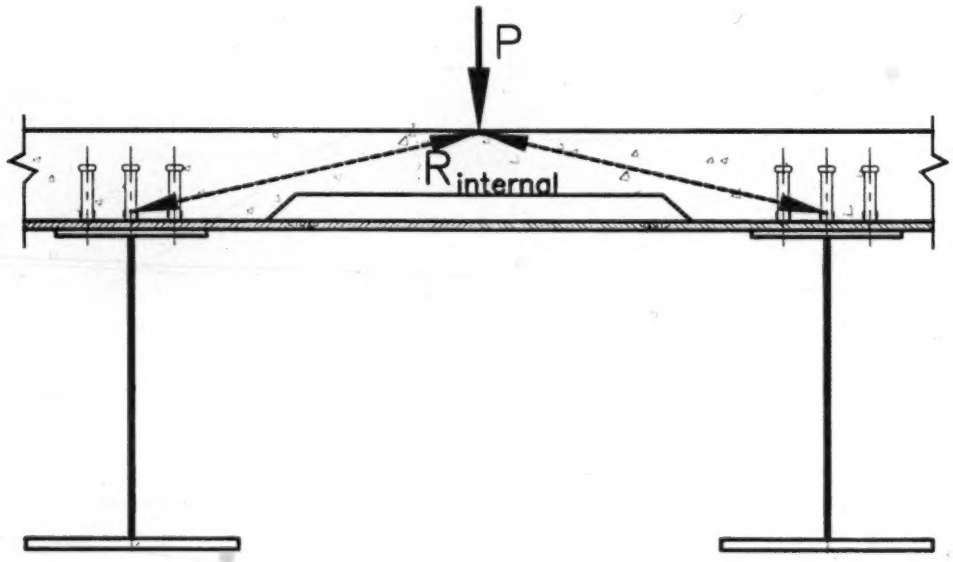

Figure 2.1 – Bridge Arching Action Model

wheel load, P, is resisted by two compressive struts, which form in the concrete deck. Through this mechanism, the load is transferred to the neighbouring steel girders. The steel strap, connected to the upper flanges of the neighbouring girders, acts as the tension tie to resist tensile stresses in the transverse direction as shown.

2.2.3 Steel-Free Deck Research Prior to Construction of Crowchild Trail Bridge

2.2.3.1 Composite Girder and Reinforced Concrete Deck Bridges

First-generation bridge deck slabs were typically designed as reinforced concrete slabs and contained approximately 30 kg of steel reinforcement per m^2 of concrete slab area. Until 1979, bridge deck slabs were only designed to behave in pure bending. However, during the mid-1970s and 1980s, internal arching action behaviour, described in the previous section, was first investigated in composite deck slabs under concentrated loads. The Ministry of Transportation of Ontario sponsored this research through an extensive load-testing program. Instead of behaving as flexural slabs as originally assumed,

researchers found that the slabs failed in punching shear at much higher load levels. Therefore, it was suggested that the amount of reinforcing steel within concrete slabs could be significantly reduced if arching action was considered. This research led to design of second-generation bridge decks with reduced amounts of reinforcing steel; approximately 20 kg of steel reinforcement per m2 of concrete slab area. Constructed in 1975, the Conestogo River Bridge near Waterloo, Ontario was the first bridge deck in the world designed with significantly less reinforcing steel by incorporating the benefits of internal deck arching action (Dorton et al. 1977).

2.2.3.2 Pioneering Steel-Free Deck Research – Simple Spans Bridges

Kong and Cheng (2000) provide a detailed summary of the early research and development of steel-free decks in the positive and negative moment regions. A brief summary of the earlier steel-free deck research prior to the construction of the Crowchild Trail Bridge is presented here.

During the late 1980s research initiated at the Technical University of Nova Scotia (TUNS) led to a complete utilization of the arching action in steel-free deck slabs. Following the genealogy of first and second-generation reinforced concrete bridge decks, steel-free bridge decks are designated third-generation bridge decks. It was proposed that internal tensile reinforcement could be eliminated altogether from concrete deck slabs if arching action was harnessed in both the longitudinal and transverse directions.

Mufti et al. (1993) constructed five half-scale deck models and tested them to failure under concentrated static loads. To control cracking caused by temperature and shrinkage in the early stages of testing, polypropylene fibres were added to the concrete deck mix. Failure modes of the first two half-scale specimens were a combination of pure bending and punching shear similar to steel-reinforced concrete decks. Transverse diaphragms did not produce sufficient transverse confinement to develop arching action within the deck. In the third lab specimen, mechanical shear connectors between the girder and the concrete deck slab provided sufficient confinement in the longitudinal direction. Transverse confinement was also improved using evenly spaced steel straps

welded to the upper flanges of girders. With the additional transverse confinement provided by the steel straps, the deck slabs failed in a punching shear failure mode. Lab tests showed a significant increase in the failure load from 173 kN to 418 kN. A fourth half-scale model proved that the steel-free deck design was also suitable for multi-girder systems. Finally, a fifth half-scale model showed that the strength of the steel-free deck did not depend on the location of the simulated wheel load. In addition, this model showed that steel straps provided more effective lateral restraint compared to diaphragms.

Subsequent tests by Newhook et al. (1996) confirmed that compression dominated the behaviour of the deck slab when sufficient transverse confinement was provided and that internal tensile reinforcement was unnecessary. Although the optimal proportion of polypropylene fibres and distribution of steel straps was not investigated at this time, the proposed steel-free concept was recommended for use in bridges. A full-scale model was also tested in laboratory conditions with satisfactory results. Lessons learned from all of these tests were incorporated into the design of the Salmon River Bridge, the first steel-free bridge deck constructed in the world. This bridge will be discussed in detail in a later section.

For simple span deck models, transverse tensile stresses were found to develop in two locations. First, tensile stressed were found to develop in the top of the concrete over the supporting girders. However, these tensile stresses were relatively low and did not affect the ultimate load capacity of the deck. Cracks that developed in the concrete deck over the supporting girders due to these tensile loads were small and did not exceed serviceability limits. Tensile stresses were also found to develop in bridge decks with transverse cantilever overhangs beyond the supporting girders. FRP reinforcement was required in the upper regions of the deck in order to support these tensile stresses.

One of the most important issues that had to be addressed before the steel-free deck design could be implemented was the short and long-term cost. For bridge owners, the initial construction cost is typically more important than the improved durability and long-term maintenance costs. Estimated construction costs by Bakht et al. (1996) were

$157/m^2$ for a conventional steel-reinforced deck and $169/m^2$ for a steel-free deck. Concrete material costs for steel-free decks, estimated by Bakht et al. (2000), were approximately 30% higher the addition of polypropylene fibres. However, the volume of concrete required for the thinner steel-free decks was approximately 30% less than used in thicker reinforced-concrete decks. Therefore the concrete material costs are about the same for each type of deck design. Due to the innovative materials used and unfamiliar construction details for a steel-free deck, labour costs and GFRP material costs are typically higher. Although these initial construction costs are slightly higher, the increased long-term durability and reduced maintenance costs were believed to offset this difference.

2.2.3.3 Steel-Free Deck Research - Continuous Span Bridges

Although the use of steel free deck technology was initially established for use in simple span concrete bridge decks, research by Dorey et al. (1996) investigated the application of steel-free decks for use in continuous bridges. In continuous span bridges, negative bending moments develop over the intermediate piers locations. A preliminary investigation was conducted at the Heavy Structures Laboratory at Dalhousie University. These tests were performed in order to investigate the cracking behaviour of composite slabs under longitudinal negative moments and to investigate the punching behaviour of a deck slab subject to global negative bending moments (Mufti et al. 1999).

Based on their experimental investigations, several conservative guidelines were recommended. The deck thickness and geometry could be designed similarly in the positive and negative moment regions. If concrete stresses exceed 60% of the flexural cracking strength of concrete, a type of FRP reinforcement was required to control the cracking and to preserve the durability of concrete. Girders supporting the steel-free deck are designed to carry the full ultimate moment in the negative moment regions. To resist the full negative moment, only the top flanges of the girders in this region needed to be increased in size. It was also noted the punching behaviour of the model bridge deck was not significantly affected by the global negative bending moments or any transverse cracks which resulted from these stresses. Overall, results from these tests indicated that

a steel-free deck design could be used in continuous bridge structures. Principles highlighted in the research were incorporated into the design of the Crowchild Trail Bridge, the first continuous steel-free deck in the world.

2.2.4 Steel-Free Deck Research After Construction of Crowchild Trail Bridge

The steel-free deck design has been further refined with additional testing and extensive research since the construction of the Crowchild Trail Bridge. Static and dynamic test results from in-service bridges, laboratory specimens, and numerical models have lead to a better understanding of steel-free bridge deck behaviour. Serviceability issues based on the performance of bridges have also been addressed in the current research.

2.2.4.1 Canadian Highway Bridge Design Code Provisions

Design guidelines have been included in the Canadian Highway Bridge Design Code (CHBDC) for steel-free bridge decks. Section 16, based on fibre-reinforced structures, was incorporated into the 2000 edition of the CHBDC. A commentary published by Bakht et al. (2000) summarizes the steel-free deck code provisions and provides detailed outlines for each of the new design guidelines. These guidelines are based on experimental, field, and model results.

In the positive moment regions, the deck slab is required to be composite with the supporting steel girders. This provides the necessary confinement in the longitudinal direction. The maximum spacing (S) between supporting girders was conservatively set at 3.0 m. The minimum deck slab thickness (t) is 175 mm and not less than $S/15$. The height of the haunch between the deck slab and top of supporting girders must be between 25 and 125 mm while the projection of the shear connectors into this haunch must be at least 75 mm. In addition, the cover above these shear connects must be at least 100 mm. An adequate amount of polymer fibres must be incorporated into the concrete mix. Transverse diaphragms, or cross frames, are required a maximum of eight m apart to support small negative transverse moments in the deck slab that develop from eccentrically placed vehicles. Since these were the first design guidelines published, many of these recommendations were conservative.

An external transverse confining system, consisting of straps, are required to connect the tops of flanges of adjacent girders in order to allow arching action to develop. This may be accomplished through the use of welded steel straps, partially studded steel straps, or any other proven method. From experimental results, it was determined that the most efficient strap spacing is between 1000 mm and 1200 mm. Therefore the strap spacing was recommended to be no more than 1250 mm. Based on experimental results, the CHBDC specifies that the minimum cross-section of a strap be given by the following empirical relationship:

$$A = \frac{F_s S^2 S_l}{(Et)} 10^9$$

where:

A = cross sectional area of strap (mm^2)

F_s = 5.0 MPa for inner transverse deck panel; 6.0 MPA for outer transverse deck panel

S = girder spacing (mm)

S_l = strap spacing (mm)

E = modulus of elasticity of strap material (MPa)

t = concrete slab thickness (mm)

Transverse edges of the deck slab are required to be stiffened by composite edge beams with adequate stiffness. Appropriate tensile reinforcement should also be provided in the cantilever overhangs regions where transverse negative moments arise

In sections over intermediate supports were negative moments arise, the CHBDC stipulates that reinforcement must be provided when tensile stresses exceed 60% of the cracking strength of concrete. Therefore the stress limit for 35 MPa concrete in an unreinforced bridge deck would be 1.77 MPa. The CHBDC also stipulates that FRP reinforcement used to control cracking in these areas may only be considered as secondary reinforcement. FRP reinforcement may not be considered as primary reinforcement that contributes to the ultimate moment capacity of the composite section.

2.2.4.2 Transverse Confinement Systems

Several types of transverse confinement systems have been investigated since the steel-free deck idea was first suggested. Currently, the most popular transverse confinement system is the welded steel strap system where the straps are welded directly to the top flanges of the girders. Fully studded straps, that contain regularly spaced shear connectors across its length, can also be used if the concrete deck is flat. Partially studded straps, on the other hand, are separated from the haunched section of the concrete deck. Cruciform straps are steel straps connected to crossbars and are fully encased in the haunched portion of the slab. Steel threaded rods may also be used and typically pass through plastic tubes embedded in the deck haunches. A significant advantage of the steel threaded rod system is that the rods can be easily replaced. Similarly, fibre-reinforced threaded bars or tendons may also be used.

Marshe and Green (1999) investigated the use of CFRP tendons to transversely pre-stress composite decks. CFRP tendons behaved as desired by providing the desired amount of transverse confinement and caused punching shear failure in the deck models. Frequently spaced intermediate diaphragms or steel beams were also effective for transverse confinement of the deck. Bakht et al. (2000) investigated cruciform straps and threaded steel rods as transverse confining systems. The results proved that the behaviour of both of these systems was satisfactory. Banthia et al. (2002) investigated the use of prestressed concrete straps partially embedded in the deck for transverse confinement. The straps provided substantial restraint to the deck slab until it cracked. Transverse prestressing of the deck slab was also found to increase the cracking threshold of the concrete deck.

An experimental study was undertaken at Akita University in Japan by Hassan et al. (2002) to understand the effects of the strength of both the concrete and confinement systems on the steel-free slab system. Several large-scale, steel-free deck slabs were subjected to static loads. External, unbonded, prestressing bars were used as the method of confinement for the test specimens. In addition, various types of concrete strength were investigated. The overall behaviour of these test slabs was similar to that of slabs

where tension straps were used for transverse confinement. However, the prestressing bars were able to delay the onset of longitudinal cracking, thus increasing the serviceability limit load of the slab specimens.

Several advantages and disadvantages are associated with each of these transverse confinement systems. However, the best transverse confinement system depends on the required transverse stiffness, geometry of the concrete deck, and spacing of the longitudinal steel girders.

2.2.4.3 Precast Concrete Steel-Free Decks

Mufti et al. (2002) briefly reported on two precast deck fatigue tests. A full-scale cast-in-place ArchDeck slab tested at Dalhousie University under simulated rolling wheel loads exhibited considerably more fatigue resistance than required. The applied dynamic loads were 40% of the static failure load of 986 kN. Another full-scale model, consisting of a non-composite precast steel-free deck slab, was tested at the University of Manitoba under dynamic loads at a level of 33% of the static failure load. The deck also sustained a population of wheel loads higher greater than that expected during the typical lifespan of a bridge. No results were given regarding the size and distribution of cracks.

These initial tests led to more recent research of steel-free deck technology by Mufti et al. (2004). This research focused on the development of a composite precast concrete deck panel without internal tensile reinforcement. These types of panels can be manufactured and delivered to a remote bridge site as individual units where cast-in-place construction is not practical. For example, this type of bridge construction is ideal where crossings are required along logging routes. Once on site these panels can be placed and made composite with the supporting steel beams. Precast arch panels were found to be durable, have longer design lives, and reduced maintenance costs.

A full-scale model test was performed to determine the performance of the precast panels under construction loads before they were made composite with girders. In addition, the behaviour of the panels under design live loads was investigated. Each panel was 2830

mm in width and 3000 mm in length with a minimum thickness of 150 mm. The concrete panels had a slight crown in the centre such that the profile resembled a shallow arch. Transverse confinement was provided by 25 mm x 50 mm steel straps. Three 22 mm-diameter shear studs at each end of the strap connected it to the concrete panel. The shear studs fit into holes pre-cut into the underside of the concrete deck panels. These shear connector holes, in addition to the gaps between panels, were filled with a quick-setting grout. Normal strength concrete (35 MPa) with typical air entrainment and synthetic fibres was used to construct the panels. The steel girders supporting the concrete deck were spaced 3.5 m apart.

Several tests were completed on the precast panels. Cyclic wheel loads and axle loads were applied at various locations along the centre and exterior panels. Testing demonstrated that the panel system could withstand concentrated wheel loads in excess of 600 kN and axle loads in excess of 900 kN. It was found that the factored wheel load of the heaviest logging truck was approximately 89% of the observed failure load of the panel. Extensive deck cracking was observed under the various applied loads. The failure mode in each of the tests was a punching failure. From the tests, the load-carrying capacity was determined to be adequate for even the heaviest off-highway vehicle used on forestry roads. Testing of the slab prior to full composite connection with the girders also showed satisfactory results, however the mode of failure changed from punching failure to a flexure failure mode. Overall, there were no safety concerns associated with the precast panel system; however, the cracks that developed early on did not meet serviceability requirements. Nominal crack-control reinforcement, consisting of either steel or GFRP bars in a crack-control grid, was recommended to reduce the onset and amount of cracking.

2.2.4.4 Serviceability Issues: Fatigue and Cracking Behaviour

Although the capacity of the steel-free deck system has been well established, a great deal of current research is focusing on the cracking characteristics and serviceability requirements of these bridge decks. Fatigue resistance of steel-free decks requires the most improvement since adequate ultimate load capacity has been shown. Longitudinal

cracking has been observed in most of the bridges and laboratory specimens. These longitudinal cracks form during the initiation of arching action. Before the transverse steel straps act in tension, the underside of the bridge deck must crack approximately midway between the girders. Longitudinal deck cracking has not been proven to directly affect the ultimate strength or safety of the bridge. However, it is recognized that wide cracks do violate the serviceability limit state of aesthetics. Furthermore, if longitudinal cracks become large enough, the durability of the deck may be jeopardized. Substantial deterioration of the concrete around the crack could result if subject to freeze-thaw cycles in the presence of water.

Recently, a number of methods for controlling the width and distribution of cracks in steel-free concrete decks have been investigated. Longitudinal cracking in steel-free decks was observed by Bakht et al. (2000) during the testing of two full-scale models in Canada. After two million cyclic loads, the FRC slab specimen had developed one predominant, longitudinal crack midway between the girders. Cracking endurance of the system was found to be relatively low as cracking originated early on during the dynamic testing. Despite the presence of the crack, the steel-free deck specimens eventually shook down to elastic and stable structures.

Further experimental investigations by Bakht et al. (2003) reported that longitudinal cracks forming at the bottom of steel-free decks would eventually develop into full-depth cracks. However, these cracks did not lead to any interruption in continuity of the top surface of the slab. Bakht et al. (2003) and Hassan et al. (2003) agreed that cracking could be limited if a nominal amount of GFRP reinforcement was incorporated into the bottom of steel-free deck. Glass FRPs are permitted by the CHBDC (2000) as secondary reinforcement. This additional reinforcement was believed to distribute the cracks and reduce the crack widths. The presence of FRP reinforcement for the purposes of crack control would not undermine the novelty of the steel-free deck system.

Longitudinal cracks in steel-free deck experiments without a GFRP mesh, noted by Hassan et al. (2003), were approximately 1 mm wide. However, longitudinal cracks in

steel-free decks with a GFRP mesh were less than 0.5 mm. Slabs with transverse prestressing exhibited similar cracking results. The ultimate load capacities of the prestressed decks were similar to that of the steel strap confined systems. Although not significantly effective, the use of higher strength concrete in the deck slab delayed the onset of longitudinal cracking.

Yang et al. (2004) investigated the effects of longitudinal cracking on girder load distribution characteristics of steel-free bridge decks. A 1/3-scale, 6-girder bridge model was constructed at Dalhousie University. The concrete deck was 8220 mm long by 3375 mm wide and 75 mm thick. Steel straps were spaced 400 mm apart in the transverse direction and were connected to the steel girders that were spaced 675 mm apart. Steel diaphragms were also spaced at 2740 mm along the length of the bridge. 65 strain gauges and one displacement transducer per girder were used to monitor the behaviour of the bridge. From the test results, it was observed that the load distribution of the steel-free deck was similar to that of a steel-reinforced concrete deck-on-girder bridge. It was also observed that the load distribution characteristics were not significantly affected by the formation of the first longitudinal crack. However, after the second longitudinal crack had formed, a small difference in the load distribution characteristics was observed. The steel diaphragms decreased the sensitivity of load distribution after cracking had occurred. Based on the initial test results, it was recommended that current analysis methods for transverse load distribution were adequate for steel-free bridge decks, even if deck cracking was anticipated.

Memon and Mufti (2004) also investigated the cracking resistance and fatigue behaviour of a full-scale deck slab model subject to 25 ton 1 Hz cyclic loading at the University of Manitoba. Although cast monolithically, the 9.0 m x 3.0 m, 175 mm thick concrete slab consisted of three equal regions. Segment A was reinforced with typical 15M steel reinforcement spaced at 300 mm in each direction. Segment B was reinforced internally with CFRP bars; 0.19% reinforcement ratio in the transverse direction and 0.13% in the longitudinal direction. GFRP bars were used for internal reinforcement in the Segment C; 0.48% reinforcement ratio in the transverse direction and 0.36% in the longitudinal

direction. Each segment contained external steel straps spaced at 1000 mm in the transverse direction. LVDTs, pi-gauges, and strain gauges were used to monitor the behaviour of the deck slab. After one million load cycles, no significant damage was observed in the concrete deck. The maximum measured deflection was 2.0 mm during the dynamic load test. Measured strains were also well below allowable limits. Longitudinal cracks that had formed were approximately 0.34 mm wide and did not appear to increase in size after one million load cycles. This crack width is acceptable by the CHBDC standards. Based on these experimental test results and analytical approach, both deck segments satisfied serviceability requirements and exhibited sufficient fatigue resistance. However, since GFRP is cheaper compared to CFRP, it was recommended that internal GFRP reinforcement and external steel straps be used to reduce the longitudinal crack with. It was concluded that a bottom later of GFRP reinforcement at a ratio of 0.25 percent is necessary in order to reduce the longitudinal crack width.

These design considerations, which attempt to reduce the amount of cracking, have led to the development of second-generation steel-free decks and will be discussed in the following section.

2.2.4.5 Second-generation Steel-Free Decks

Between 1995 and 1999, five steel-free bridge deck slabs without internal tensile reinforcement were constructed in Canada. All of these slabs developed relatively wide (approximately 1 mm), full-depth longitudinal cracks midway between the girders. These wide cracks are not aesthetically pleasing and are generally not acceptable to bridge engineers. Developers of the steel-free deck slabs agree that a nominal crack-control grid of GFRP reinforcement is a necessary addition to the steel-free deck design in order to control the rate and growth of cracks. These requirements have led to the development of second-generation steel-free decks.

Second-generation steel-free decks are designed to exhibit the same overall behaviour as the first-generation steel-free deck slabs. However, the second-generation steel-free deck design improves on the first-generation design with a crack-control mesh/grid of GFRP

reinforcement to reduce severe cracking. The amount of reinforcement required for crack control is only 13% of what would normally be required for flexure design. Two design parameters must be accounted for in the design of second-generation steel-free decks. First, the size and spacing of the steel straps used for the transverse confinement system must be determined using the same design guidelines for first-generation steel-free decks. Second, the allowable strain level in the GFRP crack control reinforcement must be less than 2000 με. These considerations ensure crack widths remain less than 0.5 mm. This limit is recommended by CHBDC (2000) where GFRP bars are used and there is no risk of corrosion. Through research at the University of Manitoba, it has been concluded that second-generation steel-free deck technology is an economical and cost-effective solution to eliminate reinforced concrete deck corrosion. In addition, GFRP bars were found to have the best fatigue resistance and prevented the formation of wide longitudinal cracks.

In the summer of 2003, the first second-generation steel-free deck slab was constructed in Winnipeg, Manitoba. This bridge will be discussed in more detail in the following section.

2.2.5 Steel-Free Bridge Decks: Field Projects

2.2.5.1 Salmon River Bridge

The Salmon River Bridge along Trans-Canada Highway 104 in Nova Scotia was the first simple span steel-free bridge deck in the world when completed in December 1995. Located in one of the harshest bridge environments, the bridge is subject to the application of de-icing slats and daily freeze-thaw cycles during the winter. Even during the summer, the ambient air contains high levels of salt-laden moisture from the Atlantic Ocean. The bridge consisted of two 31.2 m simply supported spans with a 200 mm thick concrete slab over six steel plate girders spaced at 2.7m. Girders were positioned so that transverse overhanging cantilevers in the deck were avoided. 100 mm x 14 mm steel straps were welded to the tops of the girder flanges. Weld design was governed by fatigue design guidelines. Shear studs located on the top girder flanges connected the concrete deck to the steel girders.

Since the Salmon River Bridge was the first structure to implement steel-free deck technology, it was monitored periodically during its first five years of service life. Strain sensors, consisting of foil gauges and Bragg grating-type fibre optic sensors, were mounted on the steel straps, girders, and NEFMAC grid. A remote station was set-up nearby in Halifax to monitor the performance of the bridge. It was estimated that the bridge construction cost approximately six percent more compared to a conventional reinforced concrete deck.

Several bridge loading tests were completed. Girder flange strains confirmed that the steel free deck participated fully in transverse load distribution between girders. Through a number of periodic observations during its first five years of service life, the transverse load distribution characteristics of the bridge deck have remained the same. Since these characteristics haven't changed significantly, it was concluded with confidence that the deck stiffness has remained unchanged.

Deck cracking has also been monitored periodically during the last eight years. Two types of cracks were identified in the bridge deck six months after construction. Small transverse cracks had formed near the outside edge of the deck. One continuous, longitudinal crack ran nearly the entire length of the bridge between each girder. The longitudinal cracks measured 1 mm in width and were clearly visible to the naked eye. Mufti et al. (1999) confirmed that these cracks in the deck slab had stabilized during the first five years of service life and had not spread or increased in width. Through these inspections, it has been confirmed that crack growth has ceased in the steel-free deck at a relatively early stage. Overall, these types of inspections have increased the confidence in the use of steel-free bridge decks.

No new monitoring data has been collected recently from the Salmon River Bridge. Only yearly visual inspections are completed to ensure that crack patterns are not changing. As mentioned in the previous paragraph, cracks in the deck slab had stabilized in 1999. Since then, crack mapping patterns have not changed significantly.

2.2.5.2 Kent County Road Bridge

In November 1996, the second steel-free bridge deck opened to traffic was the Kent County Road Bridge located near Chatham, Ontario over Highway 401. Since the original reinforced concrete deck had deteriorated, a new deck was constructed over the five existing steel-plate girders that were spaced at approximately 2.1 m apart. Only two of the four simple bridge spans incorporated a 175 mm-thick steel-free deck. Unlike the Salmon River Bridge, 0.82 m overhanging cantilevers were present beyond the two exterior girders. These cantilevered regions were reinforced with CFRP NEFMAC grids in the transverse direction. GFRP grids were also used in the bridge barrier wall as tensile reinforcement. To achieve full arching action within the bridge deck, 50 x 20 mm galvanized steel straps, spaced at 1.0 m intervals, were welded to the tops of the girder flanges. Due to the use of CFRP grids within the deck, the overall cost was significantly more expensive compared to that of a conventional slab. This was also the first steel-free deck slab used in a rehabilitation application.

This bridge was also instrumented with strain gauges. Static and dynamic tests were performed to determine the bridge behaviour. From test results, it was concluded that the steel-free deck acted compositely with the steel girders in the longitudinal direction. Also, the bridge deck was able to withstand a very large wheel load of 500 kN without any signs of distress. Load distribution characteristics of the bridge were somewhat improved with the steel free deck. Similar to the Salmon River Bridge, cracks developed on the underside of the steel-free deck sections. However, these cracks were quite narrow and did not follow a regular pattern. During the load tests, the crack only opened approximately 0.02 mm and then closed after the passage of the loading vehicle.

No additional load testing or vibration data has been collected from the bridge during the last seven years. The bridge is still functioning as intended after eight years of service. In September 2004, approximately eight years after construction, core samples were extracted from the reinforced concrete bridge barriers. As mentioned before, NEFMAC GFRP G-13 grids, with a 100 mm x 100 mm mesh, were used to reinforce the concrete bridge barriers. The purpose for extracting the core samples was to determine the field

durability of the glass fibres used to reinforce the concrete barriers. Alkalis in concrete are known to attack these glass fibres. Concrete cover of the GFRP grid ranged between 40 - 85 mm. At the time of writing, the test results from the core samples were not available.

2.2.5.3 Crowchild Trail Bridge

The next bridge to be constructed using a steel-free deck was the Crowchild Trail Bridge in Calgary, Alberta in September 1997. Design considerations used in the construction of the bridge will be discussed in more detail in the next chapter. However, it is important to note that this bridge was the first continuous steel-free bridge deck in the world. Also, it is interesting to note that the steel-free deck design was selected in a competitive bidding process against more expensive conventional slab designs.

2.2.5.4 Waterloo Creek Bridge

Following the construction of the Crowchild Trail Bridge, the Waterloo Creek Bridge incorporated the next steel-free deck. Located on Vancouver Island, British Columbia, the bridge was opened to traffic in March 1998. It consists of two separate, 25 m long, simply supported spans. One span carries two northbound lanes while the other span carries two southbound lanes. The northbound structure utilizes a steel free deck design while the other structure contains traditional steel reinforcement. Instead of steel girders, the Waterloo Creek Bridge was the first steel-free deck constructed on prestressed concrete I-girders. Five of these girders, spaced 2.810 m apart, were designed to carry loads in the longitudinal direction in each span. It is also the first steel free deck supported by integral abutments. Longitudinal steel reinforcement at the end of the steel-free deck ensures a monolithic connection between the deck and the abutments. The steel-free deck is 190 mm thick and contains polypropylene fibre reinforcement similar to the previous steel-free decks. Steel straps located under the deck are spaced 1.25 m apart and provide confinement in the transverse direction similar to previous bridges. This design was nearly the same cost as a conventional slab.

Data was collected from the bridge site twelve times during a period between October 1998 and June 1999. Cracking within the steel-free deck was also inspected during the site visits. Each panel between the concrete girders contained a single longitudinal crack along the length of the bridge. No additional monitoring data has been obtained from the bridge since these original tests were completed.

2.2.5.5 Lindquist Creek Bridge

The next steel-free bridge constructed in Canada was the Lindquist Creek forestry bridge located near Darfield, British Columbia. This was the first bridge to incorporate a steel-free precast panel. For this application, a steel-free design was 30% cheaper than a conventional panel construction. This bridge is located on a logging road and consists of a 24 m single span. The single lane structure consists of two steel plate girders spaced 3.5 m apart. Steel studs connect the precast concrete steel-free deck panel to the steel girders. Transverse confinement of the panels was achieved using 25 x 50 mm studded steel straps spaced at 1.0 m intervals.

Field tests performed on the bridge in March of 1998 included static and dynamic strain measurements in addition to ambient and forced vibration measurements. Testing of the bridge with 16 instruments revealed maximum measured strains of 305 $\mu\varepsilon$ in the girders. This was only 20% of the yield strain of the grade 350 A steel used for the girders. Also, the maximum deflection measured was only 11.6 mm. Load sharing between the two girders was considered to be very reasonable. Several wide cracks developed in the underside of the precast panels as a result of the absence of reinforcement. Overall, however, these tests proved that steel-free construction was reliable and safe for precast panels. No additional monitoring data has been obtained from the bridge since these original tests were completed.

2.2.5.6 Trout River Bridge

Although the Trout River Bridge was scheduled for replacement in 2003, Public Works and Government Services of Canada (PWGSC) delayed the project until 2005. This

bridge is located on the Alaska Highway within Muncho Lake Provincial Park in Northern B.C. and consists of two lanes to allow travel in each direction. Integral abutments support each end of the 65 m single-span deck superstructure. Dual trapezoidal steel box girders resist the bending moments in the longitudinal direction. Instead of using typical reinforcement, GFRP bars and galvanized steel are used to reinforce the top and bottom layers of the deck respectively. This project will expand the applications of steel free decks and will be the first steel box structure to utilize a concrete deck void of typical steel reinforcement.

Several design requirements were considered in the bridge design. The bridge is required to carry all provincial and territorial regulation loads. In order to minimize the impact on the environment, a single span bridge, 65 m in length, was selected. Since the bridge is located in a remote area, a low maintenance type of bridge was required. Therefore, durable reinforcement materials were chosen that would minimize the occurrence of corrosion and prevent deterioration of the bridge deck. GFRP bars and galvanized steel were selected to fulfill this role. Using these materials, the bridge service life is expected to be 75 years.

A Structural Health Monitoring (SHM) program will be initiated to assess the in-service performance of the innovative bridge design. In addition, data obtained will provide insight into a decision-making program to optimize the long-term maintenance cost of the bridge. The SHM program will measure the elongation of box girders due to temperature changes and restraint of the integral abutments. Strains in the GFRP reinforcement will also be measured.

2.2.5.7 Red River Bridge

During July 2003, the first application of a second-generation steel-free deck slab was implemented in a section of the Red River Bridge. The ten span, 347 m long bridge is located on the North Perimeter Highway in Winnipeg, Manitoba. The original structure was built in 1964 and consisted of a reinforced concrete slab placed above steel girders that were space 1.8 meters apart. During the winter, bridge structures in Manitoba are

subject to the application of de-icing salts and numerous freeze/thaw cycles. As a result of these severe exposure conditions, major deck rehabilitation of the Red River Bridge was necessary during the 1980's and 1990's.

The entire bridge deck of the Red River Bridge was replaced during the summer of 2003. Nine of the ten spans were replaced with a conventional 225 mm thick steel-reinforced deck slab using a highly durable ternary concrete with a projected service life of 50 years. However, one of the simple span deck sections was replaced using second-generation steel-free deck technology. Although the concrete deck in the steel-free section was also 225 mm think, conventional Portland Type 10 concrete was used. GFRP reinforcement was used for both the top and bottom mats in the internal deck panels. CFRP reinforcement was used in the negative moment regions for both the vehicular and pedestrian cantilevers of the bridge deck. Concrete bridge barriers were anchored to the bridge deck using stainless steel bars spaced at 300 mm O/C. GFRP and galvanized steel reinforcement was used within the concrete barrier. 50 mm x 30 mm steel straps spaced 1.2 m apart were tack welded to the top of the girder flanges in order to provide transverse confinement. Steel nelson studs were added to the straps to ensure that the concrete deck acted compositely with the girders. Since the existing girder studs were insufficient, haunch reinforcement was used to ensure composite action between the deck and the girders in the longitudinal direction.

The unit prices for the conventional and steel-free deck slabs were $\$993/m^3$ of concrete and $\$1103/m^3$ of concrete, respectively. The contractor's lack of familiarity with steel-free deck construction accounted for the 11% difference in construction costs. However, the steel-free deck remains a much more economical design from a life-cycle cost perspective as a result of enhanced durability and extended service life.

A structural health monitoring system, or civionic system, was designed and installed for the Red River Bridge. Instrumentation included the use of conventional strain gauges, Fibre Optic Bragg Sensors, accelerometers, and thermocouples. This instrumentation enabled the monitoring of strains within the GFRP reinforcement, CFRP reinforcement,

steel straps, and steel girders. In addition, the accelerometers installed in the traffic barriers measure the natural frequencies of the bridge. An on-site data acquisition system, video camera, and weigh-in-motion device store bridge load and behaviour information. Bridge performance results after one year of service were not available.

2.3 Conclusions from Literature Review

During the past several years, a large amount of research has focused on the development of steel-free bridge decks as a feasible alternative to reinforced concrete bridge decks. Steel-free bridge decks designed to behave in arching action have been shown to support higher loads compared to traditional bridge decks. Steel-free deck designs have been incorporated into simple-span and continuous-span bridges, and into decks with cantilever components. In addition, steel-free decks have been used in both cast-in-place and precast construction applications. Several types of confinement systems have been shown to provide adequate rigidity in the transverse direction of bridge decks. Research has also focused on the fatigue and serviceability performance of steel-free bridge decks. This hard work and creativity led to the construction of several steel-free bridges in Canada during the last ten years. Recent research has contributed to the development of second-generation steel-free bridge decks. Immediately after the construction of these bridges, load tests and ambient vibration tests were completed to capture the base-line structural characteristics and validate design assumptions. Through these research efforts and constructed bridge decks, the short-term behaviour of steel-free bridge decks has been well established. Overall, the steel-free decks investigated in the 1990s performed very well within their first years of service.

All of the steel-free bridge decks constructed during the 1990s have been in service for more than five years. Although the short-term behaviour of these bridges has been well established through brief monitoring programs, very few tests or observations have been completed since they were first constructed. For example, the Salmon River Bridge was subject to load tests immediately after construction, however, only periodical visual inspections have been completed since then to monitor the cracking patterns. Similarly, no additional tests have been investigated for the Kent County Road Bridge since static

and dynamic tests were completed in November 1996. No additional data has been collected from the Waterloo Creek and Lindquist Creek Bridges since they were first constructed. Overall, these bridge monitoring programs have not been very comprehensive and do not have clear objectives with respect to long-term monitoring or determination of long-term performance. In addition, there is currently very little published research based on the long-term field performance of new composite materials used in these structures.

Structural Health Monitoring (SHM) embodies many of the short-term objectives and goals of the previous steel-free deck bridge programs. The main objective of SHM, with respect to steel-free deck bridges, is to monitor the behaviour of these structures accurately and efficiently. SHM techniques may also be used in assessing the performance and strength of bridges under static or dynamic vehicle loads, and in the verification of innovative designs. Innovative structures, such as steel-free decks, that use new materials also require structural health monitoring. Health monitoring ensures that these new materials function as intended and their structural behaviour is satisfactory. In addition to the short-term goals highlighted by the summarized steel-free bridge tests, SHM is more beneficial using a longer timeline.

Long-term SHM could be over 10 years, 20 years, and continued throughout the entire service life of steel-free deck bridges. The monitoring process may be done continuously or periodically. Continuous monitoring is typically required if the structure is extremely important or if there is significant doubt about its structural integrity. Periodic monitoring, on the other hand, may be done once a month or once a year. For steel-free decks, long-term SHM is necessary as the true performance and strength of these bridges may become more apparent after 10 or 20 years.

Even though rigorous long-term SHM of steel-free deck bridges would be beneficial, many of the steel-free decks constructed in the 1990s have received minimal periodic monitoring since they were first constructed. The absence of long-term monitoring can be attributed to the lack of resources and funding available for these types of projects.

Additional tests should be completed as the deck cracking characteristics in many of these bridges may influence their long-term behaviour and fatigue resistance. By proving the satisfactory long-term performance of steel-free decks, bridge owners would be convinced of their benefits. With the information obtained through long-term SHM, they can accurately compare steel-free bridge deck construction to typical reinforced concrete deck construction from long-term structural and long-term cost points-of-view. Despite these observations and the benefits of proving their long-term satisfactory performance, very little research has been completed that thoroughly investigates the long-term behaviour of steel-free deck bridges.

Compared to other steel-free decks, the Crowchild Trail Bridge in Calgary has been subjected to the most amounts of load tests and ambient vibration tests since it was first constructed. The goals highlighted in the previous paragraphs are also shared by the Crowchild Trail Bridge long-term SHM program. The results and analysis of the long-term monitoring data obtained from the Crowchild Trail Bridge will be presented in the following chapters.

3.0 CONSTRUCTION, INSTRUMENTATION, AND TEST EQUIPMENT OF CROWCHILD TRAIL BRIDGE

3.1 Introduction

When constructed in 1997, the Crowchild Trail Bridge was the first continuous steel-free concrete bridge deck in the world. Steel-free deck designs had been incorporated in several bridge structures before the Crowchild Trail Bridge was constructed. However, all of the previous steel-free decks constructed were over simply supported spans. Due to the limited capacity of the existing sub-structure of the Crowchild Trail Bridge, the new super structure had to be continuous over three spans. The Crowchild Trail Bridge steel-free deck required innovative materials and a unique design to meet the load and service requirements. It is important to note the location of the bridge: southbound Crowchild Trail is one of the main road arteries into the downtown business core. Therefore, the bridge design had to be dependable to withstand the repeated traffic loading of thousands of vehicles every day.

3.2 Background of Original Crowchild Trail Bridge Structure

Located in Calgary, Alberta, the Crowchild Trail Bridge is an overpass that allows two southbound lanes of Crowchild Trail traffic to travel over University Drive. Before replacement, the original superstructure consisted of a series of simply supported, prestressed concrete box-girders, and was designed for HS20 truck loading. The original bridge remained in operation for only 20 years before structure replacement was considered due to increased truckloads and rapid deterioration.

Based on the current version of the Canadian Highway Bridge Design Code and typical truck loading, several deficiencies were identified in the original structure. Girders were determined to have insufficient bending capacity. In addition, the development and quantity of reinforcement in several structural areas were also determined to be insufficient. Therefore a new structure was required.

3.3 Materials and Design Considerations of Crowchild Trail Bridge

3.3.1 Bridge Layout and Construction Costs

Constructed in June 1997, the new Crowchild Trail Bridge superstructure replaced the old bridge deck. As a result of economic and durability concerns, a steel-free deck design was selected. Existing piers, abutments, and foundations constructed for the original bridge were reused without any modifications. The new bridge consists of three continuous spans over two pier supports measuring 29.830 m, 32.818 m, and 30.230 m for a combined total length of 92.878 m. The layout of the bridge is shown in Figure 3.1.

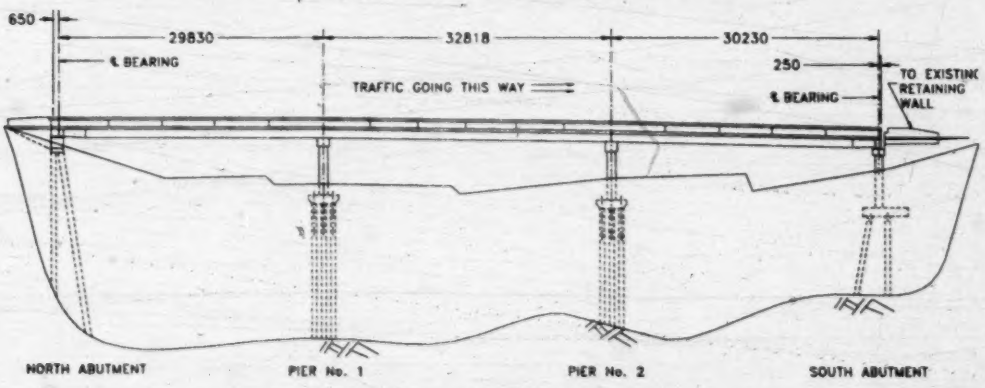

Figure 3.1 - West Elevation of Crowchild Trail Bridge

It is interesting to note that the capital cost of the steel-free deck was approximately $20,000 cheaper compared to the cost of a conventional reinforced concrete deck. Although GFRP reinforcement is not standard in bridge designs, it accounted for only 2 % of the total superstructure costs.

3.3.2 Concrete Deck

The concrete deck measures 9030 mm wide and 185 mm thick. At the interface between the concrete deck and the steel girders, the deck thickness increases to 265 mm with the addition of an 80 mm thick haunch. The concrete deck was constructed using 35 MPa concrete and consists of polypropylene fibres at a ratio of 4.5 kg/m^3. In addition to the polypropylene fibres, the concrete mix specifications for 1 m^3 included: 155 kg water,

430 kg cement, 1080 kg coarse aggregates, 680 kg fine aggregates, 50 ml / 100 kg air entrainment, and 290 ml / 100 kg superplastizer. An asphalt-riding surface covers the top of the concrete deck. The typical deck cross-section is shown in Figure 3.2.

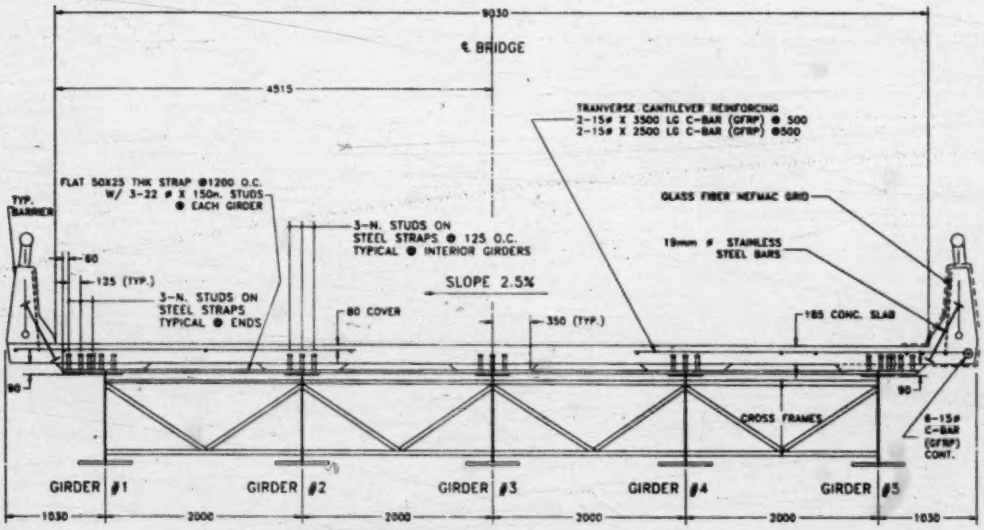

Figure 3.2 - Crowchild Trail Bridge Deck Cross-Section

Cracking of the Crowchild Trail Bridge deck was a major concern that had to be addressed during the design stage. During the winter months, the bridge experiences freezing and thawing cycles under wet conditions. These conditions could potentially lead to severe cracking within the deck. Although cracks would not significantly affect the ultimate strength of the deck, the durability of the deck would be questionable. Polypropylene fibres in the concrete mix were used to minimize and control the effects of thermal cracking and shrinkage within the bridge deck. More specifically, the fibres reduce the quantity and size of cracks.

For one-way flexural members, shear is the gradient of bending moment along the length and consists of two components: beam action and arching action. Beam action is the governing (stiffer) mechanism and occurs before cracking of the concrete deck. At service loads, shear is transferred by a combination of beam action and arching action.

Near the ultimate load the concrete cracks at the mid-span, and the load is transferred via compressive struts to the supporting girders. Therefore, under ultimate load, the Crowchild Trail Bridge deck is designed so that shear is transferred by arching action.

The concrete deck shape takes advantage of the compressive strut locations by removing a trapezoidal section from the underside of the bridge deck as shown in Figure 3.2. In this area of the deck, the compressive capability of the concrete is not required. Cracking would be more severe in this region if concrete were present due to higher tension stresses. The concrete deck is primarily designed to carry wheel loads to the neighbouring steel plate girders in the transverse direction only. Although the concrete deck does contribute to the load-carrying capacity of the bridge in the longitudinal direction to a small degree, the safety of the Crowchild Trail Bridge does not depend on this contribution. In the design, the steel girders are engineered to resist the entire longitudinal moment and are assumed to be the only structural component to transfer loads in the longitudinal direction

3.3.3 GFRP Deck Reinforcement

The concrete deck is unique due to the absence of internal reinforcing steel in selected locations. However, glass fibre reinforced polymer (GFRP) type reinforcement was placed in the concrete deck over the intermediate pier locations and in the transverse direction of the cantilever deck portions. The south span deck is reinforced internally with GFRP bars and steel bars. However, the middle span is only partially reinforced with GFRP bars and does not contain any typical steel reinforcement. Finally, the north span only contains GFRP bars in the cantilevered portions of the bridge deck located outside of the steel girders.

With a continuous bridge structure, tension stresses develop in the upper regions of the concrete deck over the piers. According to the Canadian Highway Bridge Design Code, GFRP reinforcement cannot be used as a primary reinforcement and therefore cannot be used in the calculations of the ultimate moment capacity of the composite section. However, GFRPs may be used in a secondary role in order to satisfy serviceability

requirements. Therefore, GFRP reinforcement placed in the negative moment regions is designed to reduce transverse cracking. This reinforcement reduces the quantity and size of potential transverse cracks and allows the formation of internal arches. Although cracks are not totally eliminated from the deck with this type of reinforcement, the GFRP reinforcement dictates the location of the cracks. Steel plate girders are designed to carry the entire ultimate moments in this negative bending moment region.

One meter-wide cantilevers on each side of the Crowchild Trail Bridge deck also required additional design consideration. Arching action that would typically develop between two girders cannot develop in cantilevers. GFRP reinforcement was required in the upper regions of the cantilevered sections to resist the negative bending moments.

3.3.4 Steel-Plate Girders

Five built-up steel plate girders, approximately 900 mm deep and spaced 2000 mm apart, are located below the concrete deck and are designed to carry the main structural loads in the longitudinal direction. These steel plate girders are connected together so that the bridge is continuous over both piers. To carry the full ultimate moment in the negative moment regions along the bridge, the girder size in these regions had to be increased. In the negative moment regions the top flange of the plate girder was increased from 18 x 350 mm to 32 x 600 mm and the web thickness was increased by 2 mm. In addition, the bottom flange dimensions were increased from 30 x 550 mm to 38 x 600 mm.

Four equally spaced cross-frames are located within each span and provide lateral stability for the girders. In addition, two stiffened transverse girders act as transverse diaphragms between all five girders at the intermediate pier locations. At both the north and south abutments, the five girders rest on individual bearing plates. However, at each pier location, only two bearing plates support the transverse girders that are connected to the main girders.

Double-headed shear studs were used to connect the steel girders to the concrete bridge deck. These studs are welded directly to the tops of the girder flanges. In addition to

connecting the deck and steel girders, the welded steel studs provide confinement in the longitudinal direction

3.3.5 Steel Straps

In the place of typical internal steel reinforcement, external steel tension straps were positioned directly under the concrete deck to resist tension stresses in the transverse direction. 50 x 25 mm steel bars were used as tension straps and were spaced 1.2 m apart. These steel tension straps span the distance between neighbouring girders.

The steel straps behave as tension ties in the deck arching model and contribute to the transverse flexural rigidity of the deck system. Transverse confinement was achieved using a slightly different method within the Crowchild continuous steel-free deck. Instead of welding the steel straps directly to the plate girder flanges, partially studded steel straps were used. This approach was used due to fatigue concerns.

3.3.6 Bridge Barriers

The concrete bridge barriers were based on the Ontario Bridge Barrier design and are reinforced internally with prefabricated NEFMAC GFRP grids. Double headed stainless steel studs anchor the barriers to the deck. These types of barriers continue the steel-free deck concept and provide adequate safety for traffic on the bridge.

3.4 Crowchild Trail Bridge Instrumentation and Test Equipment

3.4.1 Introduction

Traditionally, the most basic method of SHM and bridge testing has been periodical visual inspections. However, these types of inspections are limited in their effectiveness as many key bridge characteristics are not visible to the human eye. For Crowchild Trail Bridge testing, SHM tools were required to complement visual observations. A complete SHM system is made up of several tools for sensing, data acquisition, communication, intelligent data processing, data storage, and damage detection and modelling. Advances in transducer, data acquisition, and information technologies have allowed complex and continuous field monitoring with good cost effectiveness. Permanent instrumentation for the Crowchild Trail Bridge monitoring program was designed to capture its static and dynamic behaviour. However, additional instrumentation was required to collect vibration data from the bridge. Descriptions and layout of this instrumentation will be described in detail within the following sections.

3.4.2 Strain Gauges

Table 3.1 summarizes all of the permanently installed instrumentation on the Crowchild Trail Bridge. In total, the instrumentation consists of 108 strain gauges and five thermistors. 86 of the strain gauges are five mm foil strain gauges, two are glued-on fibre optic strain gauges, three are embedded fibre optic strain sensors in GFRP bars (smart bars), and 17 are electrical resistance embedded concrete strain gauges. It is important to note that all of the instrumentation is located within the north span of the bridge where internal reinforcing steel is not present. Only GFRP reinforcement is located in the cantilevered portions of the bridge deck in this span. Since a large majority of the data is obtained from the steel plate girders, locations for all of the girder strain gauges can be seen in Figure 3.3. Exact locations for all of the strain gauges is referenced in Appendix A.

Table 3.1 - Crowchild Trail Bridge Instrumentation List

Crowchild Trail Bridge - Strain Gauge and Thermosistor Setup			
Instrumentation Quantity and Description		**Location**	**Purpose of Gauge**
G-34	**5 mm foil strain gauges**	Built-up plate girders	Monitor strain distribution along webs and flanges; load sharing
T-18		Steel Tension Straps	Monitor performance of straps along length of the bridge and strain distribution along one strap
S-6		Shear Studs	Strains
C-4		Cross Frame	Investigate out-of-plane movement of cross frame under heavy loading
N-4		NEFMAC grid and barrier stainless steel rods	Strains
R-15		GFRP bars on deck reinforce.	Monitor behaviour of cantilevers and negative moment regions
RC-2		GFRP bars	Monitor performance of glue-on FOGs
RS-3		Smart bar	Monitor performance of embedded FOGs
FC-2	**Fibre Optic Sensors**	GFRP bars	Compare with foil strain gauges (RC-2)
FS-3		Smart bars	Compare with foil strain gauges (RS-3)
E-17	**Electrical resistance embedded strain gauges**	Embedded inside precast concrete blocks within deck	120 mm in length Monitor arching action in concrete deck
TH-5	**Thermistors**	4 embedded in concrete deck and 1 outside air	Determine temperature profile within the deck and ambient air temperature

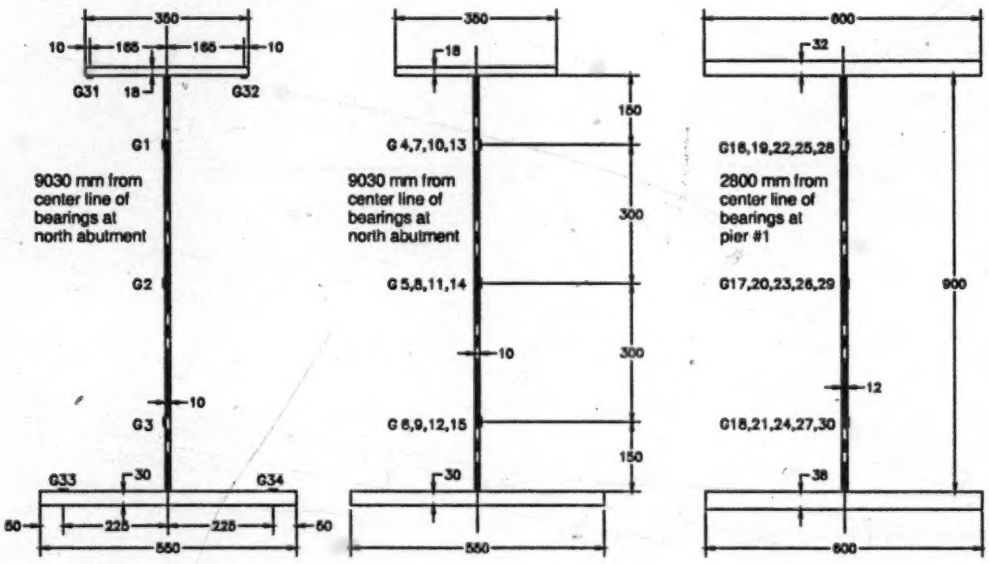

Figure 3.3 - Steel Girder Strain Gauge Configurations

3.4.3 Deflection Equipment

Additional equipment was required to measure deflections. All of the deflection measuring equipment is temporary and was only setup during load testing. During the first load tests in 1997, deflections at various points on the bridge deck were measured using surveying equipment. However, this methodology was very tedious, time consuming, and was subject to human error. In the 1998 load tests, ten cable transducers were used to measure girder deflections in two areas: near the north midspan and near Pier 1. This method was quicker and more accurate compared to the surveying method used in 1997. During the 2004 tests, five cable transducers connected to five voltage channel outputs were used to measure girder deflections. Vertical deflections of the girders were measured at a section 14.43 m from the centreline of the north abutment. This location was chosen so that deflection results from 2004 tests could be compared with 1998 deflection results taken at the same location. The cable transducer setup is shown in Figure 3.4.

Figure 3.4 - 2004 Cable Transducer Layout

3.4.4 Ambient Vibration Test Equipment

During the 1997 ambient vibration tests, eight force-balanced accelerometers manufactured by Kinemetrics (Model FBA-11) were used to capture natural frequencies and mode shapes. The accelerometers used were capable of measuring accelerations up to 0.5 g with a resolution of 0.2 μg. Accelerometers are electromechanical transducers that produce an electrical output proportional to the vibratory acceleration they are subjected to. This electrical charge is used to accurately determine natural frequencies and vibration amplitudes or mode shapes. Signal conditioners were also used to improve the quality of the accelerometer signals and were set at a cut-off frequency of 50 Hz. Ambient vibration data was first stored on the hard disk of a data acquisition computer in binary form and then transferred to a data analysis computer for numerical analysis.

Different equipment was used during the 1998 and 2004 ambient vibration tests. Four accelerometers were attached to the surface of the bridge deck with double-sided

adhesive tape in order to capture natural frequencies and mode shapes. Bruel & Kjaer Type 4370 (2) and Type 8306 (2) accelerometers were used. Type 4370 accelerometers used were capable of measuring accelerations of up to 50 g with a resolution of 100 μg. Type 8306 accelerometers used were capable of measuring accelerations of up to 5 g with a resolution of 30 μg. Compared to the equipment used in 1997, these accelerometers could measure larger accelerations with less accuracy. A computer laptop was used to record and store the vibration data. The accelerometers and data acquisition equipment that was used during the 2004 ambient vibration tests is shown in Figure 3.5.

Figure 3.5 – 2004 Ambient Vibration Equipment

3.4.5 Load Test Data Collection Equipment

When the Crowchild Trail Bridge was constructed in 1997, all of the lead wires from the strain gauges were protected in electrical conduits and were connected to a central junction box located in the north span of the bridge. This permitted the safe storage of the lead wires between tests and protected them from unfavourable ambient conditions

and vandalism. In addition, the junction box allowed for easy connection with all the wire connectors. For testing purposes, the lead wires and connectors were removed from the junction box and connected to a data acquisition system for data retrieval and storage. Figure 3.6 shows the electrical conduits carrying the lead wires directly under the bridge deck and the grey junction box used to house and store the connectors and associated wiring.

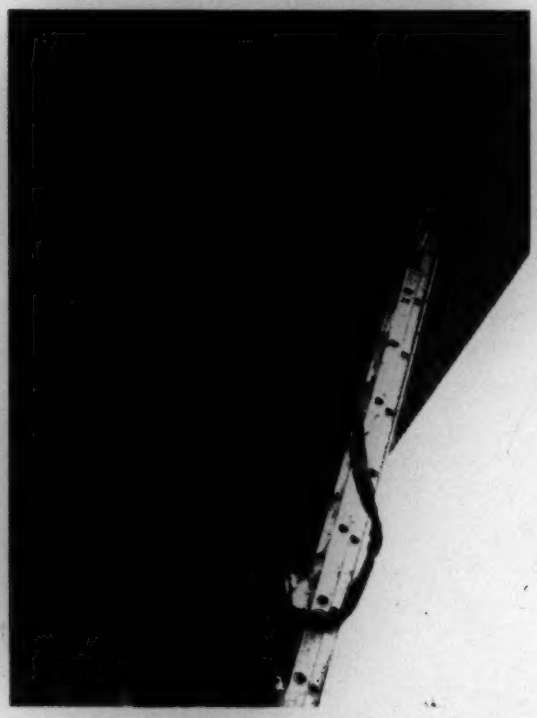

Figure 3.6 – Strain Gauge Connector Junction Box

In all of the load tests, the strain connectors were connected to a data acquisition device, which, in turn, was connected to a central computer for data storage. The DAQ performed a variety of functions including: electrical signal conditioning, supply of an external excitation voltage to all the gauges, unwanted noise filtering, and amplification of any low-level signal if required. In all of the tests, a central computer was used to store and archive all of the raw data. A Labview software program was used as an

interface between the user and the data acquisition unit in order to modify the sampling rate and amount of data collected. For all of the bridge tests, the amount of raw data collected was very important: the amount was required to be large enough to be useful, but not too large and overwhelming so that it would complicate interpretation.

For the 2004 load tests, a National Instruments data acquisition unit and Dell desktop computer were used to capture all of the strain and deflection data. The NI data acquisition unit was capable of supporting 24 strain gauges in addition to 32 voltage channels at a time. It was felt that sufficient information about the behaviour of the bridge could be captured using only 72 of the strain gauges and five of the voltage channels. Therefore, all static and dynamic load tests would have to be repeated only three times in order to collect data for the 72 strain gauges. Data acquisition equipment used for the 2004 load tests is shown in Figure 3.7.

Figure 3.7 - 2004 Data Acquisition Equipment

3.4.6 Loading Trucks

Static and dynamic loading tests required the use of loaded trucks in order to generate meaningful bridge strains and deflections. Dump trucks with hitched trailers have been used in each test. The loading truck and pup trailer used for the 2004 static and dynamic loading tests, which was typical of all the past trucks, is shown in Figure 3.8.

Figure 3.8 – 2004 Load Test Truck

However, the truck loadings were slightly different in each of the 1997, 1998, and 2004 loading tests. Although the basic truck configurations have been similar, the wheel spacing and axle loadings were slightly different for each test. Table 3.2 summarizes the total weight, individual axle loading, centre of gravity, and total length of each truck.

Table 3.2 - Loading Truck Axle Weights

Truck Year	Total Weight (kg / kN)	Truck Front Axle (kg)	Truck Rear Axle (kg)	Trailer Axle (kg)	C.G. rel. to front axle(m)	Total Length (m)
1997	36,250 kg *355 kN*	5454	14636	16160	7.73	13.18
1998	40,220 kg *394 kN*	4290	15650	20280	8.35	12.85
2004	42,380 kg *415 kN*	5630	19120	17630	7.43	13.00

Figures 3.9, 3.10 and 3.11 show the loading trucks used in 1997, 1998, and 2004 respectively. As shown in the figures, each truck/trailer consisted of three loading axles.

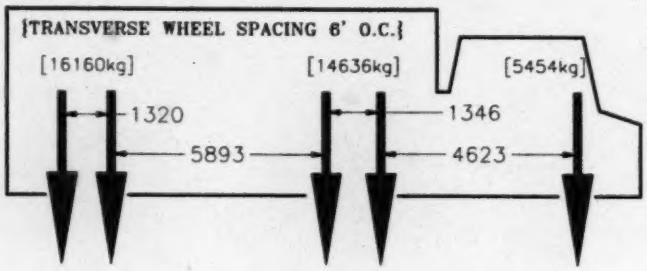

Figure 3.9 – 1997 Truck Loading

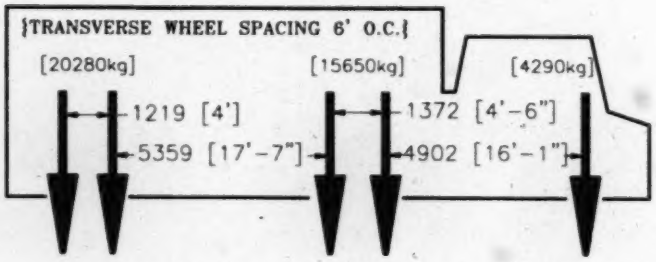

Figure 3.10 – 1998 Truck Loading

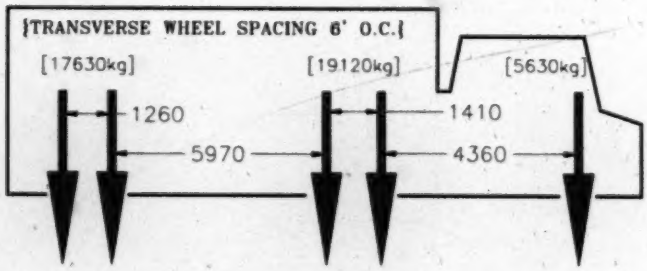

Figure 3.11 - 2004 Truck Loading

In general, the weight of the truck has gradually increased from year to year. The axle weight distributions have also varied from year to year. The centre of gravity, relative to the front axle, was calculated for each truck: the centre of gravity for the 1997 truck was located approximately 7.73 m behind the front truck axle, the centre of gravity for the 1998 truck was located approximately 8.35 m behind the front truck axle, and the centre of gravity for the 2004 truck was located approximately 7.43 m behind the front axle.

4.0 EXPERIMENTAL PROCEDURES AND RESULTS

4.1 Outline of Crowchild Trail Bridge Testing 1997 - 2004

Structural health monitoring of the Crowchild Trail Bridge was necessary in order to properly observe the behaviour of the innovative structural materials used in the continuous bridge deck. In addition, the overall structural performance of the bridge could be monitored over time. The Crowchild Trail Bridge was the first continuous span bridge in the world constructed with a steel-free deck. In order to understand the in-situ behaviour of the new bridge superstructure, a Structural Health Monitoring program was developed at the University of Alberta with guidance from ISIS Canada, the City of Calgary, and SPECO Engineering Ltd. When the structural health monitoring program was initiated in 1997 for the Crowchild Trail Bridge, three main research goals were identified: bridge performance under serviceability conditions, change of major bridge characteristics over time, and the long-term durability of the bridge. This SHM program was developed to quantify the static, dynamic, and ambient characteristics of the innovative bridge.

SHM techniques and instrumentation implemented by engineers can be considered analogous to human health check-ups administered by doctors. For example, a doctor may use special medical equipment to determine the patient's temperature, heart rate, cholesterol level, and other important characteristics. Depending on what conclusions the doctor makes from these observations, they may prescribe medicine to ensure the patient remains healthy. Similarly, an engineer can use embedded sensors and other equipment to determine strains and vibration frequencies of a bridge structure. Once this data has been collected and analyzed, appropriate measures can be taken to maintain the safety and integrity of the structure.

After the Crowchild Trail Bridge was reconstructed in 1997, several sets of tests were completed before the bridge was opened to traffic. These tests captured the baseline structural characteristics and behaviour of the bridge. Additional tests were completed in 1998 after the Crowchild Trail Bridge had been in full service for a year. Several

changes in the component performance and overall bridge behaviour were found. Six years later, in 2004, another full set of field tests were performed to determine whether any significant structural changes had occurred. Field tests consisted of ambient vibration tests to determine the natural frequencies and mode shapes of the bridge. In addition, static load tests and dynamic load tests were also completed to determine bridge strains and behaviour under known truckloads. Finally, the underside of the bridge deck was visually inspected in order to map the origin and progression of cracks as a result of normal traffic loading and other environmental factors.

Table 4.1 summarizes all of the Crowchild Trail Bridge field tests that have been completed in the first seven years of operation. Next to each test description is a number indicating the sequence of the test. For example, the number three adjacent to the ambient vibration tests for June 2004 indicates that this was the third set of ambient vibration data collected since the Crowchild Trail Bridge was first completed. Overall ambient vibration tests have been completed three times, static load tests three times, random dynamic load tests three times, planned dynamic load tests two times, and crack mapping five times. Initial tests completed in 1997 immediately after the bridge was constructed determined the baseline structural characteristics and behaviour of the bridge. Subsequent tests carried out between 1998 and 2004 determined the changing structural behaviour of the bridge

Table 4.1 - Summary of Crowchild Trail Bridge Field Tests

Date	Tests / Measurements
August 1997	• Ambient Vibration Tests (#1) - Identify initial natural frequencies and mode shapes • Static Load Tests (#1) – Measure strains and deflections • Crack Mapping (#1) – Record layout and size of cracks
September 1997	• Temperature Tests (#1) – Bridge behaviour under known temperature changes
October 1997	• Random Dynamic Load Tests (#1) – Measure strains under random traffic loading
June 1998	• Random Dynamic Load Tests (#2) – Measure strains under random traffic loading
August 1998	• Ambient Vibration Tests (#2) – Check natural frequencies and mode shapes • Static Load Tests (#2) – Measure strains and deflections under known truck load • Dynamic Load Tests (#1) – Measure strains, deflections, and accelerations under known truck load • Crack Mapping (#2) – Document locations of new cracks and estimated sizes of existing cracks
June 1999	• Crack Mapping (#3) – Document locations of new cracks and estimated sizes of new/existing cracks
July 2002	• Crack Mapping (#4) – Document locations of new cracks and estimated sizes of new/existing cracks
June 2004	• Random Dynamic Load Tests (#3) - Measure strains under random traffic loading • Ambient Vibration Tests (#3) – Check natural frequencies and mode shapes • Static Load Tests (#3) – Measure strains and deflections under known truck load • Dynamic Load Tests (#2) – Measure strains and deflections under known truck loads and known speeds • Crack Mapping (#5) – Update and document locations of new cracks and estimated sizes of existing cracks

4.2 Summary of 1997 Bridge Tests

4.2.1 1997 Ambient Vibration Test Results

On August 15, 1997, prior to the opening of traffic, ambient vibration tests were performed by a research team from the University of British Columbia. The temperature for the day was 8°C with moderate to heavy rain. These tests were important in determining the key dynamic characteristics of the Crowchild Trail Bridge. Future test results could also be compared to these initial benchmark characteristics in order to determine significant changes over time. Natural frequencies of the bridge and corresponding vertical, transverse, and torsional mode shapes were determined from the dynamic results.

During the ambient vibration testing, the bridge structure was excited by wind, human activity, and neighbouring traffic flow. No controlled external force was applied to the structure. In total, eight accelerometers were arranged to measure the vibrations at forty-six locations; fourteen different set-ups along the deck were completed. In addition, one accelerometer set-up was used near the bases of Pier 1 and 2. A spectral density normalization and averaging function (denoted as averaged normalized power spectral density (ANPSD)) was used to identify all of the natural frequencies less than 20 Hz. Thirteen natural frequencies and modes below 20 Hz were identified and are summarized in Table 4.2. The modal shape description is also noted in this table.

The fundamental frequencies for the vertical, torsional, and transverse degrees of freedom were 2.78 Hz, 3.13 Hz, and 12.84 Hz respectively. The UBC research group stressed that the resolution of the higher modes identified were not as reliable due to the limited number of measuring points and limitations in the techniques used. In addition, some of the modes were highly coupled as the methods of ambient vibration testing had difficulty handling these types of situations.

Table 4.2 - 1997 Natural Frequencies and Mode Shapes

Mode	Frequency	Description
1	2.78 Hz	1st Fundamental Vertical Mode
2	3.13 Hz	1st Fundamental Torsional Mode
3	3.76 Hz	Coupled Mode (2nd Vertical / 2nd Torsional)
4	4.05 Hz	3rd Torsional Mode
5	4.64 Hz	3rd Vertical Mode
6	5.18 Hz	Coupled Mode (4th Torsional / 1st Transverse)
7	7.13 Hz	Coupled Mode (5th Torsional / 2nd Transverse)
8	9.13 Hz	4th Vertical Mode
9	10.74 Hz	6th Torsional Mode
10	12.84 Hz	1st Fundamental Transverse Mode
11	15.77 Hz	7th Torsional Mode
12	17.68 Hz	5th Vertical Mode
13	19.29 Hz	8th Torsional Mode

4.2.2 1997 Static Load Test Results

On August 14 1997, prior to the opening of the bridge to traffic, two loaded trucks weighing 357 kN each were used to examine nine different load cases. Six of the load cases were static tests in which the two trucks were parked adjacent to each other. During the other three tests, only one truck was used for loading the bridge. Five points along each girder in the north span were monitored for deflection. Therefore, 25 girder deflection points were monitored during the test in total. The maximum measured downward deflection in the north span was 17 mm for the load case where the trucks were placed adjaeent to each other in the north span. However, when the loaded trucks were placed in the middle span, the maximum upward deflection in the north span was 7 mm. Despite the symmetrical loading of the bridge, Girder 1 exhibited the highest amount of deflection and Girder 4 exhibited the least amount of deflection.

Strain gauge readings were also obtained during the static load tests. These readings were used to find the stain distribution in the girder cross sections, the location of the neutral axis in the girders, assess the load sharing between girders, and compare the analysis results with the field test results. These results also contributed to the base structural characteristics of the bridge for future studies. Concrete strains measured were too small to be used for analysis.

Girder 1 strain gauge measurements in the positive moment region indicated that the girder response was linear and within the elastic range. The neutral axis was found to be 54.1 mm below the bottom face of the top flange in the girder web. The maximum measured tensile strain was 103 με at strain gauge location G3. In the negative moment region, the maximum projected compressive strain was 30.7 με in the top flange of the girder. In the negative moment region, the neutral axis was found to be 120 mm below the bottom face of the top flange. The change in location of the neutral axis between the positive and negative moment regions indicates the change in composite action of the member. Girder strains in the negative moment region were nearly identical; indicating that the diaphragm was very effective in girder load distribution over the pier.

Strains measured in the steel tension straps were relatively small and were below 40 με. Since no longitudinal cracks were visible, it was concluded from the 1997 test results that beam action was the primary mode for shear transfer in the transverse direction of the concrete deck.

4.2.3 1997 Dynamic Load Test Results

On October 27, 1997, dynamic measurements were obtained using a high-speed data acquisition unit. Data was scanned at a rate of 1000 Hz and electronic low-pass filters in the data acquisition unit were set at 10 kHz. Although the response of the bridge under car traffic was insignificant, the dynamic response of the bridge after the passing of a truck was recorded and analyzed. Videotape of the passing trucks was used to identify type of truck, number of axles, and passing lane.

A significant amount of electromagnetic noise had to be filtered out using commercially available software before the data could be used. An influence line was plotted to determine the response of strain gauge G3 during truck loading. From the peaks in this plot, the number of truck axles could easily be identified. Similar to the static tests, concrete strains during the dynamic tests were insignificant. Measured strains from the dynamic tests were small; strains in the T2/T3 and G3 were less than 20 με and 50 με respectively.

At the time of testing in 1997, the low strains experienced in the concrete deck and steel straps proved the bridge behaved as an uncracked composite structure. At the time of these tests, it was predicted that the behaviour of the structure would change as a result of increase cracking of the concrete due to shrinkage, thermal effects, and repeated loading.

4.2.4 1997 Crack Mapping

Crack patterns of the underside of the bridge deck were mapped out for the first time in August 1997. No longitudinal cracks were detected at this time in any of the spans. The south span, which consists of both GFRP and internal steel reinforcement, had a few transverse cracks that were less than 0.5 mm in width. The majority of these transverse cracks were located near Pier 2. The middle span is partially reinforced with GFRP bars without any internal steel reinforcement. More transverse cracks were present in this span compared to the other two spans. The north span is partially reinforced with GFRP bars in the cantilever edges only. This span contained the least amount of transverse cracks compared to the other two spans. These cracks were also approximately 0.5 mm wide.

4.2.5 1997 Temperature Tests

Afternoon temperature readings were obtained on September 25 and 26, 1997 to determine the significance of the restrained thermal effects. No traffic was present on the bridge during the tests. It was determined that temperature effects produced the most significant strains in the bridge. Strains for only a 13°C increase in air temperature were

comparable to the strains produced by the loaded trucks in the static tests. During these sets of tests, the readings of the two fibre optic sensors were also determined to be reasonable.

4.3 Summary of 1998 Bridge Tests

4.3.1 1998 Ambient Vibration Test Results

In August 1998, the second set of ambient vibration tests were completed by a research team from the University of Alberta. During the tests, one lane was permanently closed while the other lane was closed only when data was being accumulated. Ten individual tests were completed using 4 accelerometers placed at various locations to capture the natural frequencies and mode shapes. Each test lasted for 200 seconds. Eight of the tests were used to capture vertical mode shapes and two of the tests captured transverse mode shapes. Accelerometers were monitored using LabVIEW and a high-speed data acquisition system was used to obtain and store the raw data at 200 Hz.

Table 4.3 summarizes the eight natural frequencies captured under 10 Hz and the corresponding mode shapes. All of the natural frequencies and mode shapes investigated in 1998 exhibited good correlation between field and theoretical results. Compared to the UBC ambient vibration results, all of the natural frequencies were approximately 0.20 Hz lower in 1998. These results indicated that the stiffness of the bridge might have been reduced after one year of service.

Table 4.3 - 1998 Natural Frequencies and Mode Shapes

Mode	Frequency	Description
1	2.60 Hz	1st Fundamental Vertical Mode
2	2.90 Hz	1st Fundamental Torsional Mode
3	3.63 Hz	2nd Vertical Mode
4	3.85 Hz	2nd Torsional Mode
5	4.43 Hz	3rd Vertical Mode
6	5.00 Hz	3rd Torsional Mode
7	6.85 Hz	4th Torsional Mode
8	8.60 Hz	4th Vertical Mode

4.3.2 1998 Static Load Test Results

For the static load tests in 1998 one truck, with a loaded weight of 395 kN, was used. The data acquisition unit used for these tests was able to monitor 35 strain gauges simultaneously. Static load tests had to be repeated three times since the strain gauges were divided into three sets. Due to time limitations, however, the loading truck could not be positioned at every load point. The behaviour of the bridge was monitored as the truckload was positioned over 28 various load points along the bridge deck. In addition, ten cable transducers were positioned under the bridge deck to measure the vertical deflection of the girders.

Based on the deflection results, load sharing between the five girders was approximately linear. A load positioned on one side of the bridge was distributed proportionately to the other girders depending on the girder distance relative to the wheel load. Good load sharing was evident between the girders as a result of a relatively stiff deck in the transverse direction. The maximum deflection under Girder 1 was 10.3 mm downward when the truck front axle was located 15.9 m from the north abutment.

Significant conclusions were also obtained from the strain results. For example, the gauges located on Steel Strap 8 indicated the strain of the strap cycled between –15 με and 85 με as the loading truck travelled across the entire length of the bridge. The relatively low strain cycle indicated that the steel straps behaved well within the elastic range and fatigue was not critical during service loading. However, these measured strains had almost doubled compared to strains produced under similar loading in 1997. With the existence of longitudinal cracks in the deck, it was concluded that the contribution of tensile concrete in transferring shear had reduced after a year of operation.

Strains in all of the girders were also well within the elastic range and a linear strain distribution in the cross section of each girder was evident from the strain results. The maximum recorded strain for the bottom flange of Girder 1 was 104 με. Within the positive moment region of Girder 1, the neutral axis location was calculated to be 52 mm below the bottom face of the top flange; this was nearly identical to the 1997 strain results. However, in the negative moment region of Girder 1, the neutral axis shifted 70 mm downward. This result suggested a partial loss of composite action in the negative moment region.

Based on the 1998 static load field tests several overall conclusions were made. Load sharing and load redistribution by the diaphragm over pier was shown to be effective. Compared to the 1997 results, the strains in the steel straps had increased, indicating that the contribution of concrete in transferring shear had reduced. At the time of these field tests, composite action between the concrete deck and steel girders remained the same in the longitudinal direction in the positive moment region. Finally, simple beam analysis suggested the bridge stiffness had reduced approx. 3.5% from 1997 to 1998.

4.3.3 1998 Dynamic Load Test Results

Before the controlled dynamic load tests were performed, dynamic measurements from random traffic flow were also measured. The primary purpose for these tests were to ensure that the field instrumentation mounted on the bridge was still in good operating

condition. It was determined, however, that the bridge instrumentation had withstood the first winter.

The same 395 kN truck that was used for the static load test was used in the controlled dynamic load tests. Bridge dynamic behaviour under speeds of 15, 30, 40, and 55 km/hr were investigated. Temperature effects were neglected as each test lasted for a maximum of 30 seconds. As the truck passed over the deck, the bridge was excited at a frequency of 3.5 Hz, its second vertical mode shape. From the collected data, several dynamic characteristics were calculated. From the decay of free vibration motion, the damping ratio was estimated to be 1.20 %. The dynamic amplification factor was calculated to be 1.08 based on the overall deflection component and 1.15 based on the local strain component. It was also determined that the dynamic amplification factor varied nonlinearly with respect to the vehicle speed. Overall, the bridge did not deflect more under dynamic loading compared to static loading. Rather, the increased impact loading was absorbed in the torsional mode of the bridge deck.

4.3.4 1998 Crack Mapping

The location and sizes of cracks on the underside of the bridge were documented again in August 1998. It was found that after a year of operation, existing cracks documented in 1997 had increased to approximately twice their size in width. Water stain marks were also evident near the year-old deck cracks. A significant number of new transverse cracks had also formed. In addition, several longitudinal cracks had formed in the negative moment regions of the bridge deck. Several longitudinal cracks had formed at the transition between the flat and tapered parts on the underside of the bridge deck. Most of these new cracks that had formed within the first year of service were less than 0.5 mm in width. In 1998, cracks visible on the bottom surface of the bridge deck were not a serious concern from a serviceability viewpoint. Figures comparing the location and propagation of cracks during the seven-year service life of the bridge will be shown in another section.

4.4 Results of 2004 Tests

4.4.1 Introduction

In early June 2004, static and dynamic load tests, ambient vibration tests, and crack mapping were completed. This was seven years after the Crowchild Trail Bridge deck was built in 1997. Aside from crack mapping completed in 1999 and 2002, these were the first complete sets of tests conducted since August of 1998.

Table 4.4 summarizes the tests and measurements performed on the Crowchild Trail Bridge in the spring of 2004. Preliminary field tests were performed on May 31 2004 to ensure that the data acquisition equipment worked properly and that the strain sensors and connected wiring were also in acceptable working condition.

Table 4.4 - Summary of 2004 Crowchild Trail Bridge Tests

Date	Test	Measurements
May 31, 2004	Preliminary Field Tests Crack Mapping	Behaviour under normal traffic loading; size and location of new cracks since 2002.
June 6, 2004	Static and Dynamic Load Tests	Strains in several bridge components; Girder deflections
June 19, 2004	Ambient Vibration Tests	Natural Frequencies Mode shapes

As seen in Table 4.4, several strain and deflection data sets were collected during the preliminary tests. These results would be used to understand bridge behaviour under normal traffic loading conditions. Locations and sizes of new cracks in the underside of the concrete bridge deck were also observed and recorded. Drawings with cracks up to 2002 were updated with the new cracks that had formed. On June 6 2004 static and dynamic load tests were completed. A loaded truck was used to induce bridge strains and deflections. The static and dynamic load tests were similar to tests performed in 1998 so

that the results could be compared and any changes in bridge behaviour could be identified. Due to rain during the load tests, ambient vibration tests were completed two weeks later on June 19 2004.

4.4.2 2004 Preliminary Bridge Tests

4.4.2.1 Preliminary Test Methodology

Preliminary field tests and crack mapping were completed on Monday, May 31 2004, approximately one week before the loading tests. A field team from the UofA arrived at the Crowchild Trail Bridge site at 11:00 AM. Data Acquisition set-up and testing lasted for approximately six hours. The main purpose for these tests was to ensure that the data acquisition and bridge sensors were working properly. Malfunctioning wires or strain gauges could also be identified. In addition, data was collected from the bridge during normal traffic loading. This data primarily consisted of bridge strains and girder deflections while heavier trucks traveled across the bridge deck.

The junction box and wire connectors inside were in excellent condition even after seven years since their initial installation. Based on the information required, data was collected from only 72 of the total 108 strain gauges. Since the data acquisition system could only collect data from 24 strain channels at a time, the strain gauges were divided into three groups. During each test, data from one set of strain gauges was collected at a time. Table 4.5 lists the three separate sets (A,B,C) of gauges used in the preliminary tests. G-series strain gauges are located on the webs and flanges of the steel plate girders, T-series strain gauges are located on the steel tension straps, RC-series strain gauges are located on GFRP bars, E-series strain gauges are embedded in the concrete deck, S-series strain gauges are located on the shear studs, C-series gauges are located on the cross frames, and RS-series strain gauges are located on the smart bars. During the tests, measurements from five strain gauges G31-G34, T8, E2, E4, and RS3 were found to be unreliable and the data collected from these gauges was disregarded.

Table 4.5 - Strain Gauge List for Preliminary Test

DAQ Channel	SET A		SET B		SET C	
0	G1	CABLE 1	G23	CABLE 3	E2	CABLE 7
1	G2		G24		E3	
2	G3		G25		E4	
3	G4		G26		E5	
4	G5		G27		E7	
5	G6		G28		E8	
6	G7		G29		E9	
7	G8		G30		E10	
8	G9		G31		E11	
9	G10		G32		E12	
10	G11		G33		E13	
11	G12	CABLE 2	T1	CABLE 4	S1	CABLE 9
12	G13		T2		S2	
13	G14		T3		S3	
14	G15		T4		S4	
15	G16		T5		S5	
16	G17		T6		S6	
17	G18		T7		C1	
18	G19		T8		C2	
19	G20		T9		C3	
20	G21		T10		C4	
21	G22		T11		RS1	
22	G34	CABLE 10	RC1	CABLE 11	RS2	CABLE 12
23	T4		RC2		RS3	

Once the computer was set-up, several sets of data were obtained under normal traffic loading conditions. First, three sets of random data were collected during normal traffic

loading conditions. An initial test, consisting of three stages of data collection, was completed where only five deflection cable transducers and gauges in SET A were connected to the data acquisition system. During this period of data collection, care was not exercised to ensure that a truck was crossing the bridge. This initial test ensured that the data acquisition system was properly obtaining and recording data.

Next, strain gauge data was collected from the bridge when heavier trucks were present. Special care was taken to collect data as a truck would approach the bridge deck, while a truck was on a bridge, and a brief period when the truck was off the bridge. A typical truck crossing can be seen in Figure 4.1. While SET A strain gauges were still

Figure 4.1 - Preliminary Tests: Typical Truck Loading

connected to the data acquisition, five additional files of data were obtained for five different trucks. Next, four data files were obtained for SET B strain gauges. Finally, four data files were obtained for SET C strain gauges during four different truck loadings.

In the following sections, the results of the preliminary tests are summarized. These results include maximum strains, influence lines, and girder strain profiles.

4.4.2.2 Preliminary Test Results

One of the main factors in bridge behaviour is the ambient bridge temperature. Table 4.6 shows the recorded temperature and humidity at various times during data collection of the preliminary tests. An electronic temperature device was used to record the

Table 4.6 - Recorded Temperature During 2004 Preliminary Load Tests

Time	Temperature	Relative Humidity
12:10 PM	16°C	32 %
1:35 PM	17°C	27 %
2:30 PM	19°C	26 %

temperature and relative humidity. It is important to note that temperature device was located in the shade under the bridge deck near the data acquisition equipment.

Table 4.7 summarizes the maximum and minimum strains experienced by each type of strain gauge. Positive strains indicate tensile stresses and negative strains indicate compressive stresses. Also, the maximum strain range is summarized.

Table 4.7 - Preliminary Test Maximum Strain Results

SET	Gauge Type/Location	Max Strain (με)	Min Strain (με)	Strain Range (με)
SET A	G3 – Girder 1 web	82.6	-32.4	115.0
SET A	G34 – Girder 1 flange	95.1	-37.7	132.8
SET B	T3 – Steel Strap 8	36.7	-6.6	43.2
SET B	RC1 – GFRP bar	21.4	-5.2	26.6
SET C	E13 – Concrete deck	3.0	-4.2	7.2
SET C	S4 – Steel stud	2.0	-1.9	3.9
SET C	C4 – Cross frame	3.9	-17.4	21.3
SET C	RS2 – Smart bar	5.6	-1.2	6.8

From Table 4.7, it is noted that all of the strains measured were well within the elastic strain range under normal traffic loading. It is important to note that data from SET A, SET B, and SET C strain gauges were all taken at different truck loadings. Therefore it is not possible to compare strains between sets due to the possible differences in truck loadings. For example the strain range for SET C C4 was 21.3 με, however, if this gauge were loaded under a SET A or B truck, the strain would be slightly different.

The maximum girder strains were located in Girder 1 directly below the west lane where the majority of heavy traffic traveled. The maximum girder strain recorded was 95.1 με at strain gauge G34. This was expected as this particular gauge is located on the flange of Girder 1. The maximum strain recorded in the steel straps was 36.7 με in T3. Strains in the concrete deck and steel studs were very small and insignificant. All of these relatively low strains in the bridge structural components indicate that the bridge is behaving well within a satisfactory safety range.

Only dynamic readings of the strain gauges were taken during the preliminary tests; no static strain gauge readings were obtained. During the preliminary testing, no time stamp was applied to the data; therefore, all of the following figures do not indicate an exact time along the main x-axis. Figure 4.2 shows the typical dynamic response of strain gauges as a truck passes over the bridge. All of the four gauges shown in Figure 4.2 are located on Girder 1 near the middle of the north span. Strain gauges G1, G2, and G3 are located at various heights on the girder web while G34 is located on the bottom girder flange. As shown in the figure, the strain gauges situated lower on the girder experience the highest levels of strain. When the truck is located on the north span, the girder is in positive bending, and the girder strain gauges experience positive tensile stresses. However, as the truck moves over the first pier into the middle span, the girder experiences negative bending upward and the strain gauges experience negative compression stresses. Strains are relatively low once the truck moves onto the south span. Upon closer inspection of the strain readings, it is evident that three smaller peaks

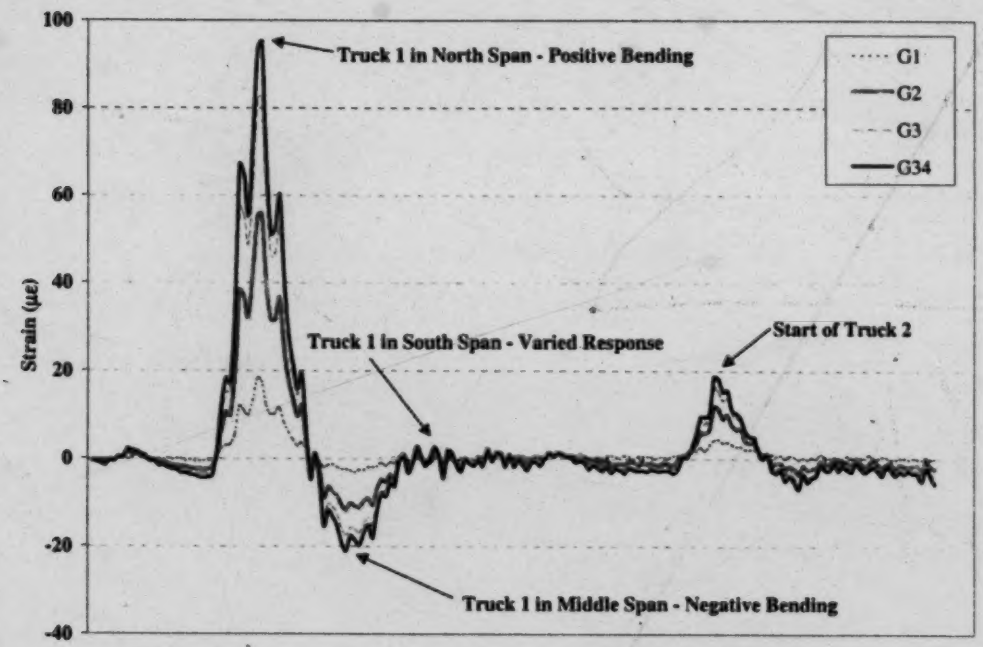

Figure 4.2 - Bridge Dynamic Behaviour: SET A Girder Strain Gauges

are within the main positive moment response. These smaller peaks indicate the exact time of individual truck axles passing over the area. The strain effects of another lighter truck can be seen near the end of the data set with similar behaviour as the first truck.

Figure 4.3 shows the linear cross section strain distribution for the plate girder during the preliminary test in the positive moment region. The strains shown were recorded at the same time instant as when the maximum strain of 95.1 με was experienced in the lower flange of the plate girder. Gauges G31 and G32 were not included in SET A and therefore the strain distribution for this cross-section is incomplete. During the full tests on June 6, the order of the channels was changed so that all of the strain gauges in this section were included in SET A. Although strain gauge G34 was believed to give unreliable results in earlier tests, the readings obtained appear to be very reasonable during the preliminary tests.

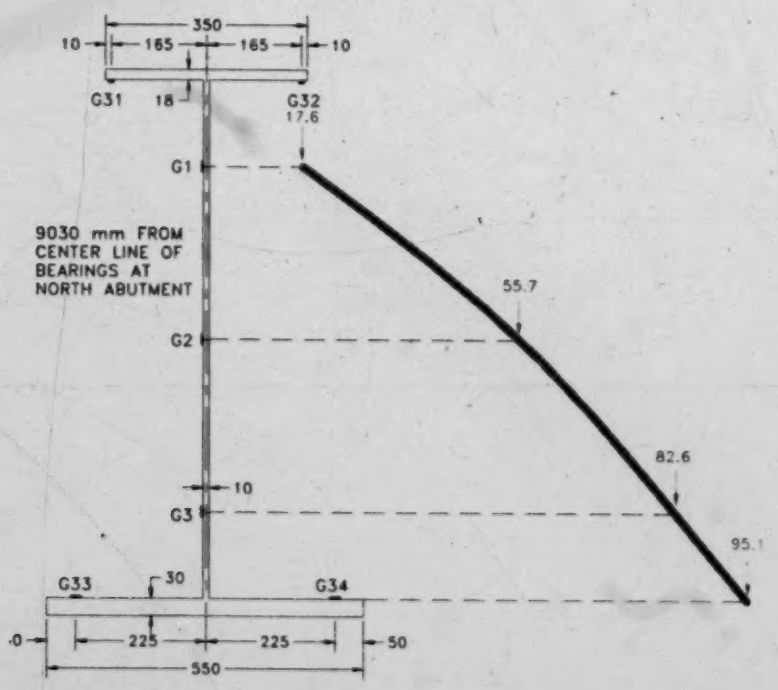

Figure 4.3 – 2004 Preliminary Tests: Strain Distribution in Positive Moment Region

4.4.3 2004 Ambient Vibration Tests

4.4.3.1 Ambient Vibration Test Methodology

Ambient vibration tests were completed on Saturday, June 19 2004. Testing began shortly after 10:00 AM and lasted for approximately three and a half hours until 1:30 PM. Accelerometers used for the ambient vibration tests were set-up in several locations to record all of the bridge natural frequencies and mode shapes. After the bridge tests were completed in 1998, it was recommended then to modify the locations of some of the accelerometers in order to better capture the transverse mode shapes of the bridge. This recommended accelerometer layout was implemented for the tests and is shown in Figure 4.4. To capture all of the desired mode shapes with only four accelerometers, twelve different set-ups were required. With this set-up, as seen in Figure 4.4, the transverse mode shapes in each span can be quantified by having an accelerometer located above each of the five girders across the width of the bridge. Accelerometers used to capture the longitudinal mode shapes were spaced four meters apart along Girder 1, the western most girder. A reference accelerometer was set-up in the middle span over Girder 1, as indicated by Setup 7. This reference accelerometer remained in the same location for the duration of all the tests. All other bridge movements recorded were normalized relative to the movement at the reference location. In addition, the reference accelerometer was used to correlate all of the different sets of tests for phase analysis to identify the mode shapes.

During the test set-up, one lane of traffic on the Crowchild Trail Bridge was continuously closed to traffic and the second lane was periodically open to allow traffic to pass through. When the accelerometers were in place and vibration data was being collected no vehicular traffic was permitted on the bridge. This process would allow the bridge and its vibrational modes to become excited by external ambient sources only. Accelerometers were attached to the concrete deck surface using two-way heavy-duty carpet tape. For each accelerometer set-up, data was collected for a total of 90 seconds at a scan rate of 200 Hz.

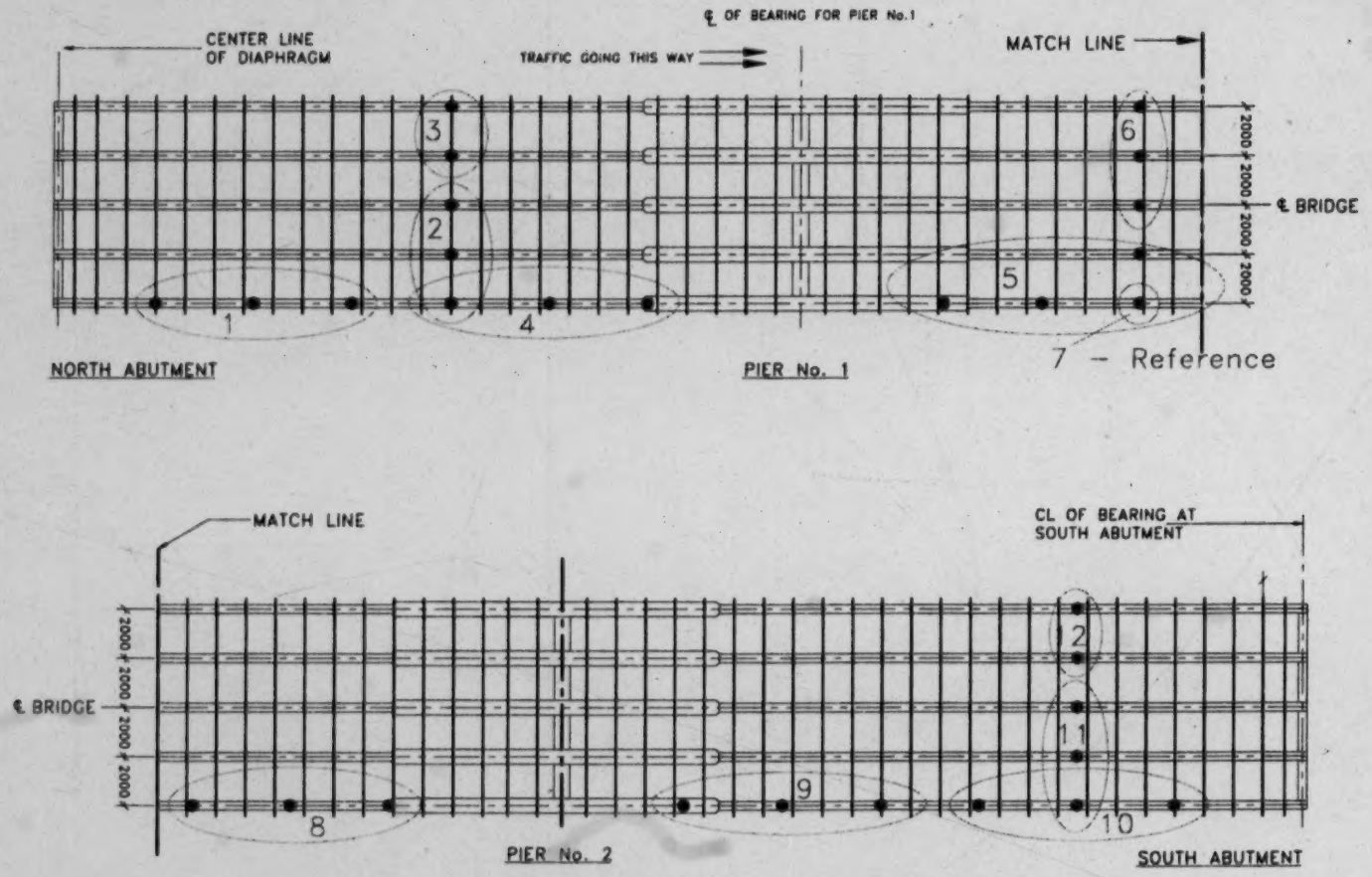

Figure 4.4 – 2004 Ambient Vibration Tests: Accelerometer Locations

During the testing, it appeared that the results from the Type 4370 accelerometers might not have been entirely reliable. Therefore, a second set of tests was completed by placing the Type 8306 accelerometers at all of the bridge locations where Type 4370 accelerometers had been used previously. The first set of tests will be referred to as the regular test set-ups and the second set of tests will be referred to as the repeat test set-ups.

The raw data files were filtered in order to separate all of the individual mode shapes. In its initial form, the raw data is in the time domain with the time in seconds along the X-axis and the magnitude in mV along the Y-axis. To determine the natural frequencies, the power spectrum was computed using a Labview program that applied Fast Fourier Transform to the raw data. The power spectrum consists of natural frequency values on the X-axis and amplitude in $[mV]^2$ along the Y-axis. Peaks on this plot indicate natural frequencies of the bridge. To determine the mode shapes, a band-pass filter was used to isolate each particular frequency. Plots obtained from this filtering procedure were also in the time domain with the time in seconds along the X-axis and the amplitude in mV along the Y-axis. The movements of the accelerometers relative to the reference location were used to obtain the mode shapes.

For most of the day, the weather was warm and sunny. Table 4.8 shows the recorded temperature during the morning of the ambient vibration tests. The electronic

Table 4.8 - Recorded Temperature During 2004 Vibration Tests

Time	Temperature	Relative Humidity
10:15 AM	17°C	35 %
11:17 AM	19°C	32 %
11:46 AM	20°C	27 %

temperature device that was used was placed in the shade on the bridge deck. Temperatures recorded on the bridge deck in direct sunlight were found to be about 10 to 20 degrees higher compared to temperatures measured in the shade.

In the following sections, the natural frequencies from the Crowchild Trail Bridge are summarized in addition to the corresponding mode shapes.

4.4.3.2 Natural Frequency Results

The natural frequencies found from the test results are shown in Table 4.9. Several methods were used to calculate the natural frequencies. First, natural frequencies were calculated for each accelerometer at each placement. Depending on the placement of the

Table 4.9 - 2004 Crowchild Trail Bridge Natural Frequencies

Mode	Frequency	Description
1	2.80 Hz	1st Fundamental Vertical Mode
2	3.16 Hz	1st Fundamental Torsional Mode
3	3.78 Hz	2nd Vertical Mode
4	4.19 Hz	2nd Torsional Mode
5	4.66 Hz	3rd Vertical Mode
6	5.36 Hz	3rd Torsional Mode
7	6.89 Hz	4th Torsional Mode
8	8.29 Hz	4th Vertical Mode

accelerometer, some frequencies were more dominant than others. For example, an accelerometer placement in the transverse direction would tend to be more influenced by transverse modes. By looking at the natural frequencies for each placement, trends could be identified for the overall bridge behaviour.

Summing the power spectrum results from each individual accelerometer test set-up also identified natural frequencies. By summing all the results, the natural frequencies of the bridge were more easily identified. Figure 4.5 graphs the sum of the power spectrum results of the two 8306 accelerometers. Figure 4.5 contains the results from all of the test

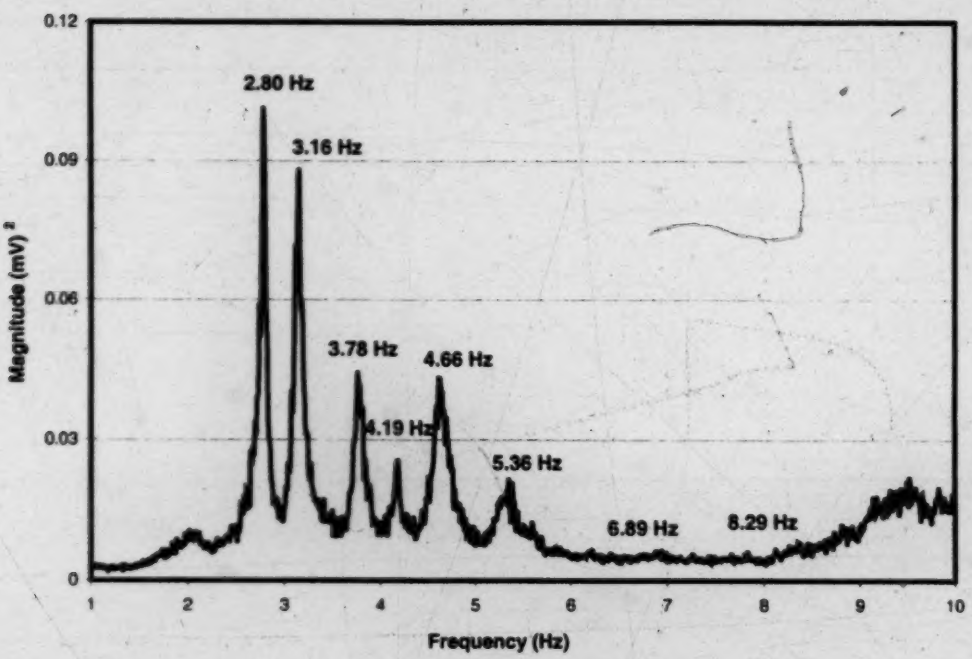

Figure 4.5 - Power Spectrum Results: 2004 Crowchild Trail Bridge Natural Frequencies

set-ups including the regular test set-ups and repeat tests set-ups. The dominant peaks in the plots represent the bridge natural frequencies. These are the frequencies that are experienced by the bridge most frequently and are captured by the accelerometers. The first six natural frequencies are the most easily identified by sharp, distinct peaks in the graphs. However, the last two natural frequencies of 6.89 Hz and 8.29 Hz are not as clear and distinct compared to the first six natural frequencies.

Natural frequencies most exemplified in the north, middle and south spans were also analyzed. Figures 4.6, 4.7, and 4.8 show the sum of power spectrum results from the Type 8306 accelerometer that was repositioned for every test. Power spectrum results from the reference accelerometer were not included in these graphs. Figure 4.6 sums all of the power spectrum results from the Type 8306 accelerometer set-ups in the north span. Similarly, Figure 4.7 sums the entire power spectrum results from the Type 8306 accelerometer set-ups in the middle span, not including the results from the reference

accelerometer. Finally, Figure 4.8 sums all of the power spectrum results from the Type 8306 accelerometer set-ups in the south span.

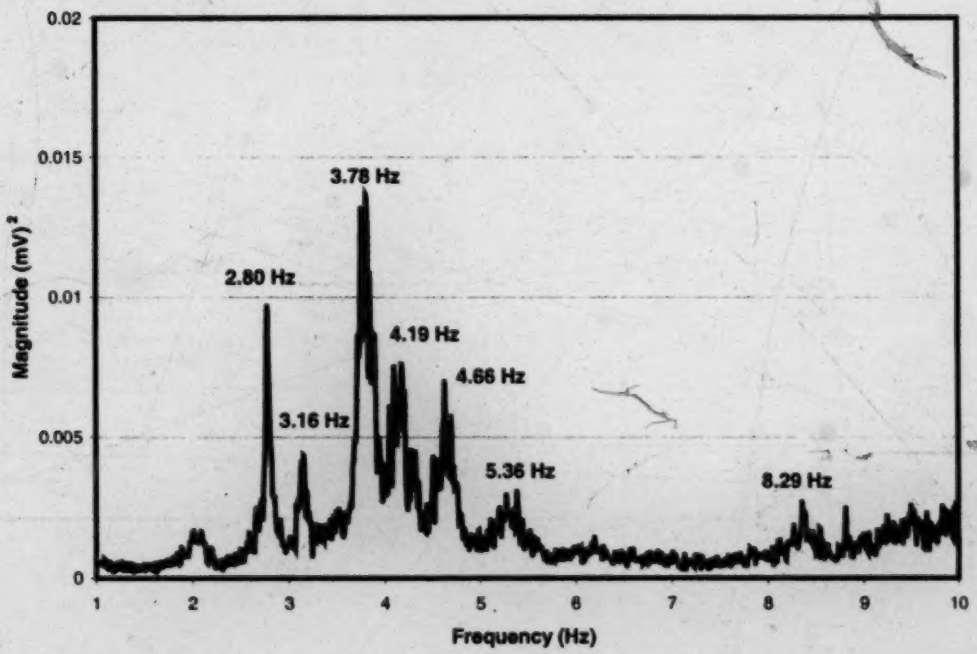

Figure 4.6 - North Span: Sum of 8306 Accelerometer Power Spectrums

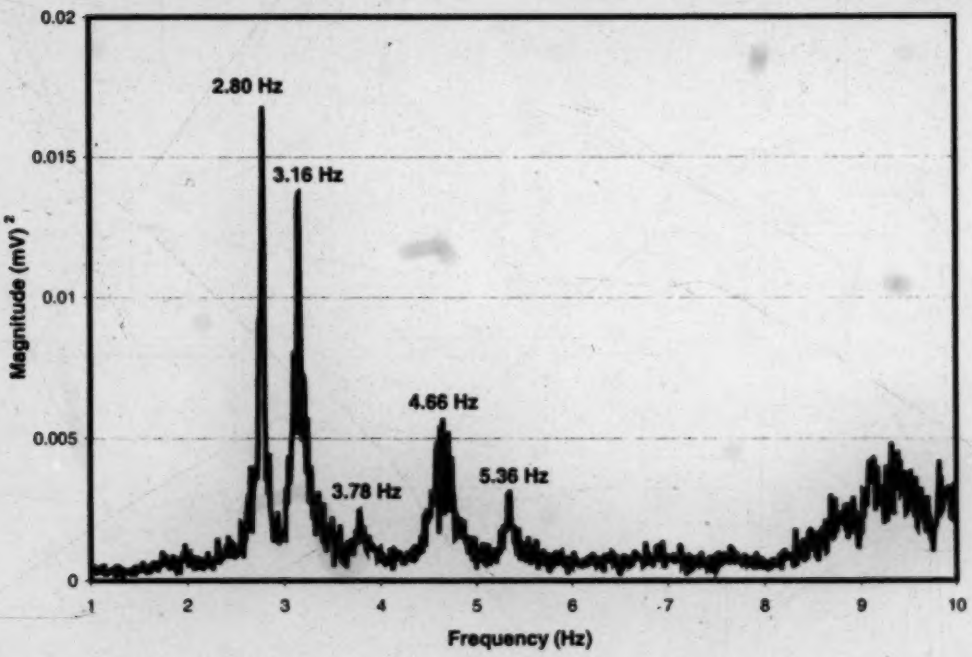

Figure 4.7- Middle Span: Sum of 8306 Accelerometer Power Spectrums

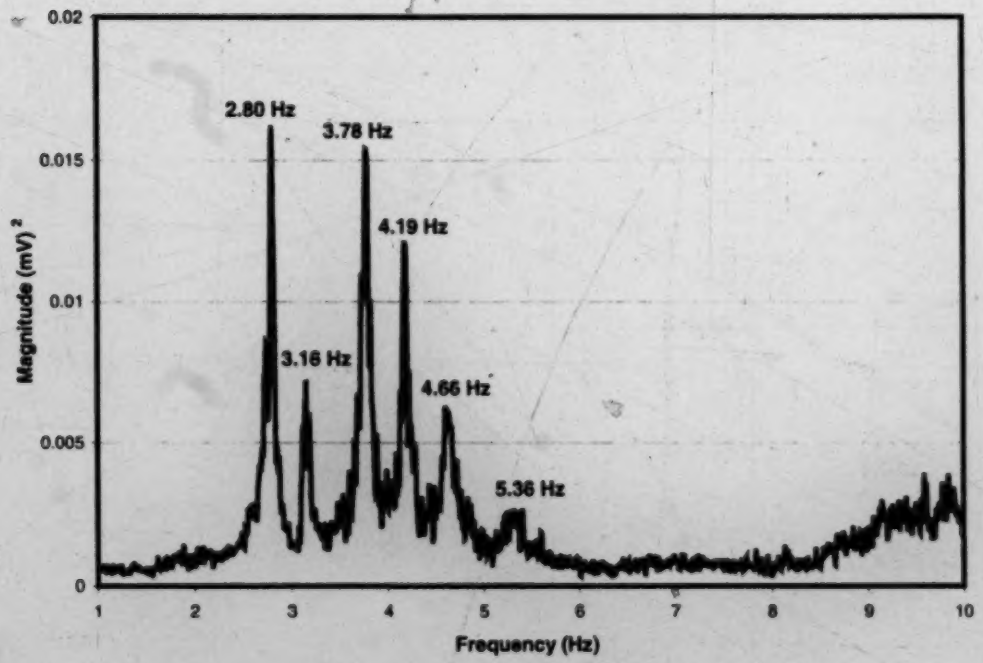

Figure 4.8 - South Span: Sum of 8306 Accelerometer Power Spectrums

Most of the bridge natural frequencies can be identified in the north span; however, the 6.89 Hz frequency is not evident. In this span, the first three vertical frequencies/mode shapes are more predominant compared to the first three torsional frequencies/mode shapes. Only five of the first eight natural frequencies are clearly evident in the middle span. The 4.19 Hz frequency and the seventh and eighth frequencies are not evident from the middle span power spectrum results. Also, the first two natural frequencies at 2.80 Hz and 3.16 Hz are significantly more predominant compared to the other natural frequencies shown in the power spectrum. In the south span power spectrum the first six natural frequencies are clearly evident. Similar to the north span, the first three vertical frequencies/mode shapes are more predominant relative to the first three torsional frequencies/mode shapes. The last two natural frequencies are not evident from the power spectrum results of the south span.

4.4.3.3 Mode Shape Results

Mode shapes of the bridge deck were also identified. In order to create the mode shapes, all of the recorded accelerometer movements were normalized relative to the reference accelerometer. After this step the magnitudes were further modified so that the maximum normalized amplitude in any of the spans had a value of 1.0 for each mode shape. Therefore, the average normalized amplitudes of other bridge deck locations are less than 1.0. The eight mode shapes corresponding to the eight natural frequencies are shown in Figures 4.9, 4.10, 4.11, and 4.12. Both three-dimensional isometric views and the west elevation views of each mode shape are shown in the figures. In each figure, the horizontal axis is the distance in meters from the north abutment. The vertical axis is the average normalized magnitude of excitation for each mode shape.

The mode shapes shown in the figures were obtained from the accelerometers placed along Girder 1. Each figure contains two mode shapes: a vertical mode shape and a torsional mode shape. Vertical and torsional mode shapes plotted in the same figure are nearly identical in shape. Looking at the mode shapes in the transverse direction identified the two types of mode shapes. If the mode shape in the transverse direction was near horizontal, it was considered to be a vertical mode shape. This indicates that

neighbouring girders vibrate in phase with each other, thus producing 3D vertical mode shapes as seen in the figures. However, if the mode shape direction was not horizontal, then it was considered to be a torsional mode shape. This indicates that neighbouring girders vibrate out of phase relative to each other, thus producing 3D torsional mode shapes as seen in the figures.

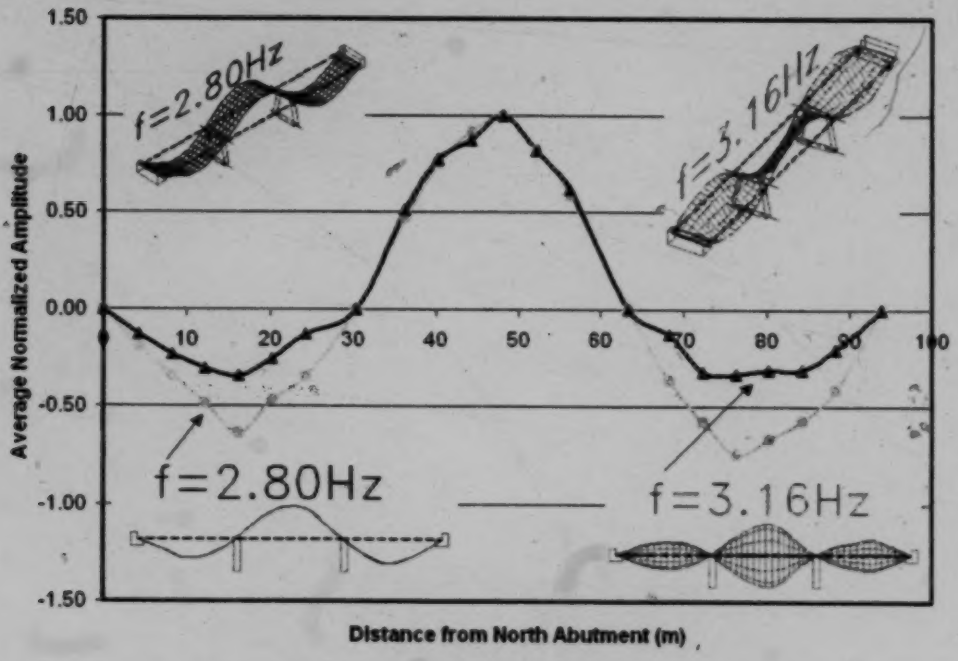

Figure 4.9 - First Vertical and Torsional Mode Shapes

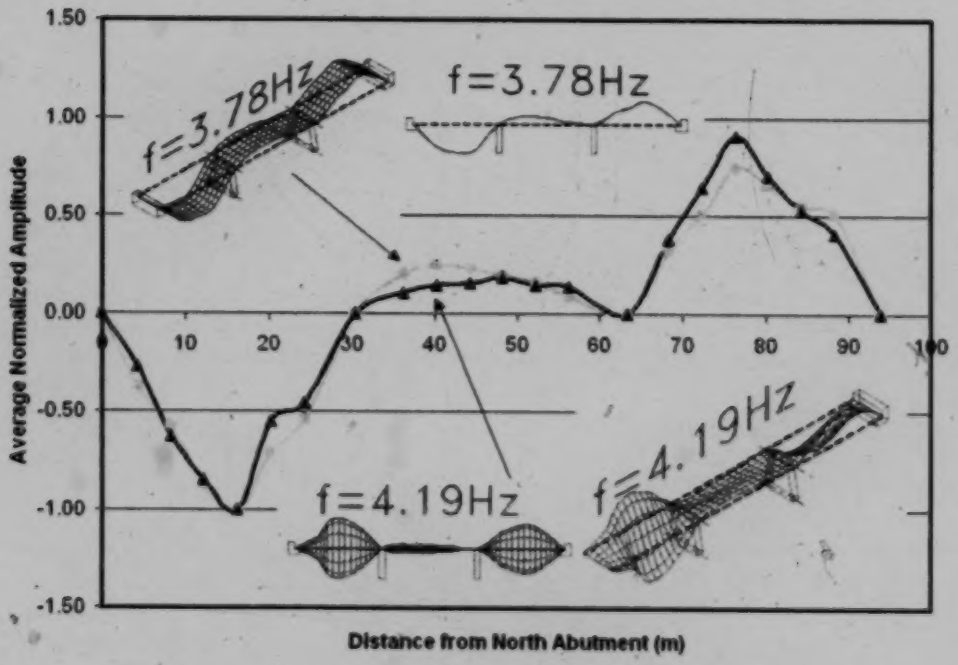

Figure 4.10 - Second Vertical and Torsional Mode Shapes

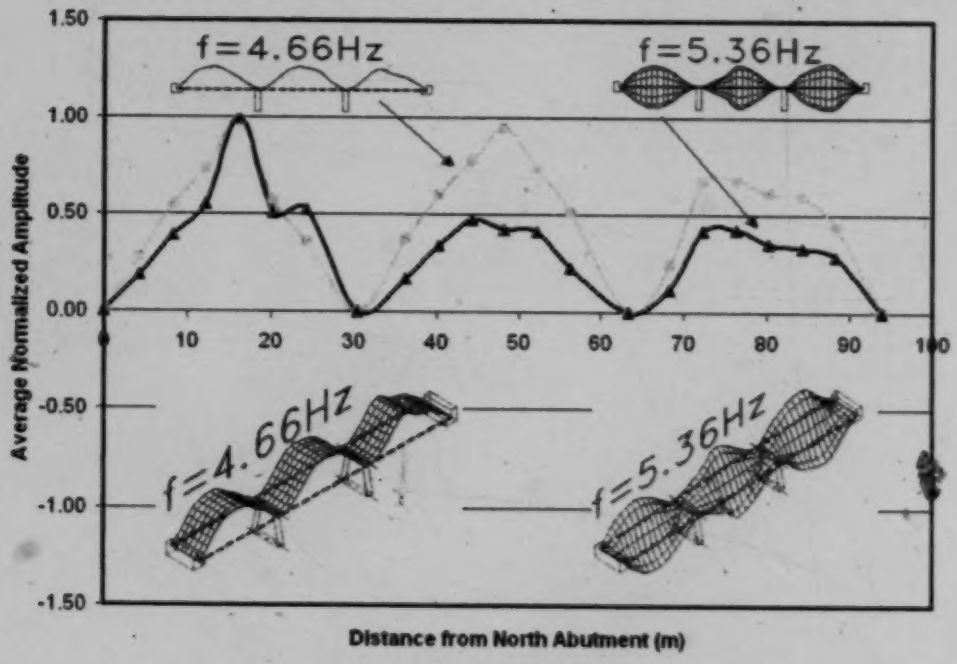

Figure 4.11 - Third Vertical and Torsional Mode Shapes

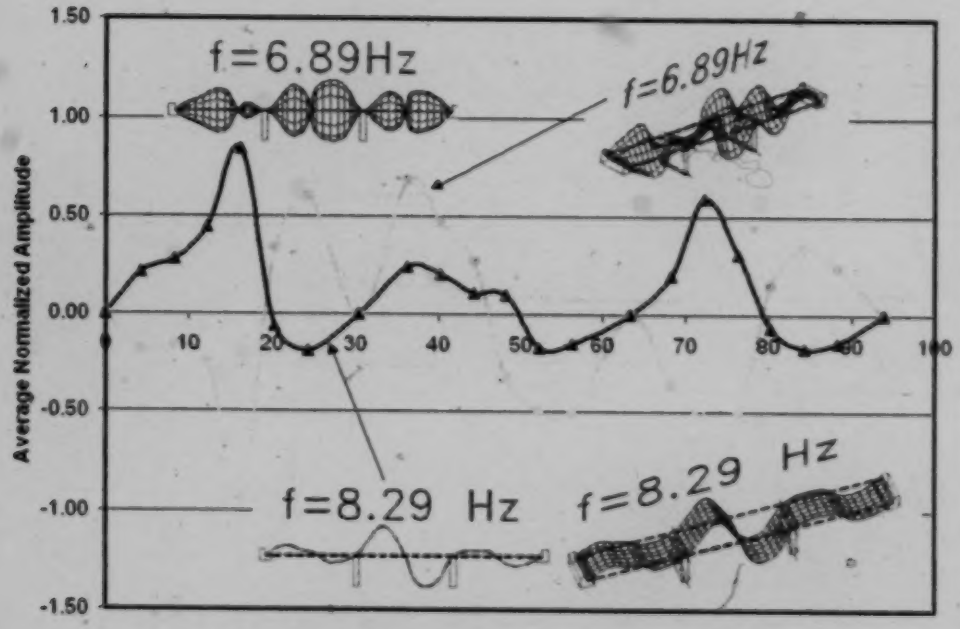

Figure 4.12 - Fourth Vertical and Torsional Mode Shapes

4.4.4 2004 Static and Dynamic Load Tests

4.4.4.1 Loading Test Methodology

Static load tests were completed on Sunday, June 6 2004. Testing set-up began at approximately 6:30 AM. The City of Calgary provided an electrical generator, a ladder, and traffic control. Similar to the ambient vibration tests, the west-facing traffic lane was completely closed for the duration of the tests and the east-facing lane was open intermittently between tests when data was not being collected. Pavement markings were laid out to indicate static load points as shown in Figure 4.13. However, before the individual load points were marked out on the bridge deck, the location of both bridge piers was determined. The location of both piers was measured

Figure 4.13 - Static Load Point Location Markings

from both the north and south abutments. Once these benchmark locations were determined, the actual loading points were marked. Figure 4.14 indicates the static load point locations on a plan view of the Crowchild Trail Bridge Deck. The front passenger-side truck axle would be positioned above these points. As seen in Figure 4.14, all of the

static loading points were located exactly midway between Girder 1 and Girder 2. This location was chosen to investigate load sharing between girders in addition to other bridge properties. For comparison with previous static loading results, the load point location numbers were left the same. As indicated in Figure 4.14, some of the loading points were omitted in order to save time during field testing.

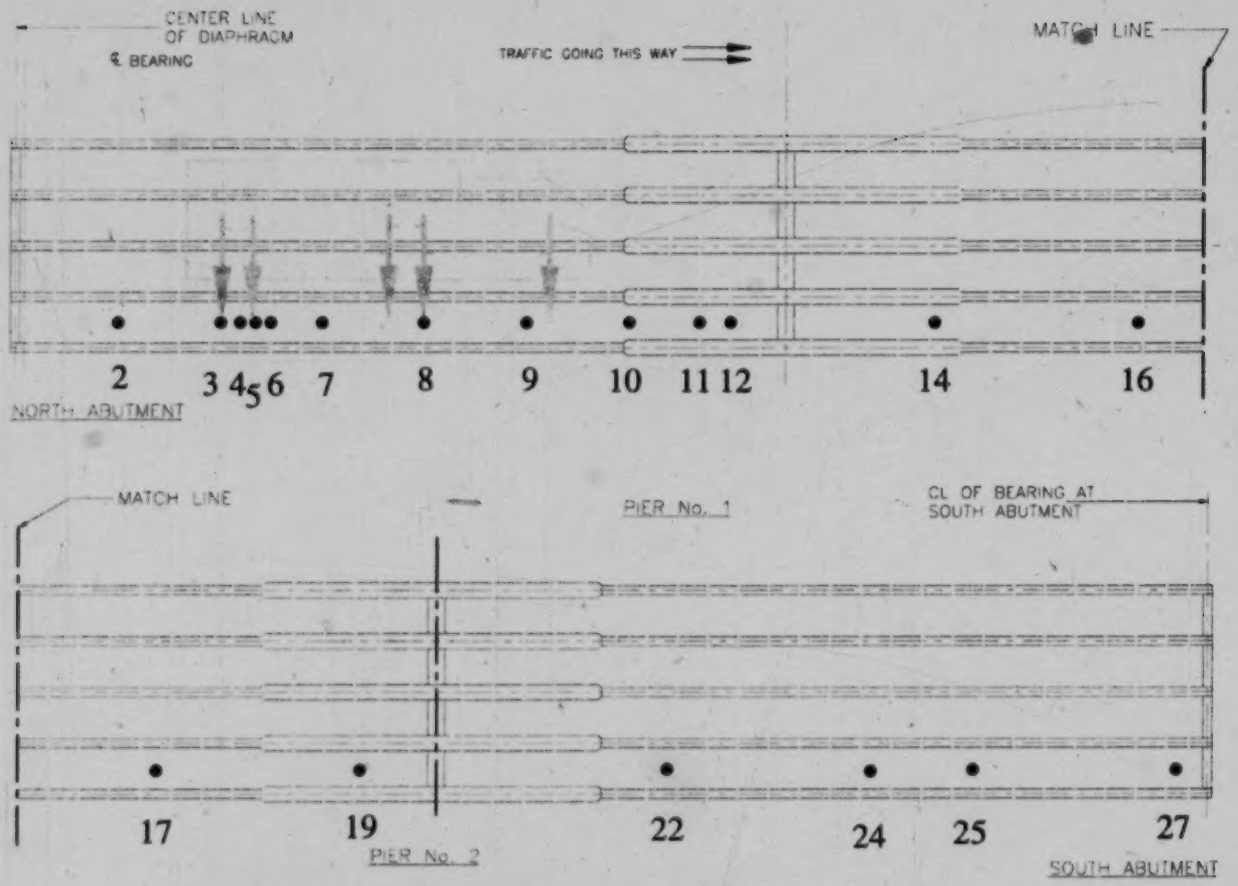

Figure 4.14 – 2004 Static Loading Point Locations

Most of the loading points in the north span were tested since the majority of instrumentation is in this span. In the middle and north spans, only half of the recommended loading points were tested in order to save time. However the tested loading points were sufficient enough to give an overall idea of bridge behaviour and would yield enough data to be used to calculate influence lines.

In order to group all of the strain gauges from Girder 1 together, channel cable 2 from SET A and channel cable 3 from SET B had to be switched. Table 4.10 shows the revised channel sets. The temperatures and relative humidities were again recorded throughout the duration of the tests. This was done in the event that a sudden change of weather or temperature may influence the behaviour of the Crowchild Trail Bridge. Table 4.11 shows the recorded temperature and relative humidity throughout the duration of the tests. At the start of the tests at 8:00 AM the weather was clear with relatively warm temperatures. However, at approximately 10:00 AM, heavy precipitation began and would continue for the remainder of the testing period. As can be seen in Table 4.11, once the heavy precipitation began, the temperature decreased steadily while the relative humidity increased sharply. Despite the precipitation, the static and dynamic loading tests were completed. As a result of the wet bridge deck surface, however, the ambient vibration tests were rescheduled two weeks later

Table 4.10 - List of Strain Gauges for Load Tests

DAQ Channel	SET A		SET B		SET C	
0	G1	CABLE 1	G23	CABLE 2	E2	CABLE 7
1	G2		G24		E3	
2	G3		G25		E4	
3	G4		G26		E5	
4	G5		G27		E7	
5	G6		G28		E8	
6	G7		G29		E9	
7	G8		G30		E10	
8	G9		G31		E11	
9	G10		G32		E12	
10	G11		G33		E13	
11	G23	CABLE 3	T1	CABLE 4	S1	CABLE 9
12	G24		T2		S2	
13	G25		T3		S3	
14	G26		T4		S4	
15	G27		T5		S5	
16	G28		T6		S6	
17	G29		T7		C1	
18	G30		T8		C2	
19	G31		T9		C3	
20	G32		T10		C4	
21	G33		T11		RS1	
22	G34	CABLE	RC1	CABLE	RS2	CABLE
23	T4	10	RC2	11	RS3	12

Table 4.11 - Recorded Temperature During 2004 Load Tests

Time	Temperature	Relative Humidity
8:10 AM	15°C	44 %
9:22 AM	17°C	36 %
10:03 AM	16°C	53 %
11:08 AM	12°C	77 %
12:37 PM	10°C	88 %

Loading tests began shortly after 8:00 AM. First, SET A strain gauges were connected to the data acquisition unit. Four sets of dynamic readings were taken while the loading truck passed over the bridge deck at various speeds; two at 15 km/hr, one at 30 km/hr, and one at 55 km/hr. Next, static tests were completed with SET A strain gauges still connected to the data acquisition unit. In total, the truck was positioned along the bridge deck at 19 different load points as outlined before. Five static readings per load point were completed with the data acquisition unit. The five readings were averaged to give the actual static strain. Zero readings were recorded after the loading points in each span were completed; a total of four sets of zero readings were taken for each strain gauge set. Zero strain readings would be subtracted from the loading point strains to give the actual strains.

This testing methodology was used again with strain gauge SETS B & C. Dynamic and static readings were taken for each strain gauge set in exactly the same manner as was completed for SET A. Dynamic readings were completed for speeds of 15 km/hr, 30 km/hr, and 55 km/hr. Static readings were also completed for all 19 loading points. Midway through the loading tests, when SET B was connected to the data acquisition unit, heavy rain began and continued through the remainder of the loading tests. As a result, the loading tests required additional time to complete.

After typical static and dynamic load tests, a couple of tests were completed to investigate the dynamic effects of a bump and braking on the bridge deck surface. 2X6 wood planks were placed near the mid-span of the north span on static Load Point 8. As

the truck ran over the wood planks, an impact load was simulated. Data was recorded as the truck ran twice over the planks at a speed of 55 km/hr. The dynamic effects of braking on the bridge deck from speeds of 15 km/hr and 30 km/hr were also recorded. All of the static and dynamic tests were completed at approximately 1:00 PM.

Deflections of the five girders were monitored during the static and dynamic load tests. Five cable transducers were used to measure the vertical displacement of the plate girders. The girder deflections were measured at the approximate mid-span location in the north span. This was directly below Tension Strap 13.

4.4.4.2 Static Test Results

Static tests were completed at 19 different loading points along the length of the bridge between Girder 1 and Girder 2. Table 4.12 shows the maximum strains recorded during the static tests and the corresponding loading point location. Positive strains indicate tensile stresses and negative strains indicate compressive stresses.

Table 4.12 - Static Test Maximum Strain Results

SET	Gauge Type/Location	Max Strain (με)	Min Strain (με)	Strain Range (με)
SET A	G3 – Girder 1 web	89.4 (L*9)	-17.4 (L*19)	106.8
SET A	G33 – Girder 1 flange	92.9 (L*9)	-17.9 (L*19)	110.8
SET A	G34 – Girder 1 flange	101.3 (L*9)	-19.7 (L*19)	121.0
SET B	T3 – Steel Strap 8	79.2 (L*9)	-5.8 (L*2)	85.0
SET B	RC1 – GFRP bar	58.1 (L*12)	-6.3 (L*27)	64.4
SET C	E13 – Concrete deck	24.6 (L*9)	-5.8 (L*17)	30.4
SET C	S4 – Steel stud	9.5 (L*9)	-0.9 (L*2)	10.4
SET C	C4 – Cross frame	3.0 (L*16)	-63.5 (L*9)	66.5
SET C	RS2 – Smart bar	13.5 (L*12)	-3.0(L*25)	16.5

All of the strains recorded were well within the elastic range and therefore the suitable level of safety. As shown in Table 4.12, most of the maximum strains occurred when the front axle of the truck was positioned at Loading Point 9. At this position the truck's centre of gravity would have been near the centre of the north span, thus producing the maximum strain effects. The majority of the minimum strains, or compressive strains, occur when the truck is positioned in the middle span of the bridge. At this position, the weight of the truck causes a negative bending moment in the north span of the bridge and causes the compressive strains as indicated. G33 and G34 experienced the greatest amount of strain because they are located on the bottom flange of Girder 1. The steel studs exhibited the lowest amount of strain.

Influence lines were constructed from strain results of all the different truckload points. Figure 4.15 shows the influence lines for several strain gauges located on Girder 1.

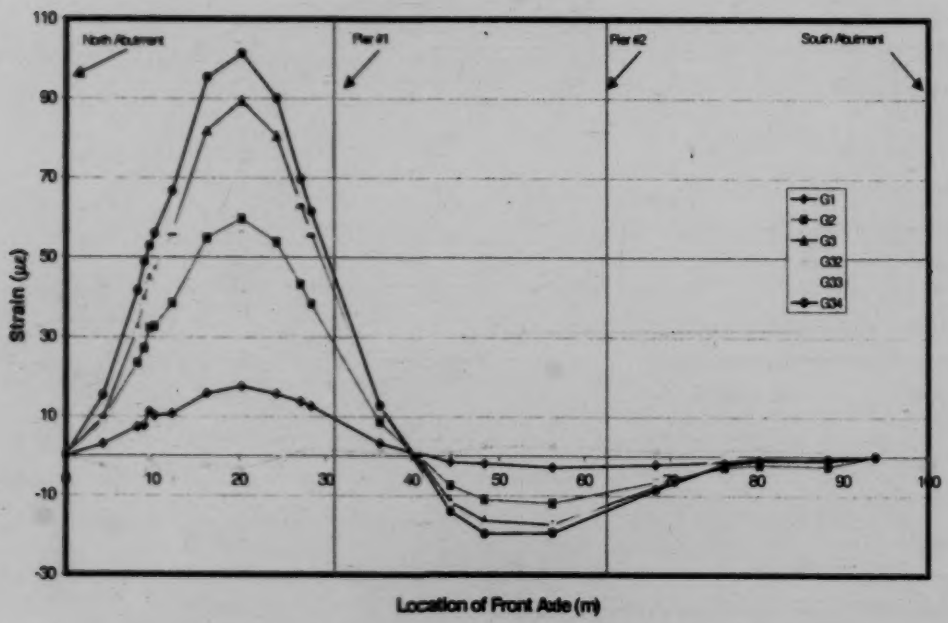

Figure 4.15 Static Response: Influence Lines of Girder Strains

The Y-axis indicates the level of strain recorded from the strain gauge while the X-axis indicates the position of the truck front axle relative to the north abutment. The approximate location of Pier 1 and Pier 2 are also indicated. Six influence lines are shown in this figure including G1, G2, G3, G32, G33, and G34.

G3, G33, and G34 show the highest levels of strains because they are located on the flange and lower portions on the web of the plate girder. The highest levels of strain in the plate girder are experienced when the truck is positioned on the north span. As the truck first moves onto the middle span, the positive strains are gradually reduced. Although the front axle of the truck is past Pier 1, the centre of gravity of the truck initially remains on the north side as the positive strains indicate. The truck centre of gravity is over Pier 1 when the front axle reaches 40 meters past the north abutment. This is indicated by a zero strain level in the girder gauges. The north span plate girder experiences a negative moment and subsequent compression strains as the centre of gravity of the truck shifts into the middle span. When the truck is over the south span, the strains in the north span approach zero. Therefore, very little loading effects are experienced when the truck is in the south span. Influence lines for other selected strain gauges can be found in Appendix B.

Strain profiles in the positive and negative moment regions can also be analyzed from the static test results. Strain Gauges G1 - G3, and G31-G34 were mounted on Girder 1 at the same cross section. At 9030 mm from the centre line of north abutment bearings, these gauges are located in the positive moment region of the plate girder. Figure 4.16 shows the maximum strains recorded at this cross-section during the static load tests.

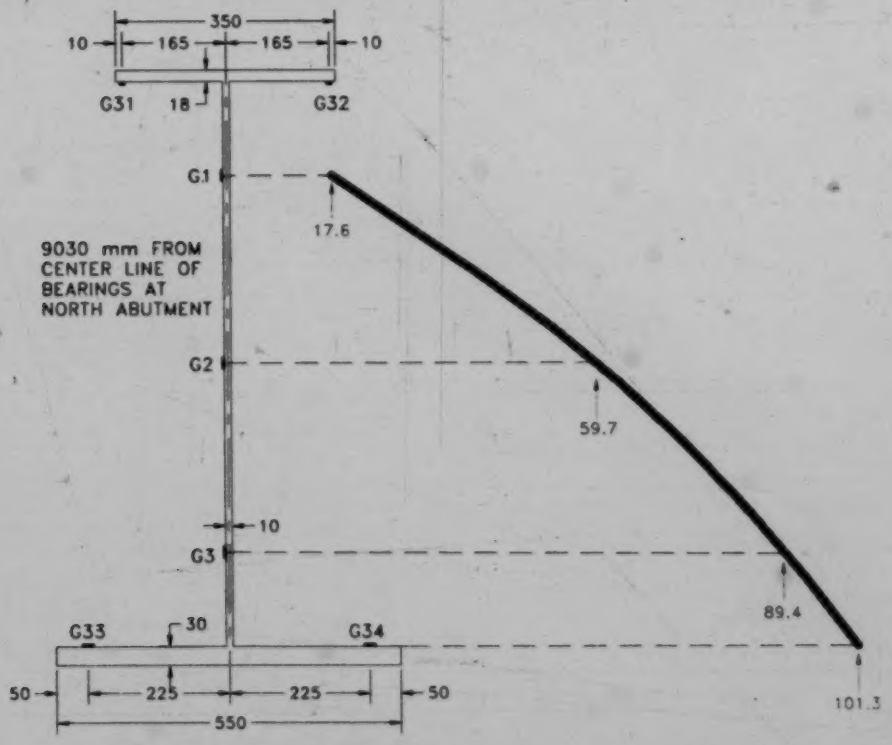

Figure 4.16 - 2004 Positive Moment Region Strain Distribution

These maximum positive moment strains occurred when the front axle of the truck was positioned at Load Point 9, approximately 20 meters from the expansion joint above the north abutment. The maximum strain in the bottom girder flange is 101.3 με. The strain distribution is approximately linear. Although no reasonable results could be obtained from G31 or G32, the current results could be extrapolated to obtain the approximate

location of the neutral axis. From the current results, the neutral axis is located approximately 50 mm below the bottom surface of the top flange.

Strain results could also be used to form the strain profile in the negative moment region. Figure 4.17 shows the strain profile in the negative moment region. Results from strain gauges G16, G17, and G18 were used to plot the strain profile. These gauges are also located on Girder 1, however, they are located in the negative moment region at approximately 2800 mm north of the centre line of Pier 1.

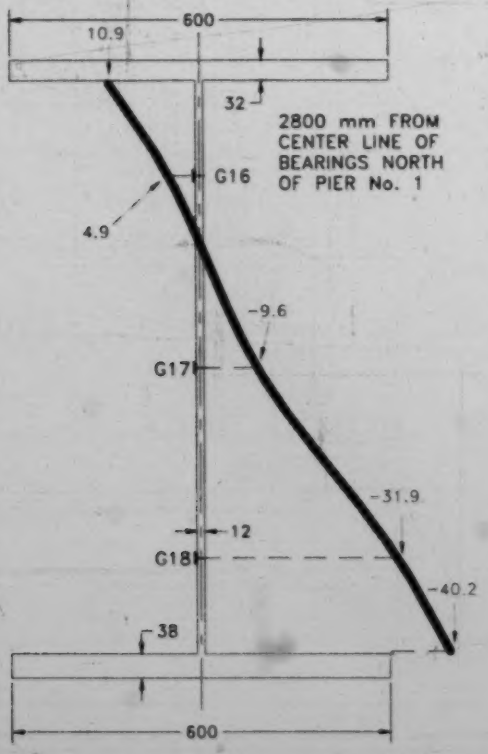

Figure 4.17 - 2004 Negative Moment Region Strain Distribution

Although only the results from three gauges were used, strains were extrapolated to obtain approximate values at the flange portions as shown on the figure. Again, an approximate linear strain profile is apparent. The maximum compression strain is 19.7 με located in the bottom flange of the plate girder. These maximum strains occurred when the front axle of the truck was positioned over Loading Point 19 at approximately

25.8 meters south of the centre line of Pier 1. Using the strain results, the neutral axis is located approximately 250 mm below the bottom face of the top flange.

Load sharing between the five girders was also analyzed by looking at the tension strain results. Results were compared from the lowest strain gauge position on each girder web. These gauges included G3, G6, G9, G12, and G15 from Girders 1, 2, 3, 4, and 5 respectively. Figure 4.18 shows the maximum strains recorded from each gauge. All of

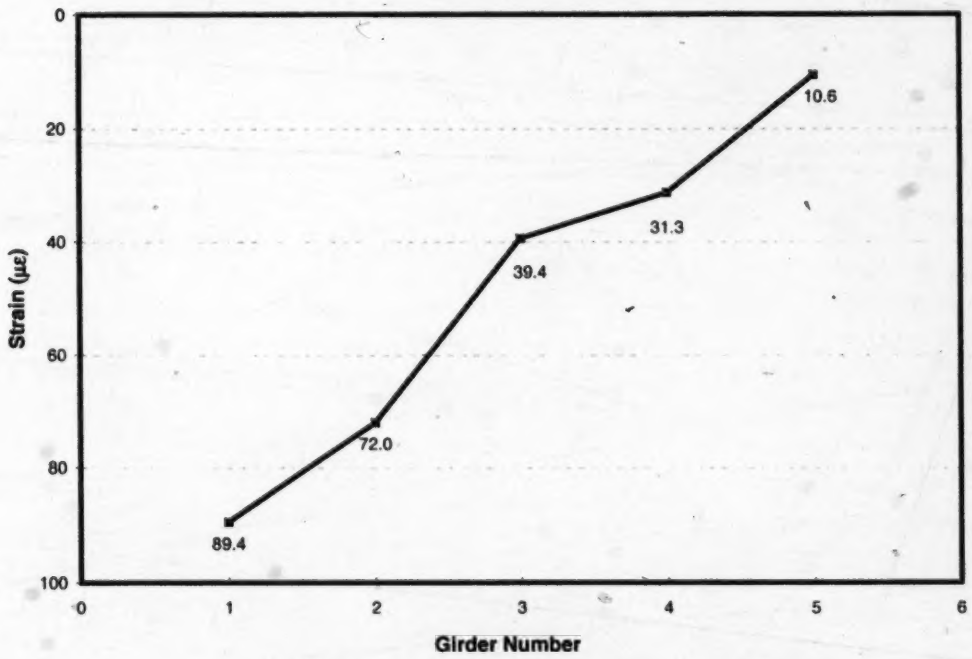

Figure 4.18 - Load Sharing Indicated By Girder Stains

the readings were taken when the loading truck produced maximum strains by being positioned on Loading Point 9. However, all of the readings were not taken during the same test since G3 and G6 were included in SET A and G9, G12, G15 were included in SET B. These results may have been slightly different if all of the strain readings were obtained during the exact same test. G3 on Girder 1 experiences the most strain and G15 on Girder 5 experiences the least amount of strain. This is as expected as the loading truck is on the west-facing lane and the front passenger-side axles are directly between

Girders 1 and 2. From the figure, the load sharing is approximately linear between all five girders. With the exception of Girder 3, there is approximately a 20 με increase in strain between neighbouring girders the closer one gets to the loaded truck.

During the static load tests, deflections of all the five girders near the middle of the north span were monitored. The maximum measured upward and downward deflections for each girder is show in Table 4.13. Maximum downward deflections occurred when the truck was positioned on Static Loading Point 10. However, maximum strains occurred

Table 4.13 - Maximum Measured Deflections From Static Tests

Location	Maximum Upward Deflection (mm)	Maximum Downward Deflection (mm)
Girder 1	4.3	-12.3
Girder 2	3.3	-10.7
Girder 3	2.6	-7.1
Girder 4	2.0	-4.6
Girder 5	1.3	-2.2

when the truck was situated over Loading Point 9. This is because all of the girder strain gauges are located closer to the north abutment compared to the cable transducers, which are located closer to the middle of the span. Therefore, the different loading truck positions produce maximum effects depending where the measuring gauges are located. Maximum upward deflections occurred when the truck was positioned on static Loading Point 19. From the results in Table 4.13, the maximum measured deflection is 12.3 mm downward for Girder 1. Considering the downward and upward deflection, Girder 1 had a total range of motion of 16.6 mm during the static load tests.

The cable transducer deflection readings exhibit good agreement with the girder strain readings. For the tests, it was assumed that the truck was positioned exactly midway between the Girder 1 and Girder 2. The results may vary somewhat depending on the

actual position of the truck, however, these results are sufficient to determine the girder load sharing characteristics and the overall bridge behaviour.

Figure 4.19 shows the influence line for the north span girder deflection as the position of the loaded truck changed during the static tests. All of the girders deflect downward as

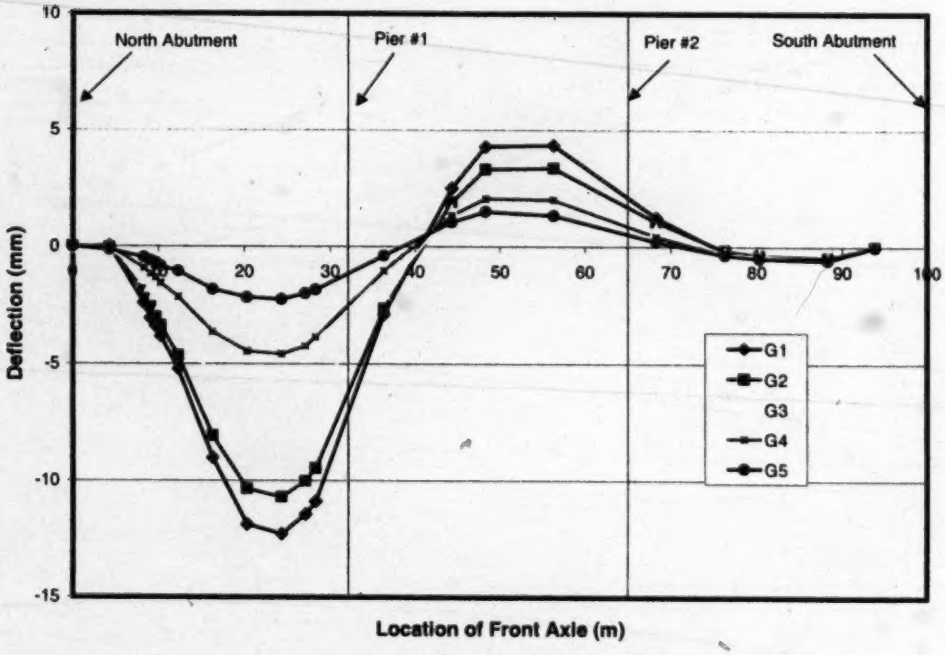

Figure 4.19 - Girder Deflection Influence Line

the truck travels onto the north span. When the front axles of the truck reach the location of the first pier, some girder deflection is present as the centre of gravity of the truck remains over the north span. However, when the front axles of the truck reach approximately 40 meters past the north abutment, the girders begin to deflect upward as a negative moment is introduced into the north span. As the truck passes onto the far south span, the north span girders again deflect downward a relatively small amount.

4.4.4.3 Dynamic Test Results

Several sets of dynamic tests were recorded at various truck speeds. The same loading truck that was used in the static tests was also used for the dynamic tests. Dynamic effects of truck speeds at 15, 30, and 55 km/hr were investigated. Table 4.14 shows the maximum strains recorded during the dynamic tests.

Table 4.14 - Maximum Strains from Dynamic Test Results

SET	Gauge Type/Location	Max Strain (με)	Min Strain (με)	Strain Range (με)
SET A	G3 – Girder 1 web	96.1	-19.2	115.3
SET A	G33 – Girder 1 flange	102.0	-20.1	122.1
SET A	G34 – Girder 1 flange	109.9	-19.2	129.1
SET B	T3 – Steel Strap #8	74.3	-5.2	79.5
SET B	RC1 – GFRP bar	62.8	-8.3	71.1
SET C	E13 – Concrete deck	47.5	-4.0	51.5
SET C	S4 – Steel stud	10.5	2.5	13.0
SET C	C4 – Cross frame	1.7	-59.0	60.7
SET C	RS2 – Smart bar	14.1	-2.9	17.0

Positive strains indicate tension strains while compressive strains indicate compressive strains. All of the maximum girder strains resulted from the truck speed of 30 km/hr. However, maximum strains in the other bridge structural components were caused at various speeds. As can be seen from the results, all of the maximum strains from the dynamic tests are well within the elastic range.

Influence lines for several of the bridge components were plotted. Figure 4.20 shows the typical dynamic response of strain gauges G3 and G34 as the loading truck passed over

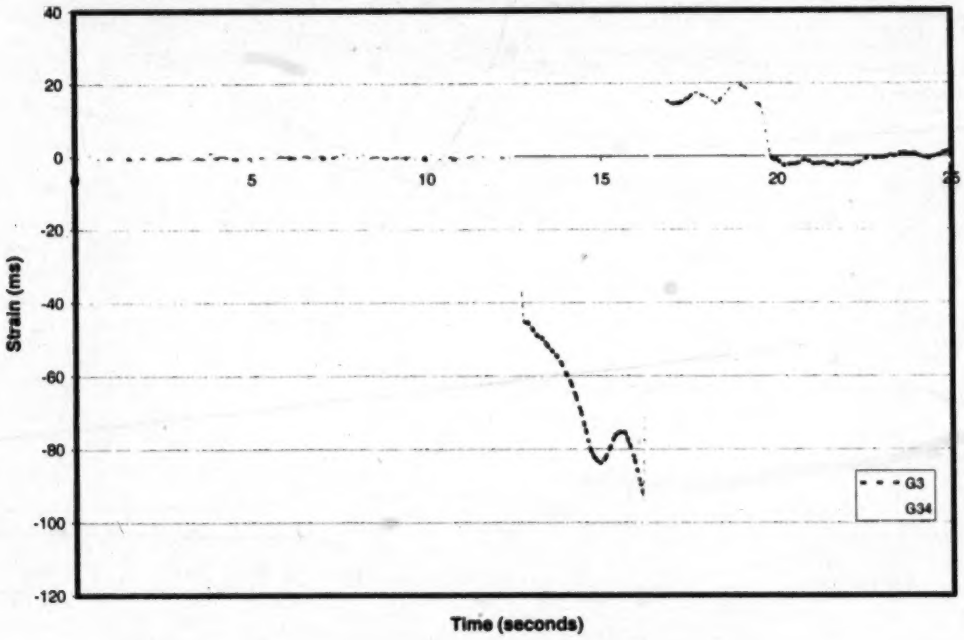

Figure 4.20 - Dynamic Response of Girder Strain Gauges

the bridge at 30 km/hr. These figures are very similar to the influence lines plotted from the static response. However, the response of the strain gauges is sharper compared to the static response plotted earlier. The strain virtually jumps from zero as the truck passes over the deck.

To obtain the dynamic behaviour of the Crowchild Trail Bridge in 1998, data was scanned at a rate of 500 Hz. With the new data acquisition used for the 2004 tests, however, only averaged data readings were recorded. The strain response was sampled at a similar frequency compared to the 2004 tests, but groups of 60 readings were averaged at a time and only the averaged readings were stored. With this technique, higher frequency noises were not captured and the dynamic results could be viewed directly without the use of any low-pass filters. Although this made it easier to determine the

overall behaviour of the bridge response, many of the detailed dynamic properties could not be calculated as a result of this averaging technique. With the averaged data, it was not possible to decouple the dynamic response from the static response. Strains recorded during the dynamic tests may not have been the actual maximum results due to the averaging effects. Without clear static and dynamic values, the impact factor could not be calculated. As a result of the rain during dynamic testing, accelerometers could not be positioned to capture the free vibration motion of the bridge deck. Therefore the damping ratio could not be calculated.

Deflections were higher when the truck was traveling at lower speeds compared to higher speeds. Table 4.15 shows the maximum upward and maximum downward girder deflections from the dynamic load tests.

Table 4.15 - Measured Deflections from Dynamic Tests

Location	Maximum Upward Deflection (mm)	Maximum Downward Deflection (mm)
Girder 1	4.5	-13.2
Girder 2	3.5	-10.8
Girder 3	2.7	-6.9
Girder 4	2.3	-4.1
Girder 5	1.8	-1.6

Girder 1 exhibits the greatest range of deflection as would be expected considering that the loading truck was positioned on the west lane of the bridge. Considering both the maximum upward and downward bridge deflection, the total range of movement for Girder 1 is 17.7 mm.

4.4.5 2004 Bridge Visual Inspection

4.4.5.1 Bridge Deck Crack Mapping

Thorough field tests and crack mapping of the Crowchild Trail Bridge were completed in 1997 and 1998. Since then, crack mapping of the underside of the Crowchild Trail Bridge has been completed another three times: in June 1999, July 2002, and most recently in June 2004. This section will summarize the results from the 2004 crack mapping. A complete comparison and analysis of the deck cracks over the first seven years of the service life of the bridge will be presented in the next chapter. Figures showing the location of all the cracks will also be presented in the next chapter.

Overall, relatively few new cracks could be seen on the underside of the bridge deck since July 2002. Within the last two years of service life, the rate of crack growth has significantly been reduced. In the north span only a few new transverse cracks have randomly formed. Another noticeable change was the extension of the longitudinal crack between girders two and three to Pier 1. Several new transverse cracks had also formed in the middle span. However, no new longitudinal cracks had formed in this region. Similarly, there were also several new random transverse cracks in the south span. Most of the new transverse cracks that had formed were less than 0.5 mm thick. With the naked eye these cracks were somewhat difficult to detect. Drivers underneath the Crowchild Trail Bridge would not be affected or even aware of the existing cracks. Therefore, these small deck cracks would not affect drivers' confidence of using the bridge.

4.4.5.2 Bridge Deck Leakage

As a result of heavy precipitation that occurred during the bridge loading tests, water was observed to penetrate through the bridge deck at several crack locations. Figures 4.21 and 4.22 show water leakage through cracks on the underside of the bridge deck. Distinct water stains from previous leakage were also noted in the same areas.

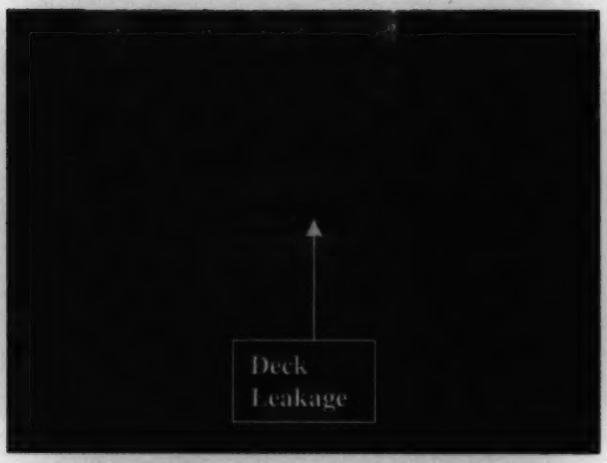

Figure 4.21 - Bridge Deck Leakage Near Strap

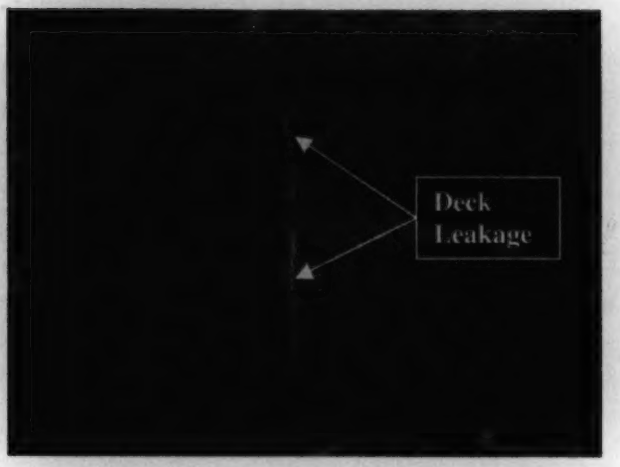

Figure 4.22 - Bridge Deck Leakage at Deck Haunch

This leakage results from cracks that have propagated completely through the bridge deck over time. In Figure 4.27 leakage is shown along a transverse crack at a construction joint. Figure 4.28 shows leakage along a longitudinal crack in the concrete deck haunch. Here the moisture has fully penetrated the crack and is migrating toward the steel plate girder where more potential damage could occur.

Figure 4.23 on the following page shows the approximate locations of these water leaks and water stains on the underside of the deck. Please note that this drawing is not drawn to scale to accurately represent the relative sizes of the steel girders and straps. Also, the water-stained areas on the bridge deck were intentionally drawn larger than what was actually observed in the field. From the figure, it is noticed that the middle span, which was reinforced internally with only GFRP bars, contained the most amount of areas affected by water leakage. The south span, which was the only span to contain a small amount of internal steel reinforcement, contained the fewest affected areas. Most of the water leakage occurred at cracks orientated in the transverse direction. Water leakage was noted to occur at several cold joint locations.

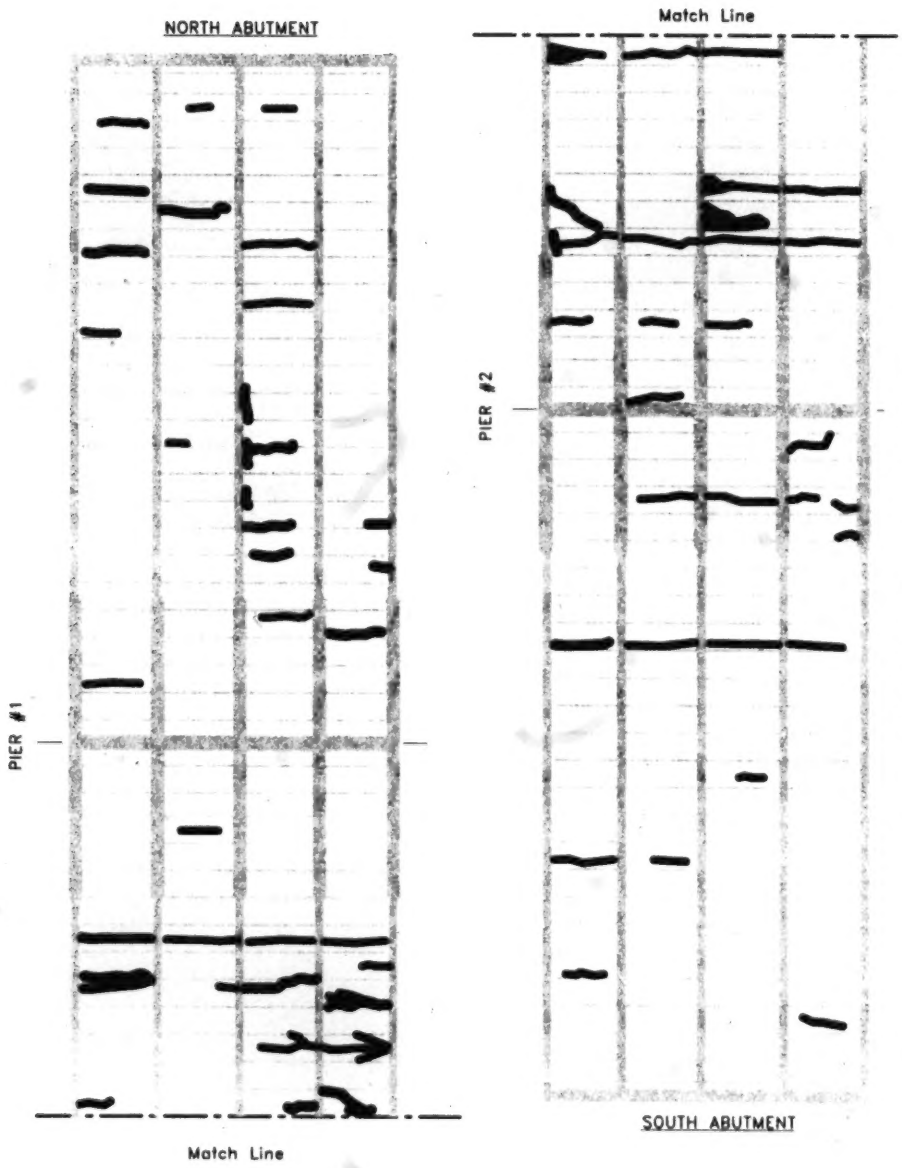

Figure 4.23 - Bridge Deck Leak Locations

4.4.5.3 Bridge Barrier Cracks

Visible vertical cracks were also located along both sides of the concrete bridge barrier. Figures 4.24 and 4.25 show the typical cracking pattern along the concrete side barriers

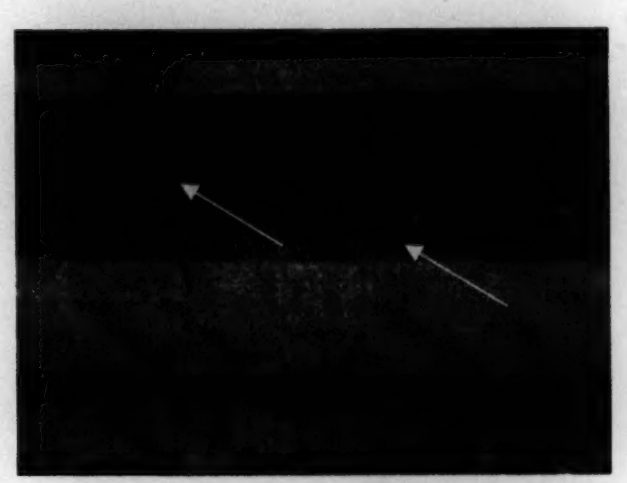

Figure 4.24 - Cracking in the Concrete Bridge Barriers (Interior)

Figure 4.25 - Cracking in the Concrete Bridge Barriers (Exterior)

viewed from both sides. Figure 4.24 shows the view from the road surface of the bridge and Figure 4.25 is the external view of the concrete barrier. As seen in the figures, the cracks were spaced approximately 600 mm to 1000 mm apart along the barriers. Internal

reinforcement used in the concrete barrier consisted of prefabricated NEFMAC GFRP grids. In addition, double headed stainless steel bars anchor the barriers to the bridge deck. Cracks in the barriers were the most visible areas of damage.

5.0 ANALYSIS AND COMPARISON OF RESULTS

5.1 Introduction

Structural health monitoring of the Crowchild Trail Bridge was necessary to investigate the behaviour of the innovative materials used within the continuous steel-free deck. Since the Crowchild Trail Bridge was reconstructed in 1997, several sets of field tests have been completed before and after it was opened to traffic. Field tests consisted of ambient vibration tests to determine the natural frequencies and mode shapes of the bridge. In addition, static load tests and dynamic load tests were also completed to determine bridge strains and behaviour under known truckloads. Finally, the underside of the bridge deck was visually monitored in order to map the origin and progression of cracks. The first tests highlighted the baseline structural characteristics and behaviour of the bridge. Additional tests were completed in 1998 after the Crowchild Trail Bridge had been in full service for a year. Six years later, in 2004, another full set of field tests were performed to determine whether any structural changes had occurred.

5.2 Comparison of Preliminary, Static, and Dynamic 2004 Test Results

In June 2004, several tests were completed including preliminary, static, and dynamic tests. Preliminary tests were performed under random traffic loading and ensured that the instruments monitoring the bridge were functioning properly. Static and dynamic tests were completed under know truck loads. Table 5.1 compares the maximum strains from the preliminary tests, static tests, and dynamic tests. Compression strains and tension strains are not differentiated by sign convention from each other. By comparing the results of these tests, the validity of each test may be confirmed. Also, it is useful to compare the bridge response to various types of loading including random loading and controlled loading.

Table 5.1 - Comparison of 2004 Preliminary, Static, and Dynamic Test Strains

Gauge Type/Location	2004 Maximum Strains (με)		
	Preliminary Test	Static Tests	Dynamic Tests
G3 – Girder 1 web	82.6	89.4	96.1
G33– Girder 1 flange	-	92.9	102.0
G34 – Girder 1 flange	95.1	101.3	109.9
T3 – Steel Strap 8	36.7	79.2	74.3
RC1 – GFRP bar	21.4	58.1	62.8
E13 – Concrete deck	4.2	24.6	47.5
S4 – Steel stud	2.0	9.5	10.5
C4 – Cross frame	17.4	63.5	59.0
RS2 – Smart bar	5.6	13.5	14.1

From Table 5.1, it can be seen that the maximum strains in the girders are relatively similar between all three tests. Strains in the other components of the bridge are significantly smaller in the preliminary tests compared to the static and dynamic load tests. This difference may be attributed to unknown truckloads and wheel positions. Girder strains are the highest under dynamic loading. This is due to the impact loading of the truck. Overall, this comparison proves that the instruments monitoring the bridge were functioning properly during each of the three tests. In addition, this simple comparison proves that the data obtained is reliable.

These results suggest that total weight of regular traffic over the bridge may be similar in weight to the loading truck used In each test, the girders are carrying similar traffic loads because the strains in the main load-carrying plate girders are the same. However, normal traffic may travel on a different location of the bridge deck so that strains in other structural components are lower. As described previously, during the controlled loading tests, the front axle of the truck was positioned midway between Girder 1 and Girder 2. As shown in Table 5.1, this location produces higher strains in the other structural

components of the bridge including the carbon reinforcement in the bridge deck, the steel straps, and the cross frame. Normal traffic will travel in a random fashion and may not be positioned in a location that produces the maximum strain effects in other bridge structural components.

Deflection results are compared between the static and dynamic strain results. Table 5.2 summarizes and compares the maximum deflections of the static and dynamic results.

Table 5.2 – Comparison of 2004 Maximum Deflections

Location	**Maximum Upward Deflection (mm)**		**Maximum Downward Deflection (mm)**	
	Static	**Dynamic**	**Static**	**Dynamic**
Girder 1	4.3	4.5	-12.3	-13.2
Girder 2	3.3	3.5	-10.7	-10.8
Girder 3	2.6	2.7	-7.1	-6.9
Girder 4	2.0	2.3	-4.6	-4.1
Girder 5	1.3	1.8	-2.2	-1.6
Average	***2.7***	***3.0***	***-7.4***	***-7.3***

Relatively few differences exist in the deflections between the static and dynamic results. The upward deflections are very similar. However, there are some slight differences in the downward deflections. Girder 1 and 2 deflections are higher in the dynamic results compared to the static results. However, Girder 3, 4, and 5 deflections are higher in the static results compared to the dynamic results. These results suggest that the loading truck may have been closer to the west side traffic barrier during the dynamic tests. This would have caused higher eccentricity in the loading with relatively higher deflections in Girders 1 and 2 and relatively lower deflections in Girders 3, 4, and 5.

5.3 Comparison of Ambient Vibration Results

5.3.1 Ambient Vibration Test Overview

Ambient vibration tests have been complete three times on the Crowchild Trail Bridge since the new deck was constructed in 1997. Bridge deck natural frequencies and mode shapes were calculated from the results of each field test. A team from UBC measured the natural frequencies and mode shapes of the Crowchild Trail Bridge immediately after construction was completed and before it was opened to traffic. After one year of operation, a team from the UofA measured the vibration characteristics of the bridge again in 1998. Finally, another set of ambient vibration tests was obtained six years later in 2004.

Careful comparison of the ambient vibration test results can provide insight into the current status of the Crowchild Trail Bridge. Vibration characteristics of the bridge depend on its physical properties such as mass, stiffness, and boundary conditions. Variations of these properties over time will directly influence its modal parameters. Therefore, changes in modal parameters and natural frequencies can be used to locate and quantify changes in the overall behaviour and structural damage of the Crowchild Trail Bridge.

5.3.2 Comparison of Natural Frequencies

Table 5.3 lists the eight predominant natural frequencies below 10 Hz and their corresponding mode shapes for each field test. In general, the natural frequencies measured in 1998 were approximately 0.20 Hz lower than the frequencies measured in 1997. To account for this change, it was speculated that the stiffness of the bridge reduced within the first year of operation.

However, in 2004, the first six measured natural frequencies were closer to the results that were measured in 1997. Although the last two natural frequencies were difficult to quantify from the 2004 results, they are relatively close to the 1998 results.

Table 5.3 – Crowchild Trail Bridge Natural Frequencies

Mode Shape Description	Ambient Vibration Test Results		
	September 1997	August 1998	June 2004
1st Vertical Mode	2.78 Hz	2.60 Hz	2.80 Hz
1st Torsional Mode	3.13 Hz	2.90 Hz	3.16 Hz
2nd Vertical Mode	3.76 Hz	3.63 Hz	3.78 Hz
2nd Torsional Mode	4.05 Hz	3.85 Hz	4.19 Hz
3rd Vertical Mode	4.64 Hz	4.43 Hz	4.66 Hz
3rd Torsional Mode	5.18 Hz	5.00 Hz	5.36 Hz
4th Torsional Mode	7.13 Hz	6.85 Hz	6.89 Hz
4th Vertical Mode	9.13 Hz	8.60 Hz	8.29 Hz

5.3.3 Comparison of Mode Shapes

Figures 5.1 to 5.8 compare the first eight mode shapes captured in 1998 and 2004. From the results, it is evident that the first vertical and torsional 1998/2004 mode shapes are nearly identical. The second vertical and torsional 1998/2004 mode shapes are very similar as well, however, they do not match as close compared to the first two mode shapes. The general shapes of the third vertical and torsional 1998/2004 mode shapes are similar, however the magnitude of the 2004 mode shape is consistently lower compared to the 1998 mode shape. It is also interesting to note the third torsional mode shape from the 2004 results. The 2004 mode shape in the north span is nearly the same compared to the 1998 results. However, the 2004 mode shape magnitude gradually declines in the middle span and again in the south span. Magnitudes from the 1998/2004 fourth vertical and horizontal mode shapes are generally the same. However, the last two (4th vertical and 4th torsional) mode shapes were the most difficult to obtain from the raw data. Although the general shapes of the modes are similar, the results from the 4th vertical and 4th torsional modes exhibited the least compatibility.

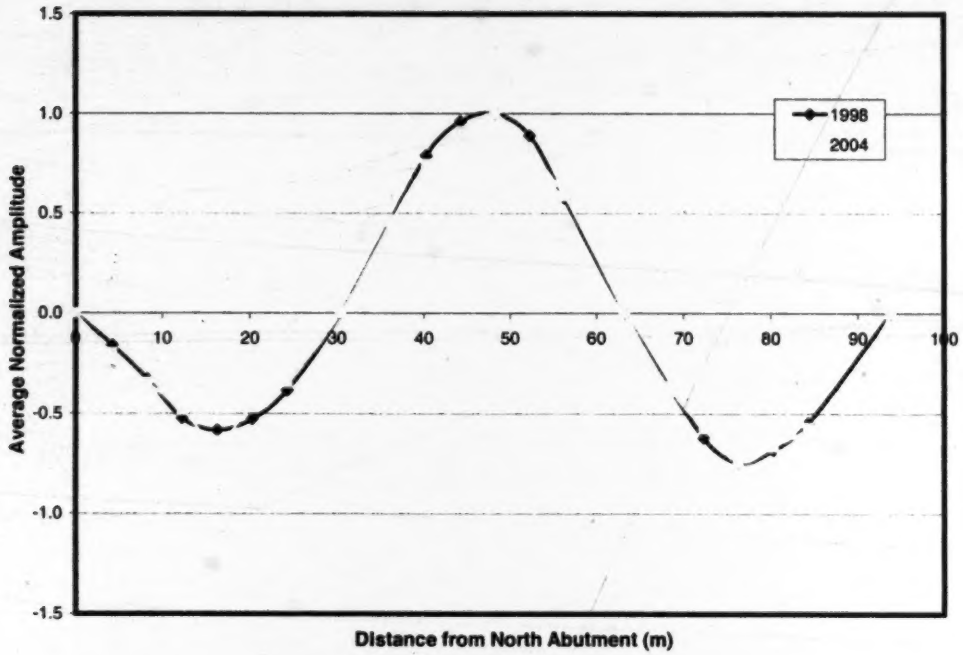

Figure 5.1 - 1st Vertical Mode Shape: Comparison of 1998 and 2004 Results

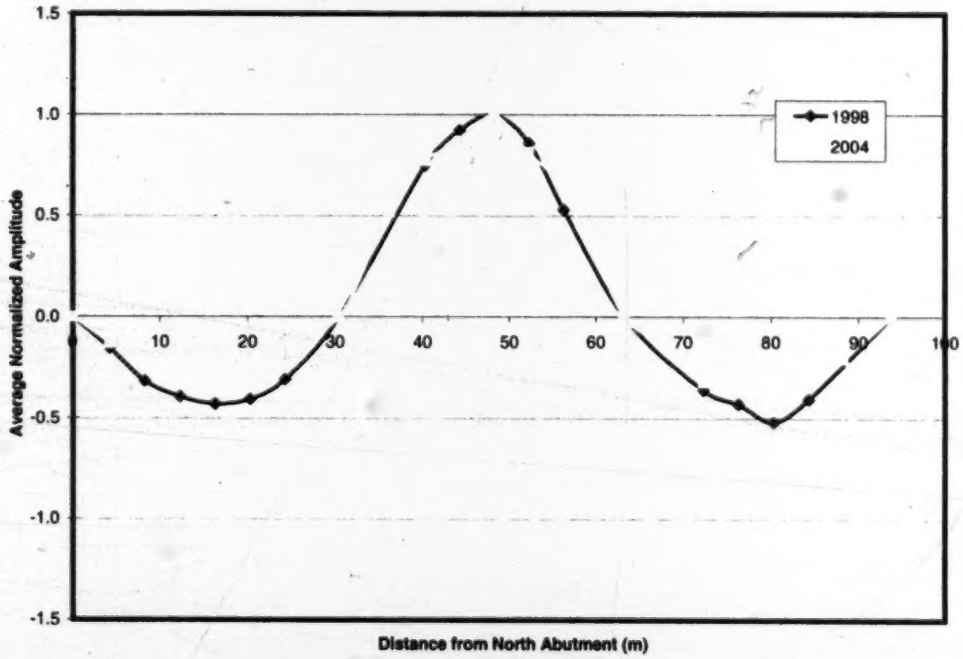

Figure 5.2 - 1st Torsional Mode Shape: Comparison of 1998 and 2004 Results

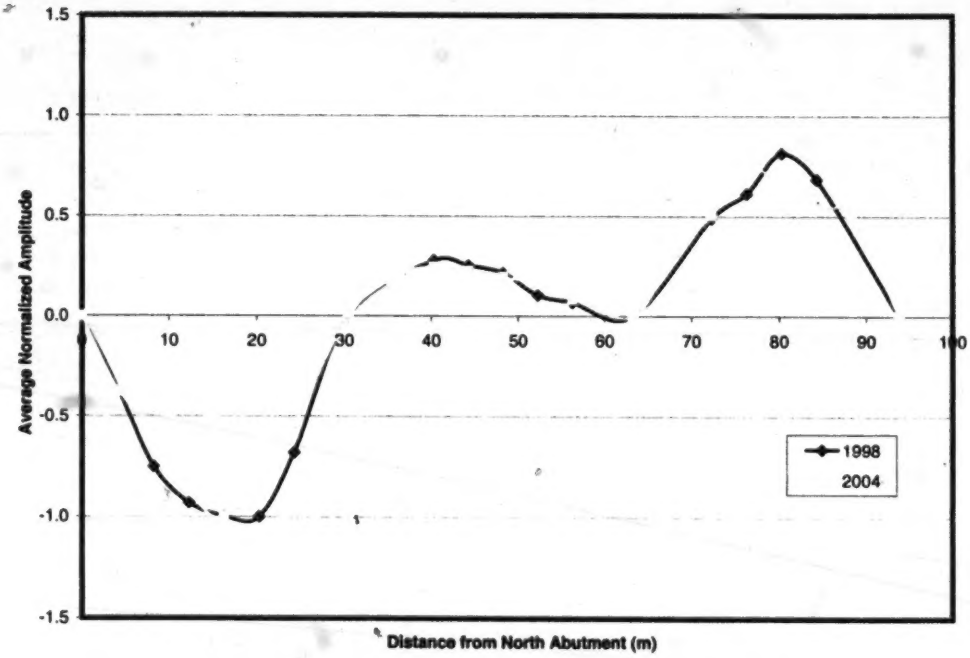

Figure 5.3 - 2nd Vertical Mode Shape: Comparison of 1998 and 2004 Results

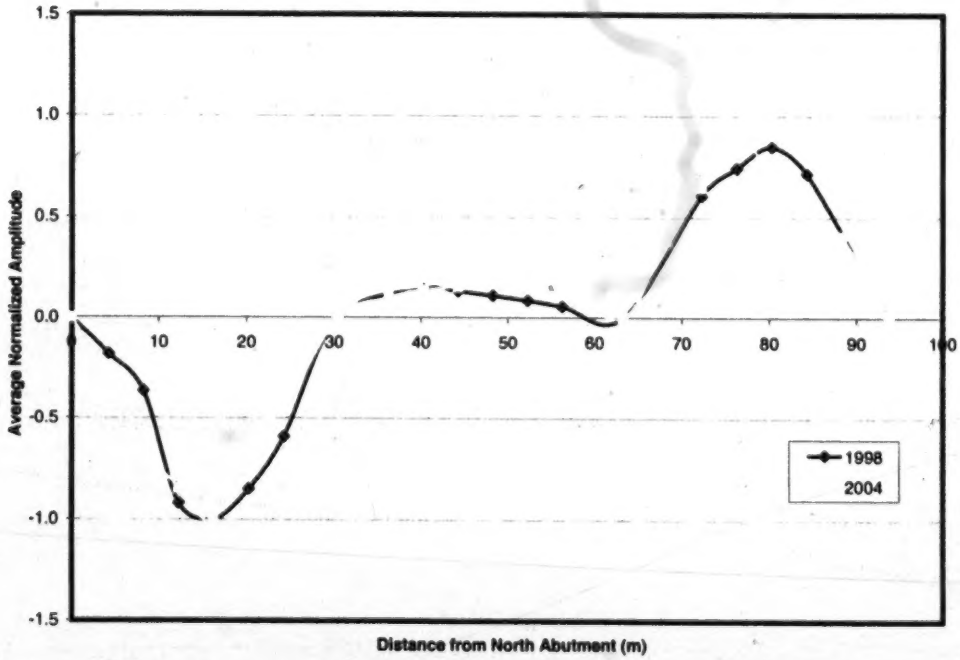

Figure 5.4 - 2nd Torsional Mode Shape: Comparison of 1998 and 2004 Results

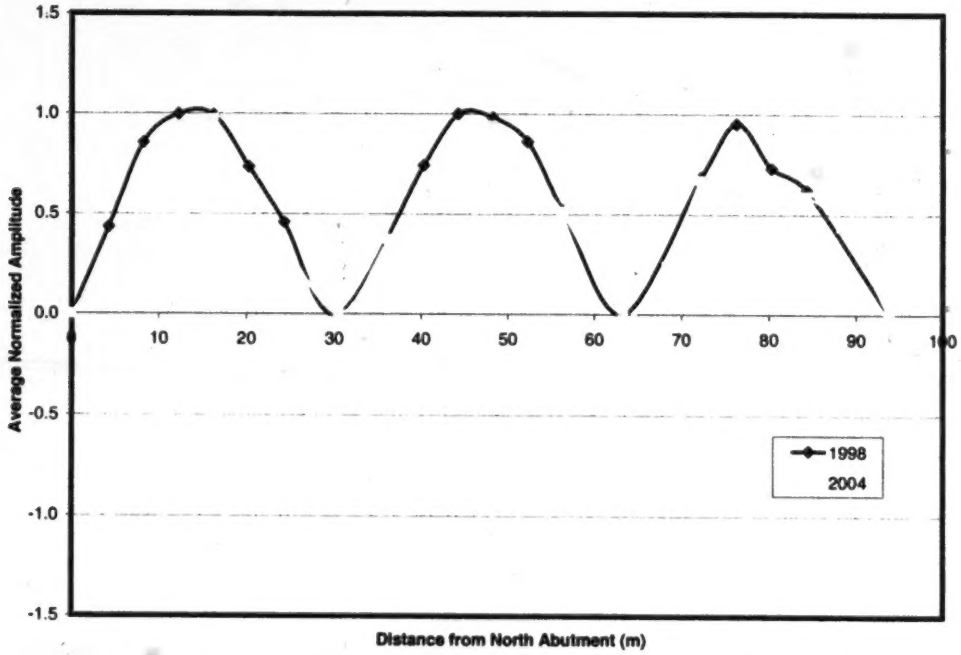

Figure 5.5 - 3rd Vertical Mode Shape: Comparison of 1998 and 2004 Results

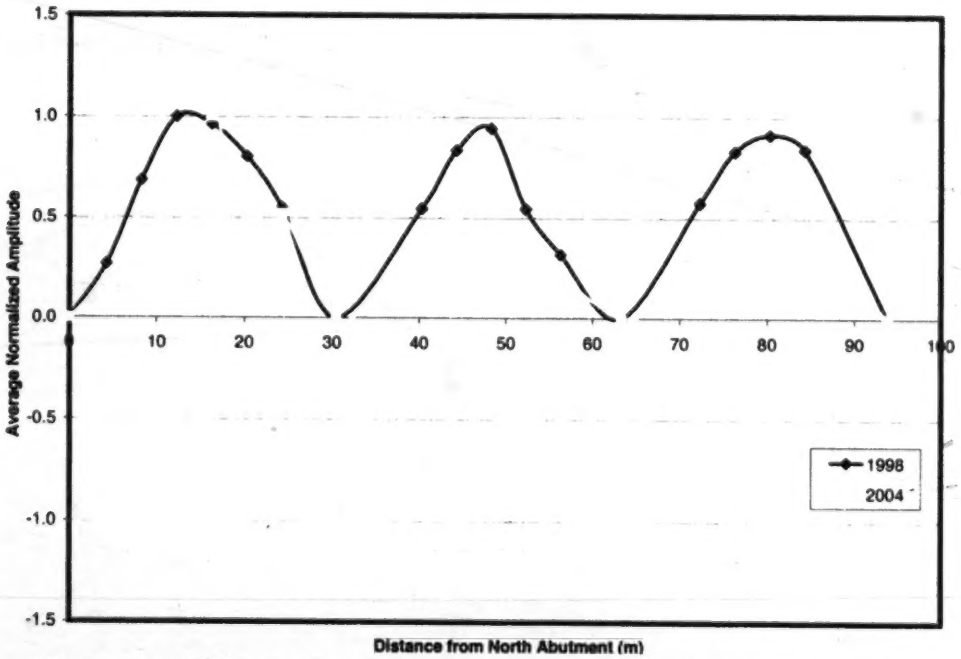

Figure 5.6 - 3rd Torsional Mode Shape: Comparison of 1998 and 2004 Results

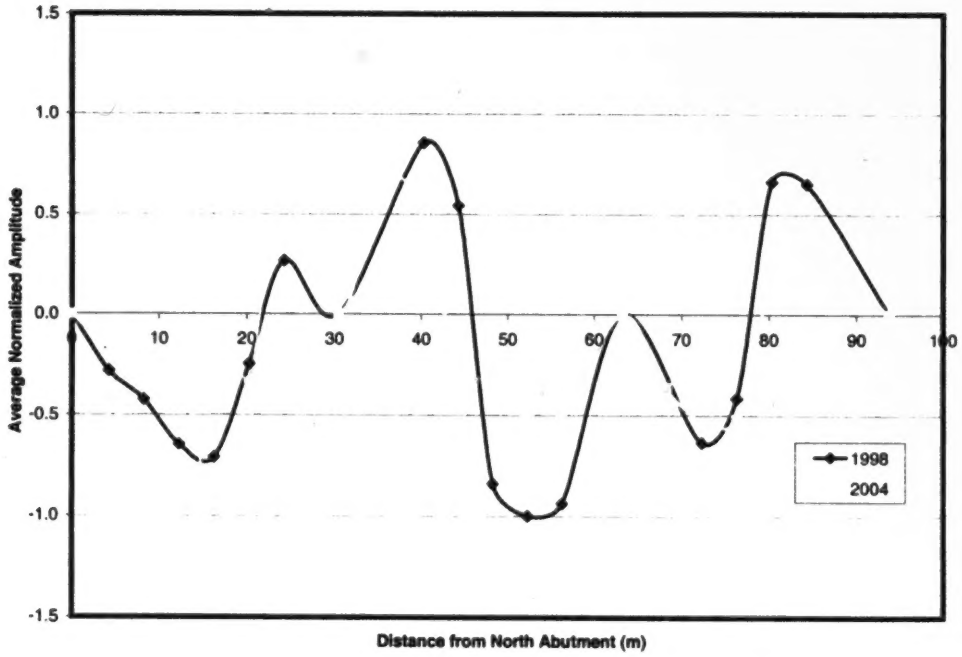

Figure 5.7 - 4th Veritcal Mode Shape: Comparison of 1998 and 2004 Results

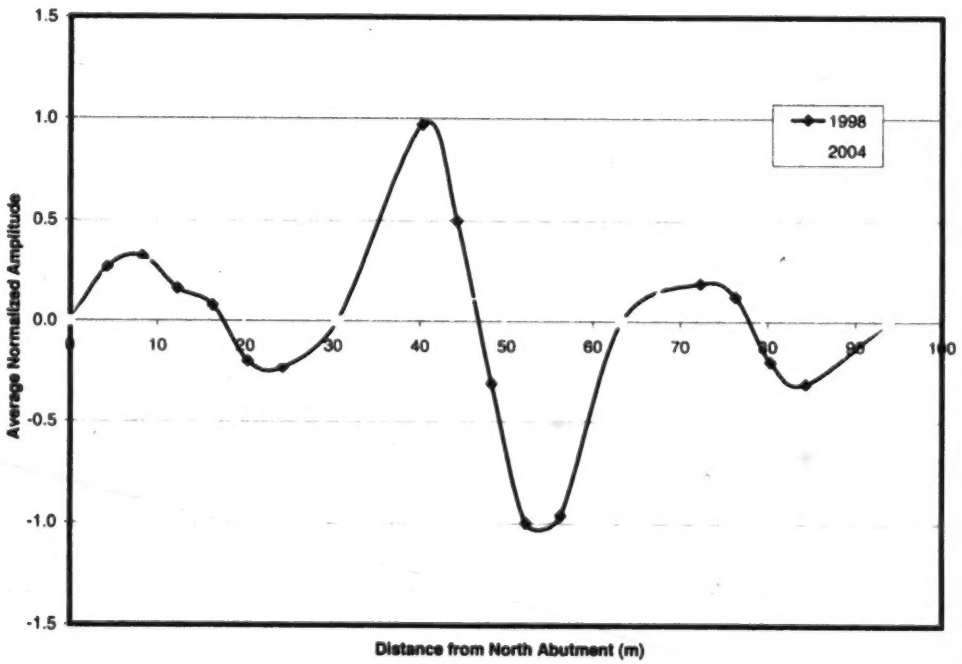

Figure 5.8 - 4th Torsional Mode Shape: Comparison of 1998 and 2004 Results

5.3.4 Discussion of Ambient Vibration Results

In the literature, there are several explanations for observed changes in natural frequencies. In addition to changes in bridge stiffness due to cracking or structural damage, the dynamic behaviour of a bridge may also be influenced by environmental factors. In particular, changes in the ambient temperature are very important because it changes boundary conditions and induces axial stresses within the bridge deck. In the case of asphalt, temperature changes can greatly affect the material stiffness and properties. However, concrete material properties are not significantly affected by temperature changes. Cunha et al. (2003) and Peeters et al. (2001) found that for a temperature range of 50°C during ambient vibration tests for the Z24 Bridge in Switzerland, the first natural frequency varied by as much as 0.5 Hz. The relationship was bilinear and most of the variation in the natural frequency occurred between 0°C and –5°C. Careful analysis showed that non-linearity was related to the variation of thermal inertia of the thick asphalt layer and concrete deck. Below freezing, the asphalt layer was found to contribute significantly to the overall stiffness of the bridge. The second natural frequency was also bilinear, however, the value increased during positive temperature increases.

Desjardins et al. (2000) also noted significant variability in modal parameters from various monitoring datasets obtained from the Confederation Bridge in PEI. He concluded that observed changes in modal or dynamic properties were a result of the following effects:

- Environmental effects such as temperature, relative humidity, wind
- Differences in the loading scenarios
- Computational inaccuracies and modeling assumptions
- Stiffness degradation due to deterioration or damage

One of the most notable damage detection tests was first completed by Farrar et al. (1999) on the I-40 Bridge in Albuquerque, New Mexico. Significant findings from their research can be used to explain changes in the ambient vibration data obtained from the

Crowchild Trail Bridge. For the I-40 Bridge tests, significant changes in natural frequencies and mode shapes were observed only after large amounts of structural damage had been induced; even then the natural frequency changes were less than 8%. It was noted that differences in obtained data are inevitable with test-to-test repeatability and changing test conditions. For future tests, they recommended that the sensitivity of modal test results to environmental conditions and test procedures be quantified. They also noted that a temperature differential of 25°C influenced the natural frequency of another bridge by as much as 0.4 Hz. Ward (1984) reported that under normal circumstances the stiffness of a bridge should decrease as it cracks or corrodes away, however, this tendency could be masked by changes in the support conditions.

Therefore, changes in the Crowchild boundary supports and ambient conditions may have contributed to the observed changes in natural frequencies. Clearly, variations in the natural frequencies and mode shapes of the Crowchild Trail Bridge over time are not strictly related to changes in stiffness or structural damage. Changes in support conditions, temperature, other environmental factors, and test procedures may also contribute to variability in the measured dynamic behaviour.

5.4 Comparison of Static Loading Results

Static loading tests have been performed three times since the Crowchild Trail Bridge was constructed. In all of the static loading tests from 1997, 1998, and 2004 the truck weights were relatively the same as summarized in a previous section. In this section, maximum strains and deflections, girder strain distributions, and girder neutral axis locations will be compared.

5.4.1 Comparison of Maximum Static Strain Readings

Table 5.4 compares the maximum strain results from 1997, 1998, and 2004 caused by the static truck loadings. It is important to note that the results in the table do not specify if the strains are in tension or compression. Overall, the results from the various tests indicate that all of the obtained strain data is reliable and the differences in strain range for most of the bridge components is relatively small.

Table 5.4 - Absolute Maximum Measured Static Strains

Gauge Type/Location	Maximum Static Strains		
	1997 Strains (με)	1998 Strains (με)	2004 Strains (με)
G3 – Girder 1 web	103.0	97.1	89.4
G33 – Girder 1 flange	94.0	100.5	92.9
G34 – Girder 1 flange	97.0	108.7	101.3
T3 – Steel Strap 8	57.0	89.2	79.2
RC1 – GFRP bar	120.0	39.8	58.1
E13 – Concrete deck	90.0	20.7	24.6
S4 – Steel stud	24.0	16.0	9.5
C4 – Cross frame	64.0	58.4	63.5
RS2 – Smart bar	34.0	31.5	13.5

The highest girder strains were recorded during the 1998 static loading tests. However, there is less than a 10% difference in measured girder strains between 1997, 1998, and 2004. The relatively small differences in measured girder strains may be attributed to the slight variability in truck weights and truck loading location, and very slight differences in bridge stiffness. It is also important to note that the static load point locations may not cause the highest strains; the maximum strains may occur at a truck position between designated loading points. Overall, this comparison indicates that the condition of the bridge girders has remained unchanged during the first seven years of service life. In previous reports, it was concluded that the measurements from strain gauges G33 and G34 were unreliable due to poor connections with the steel girder. Although tension strains in gauge G33 are consistently lower than gauge G34, an average of the two strain readings gives a clear indication of the girder flange behaviour.

Strains in the other monitored components have not changed significantly between 1998 and 2004. Strains in the other steel members, the cross-frame, steel strap, and steel studs, are nearly identical for the 1998 and 2004 results. For example, the gauges located on

Steel Strap 8 indicated the it cycled between strains of –15 με and 85 με as the truck travelled across the entire length of the bridge in 1998. In 2004 the strains in the steel strap ranged between –5.8 με and 79.2 με. This relatively low strain cycle indicates that the steel straps behaved well within the elastic range and fatigue was not critical during service loading. However, these measured strains are approximately double the strain values produced under similar loading in 1997. Higher strains in the steel straps indicate that arching action within the deck is more prominent since 1997.

5.4.2 Comparison of Deflections and Girder Load Sharing

Significant changes in the bridge stiffness over time can be detected by analyzing the load sharing between the girders. First, it is important to summarize again the differences in each of the load tests. In the 1997 test, the passenger-side wheels were positioned approximately 750 mm from the edge of the bridge barrier. However, in the 1998 and 2004 tests, the passenger-side wheels of the truck where positioned further away from the edge of the bridge barrier at a distance of 1000 mm. As summarized in a previous section, the 1998 truck was approximately 4000 kg heavier than the 1997 truck. In turn, the 2004 loading truck was approximately 2000 kg heavier than the 1998 truck or 6000 kg heavier than the 1997 truck.

Figure 5.9 highlights the load sharing between girders based on the deflection measurements from 1997, 1998, and 2004. As seen in the figure the load sharing characteristics among the girders had not changed significantly from 1997 to 2004. At a transverse section, the deflected shape of the girders is very close to a straight line. Load sharing is characterized by the load–carrying contribution of girders not directly loaded by the truck. Adequate load sharing among the girders suggests a relatively stiff deck in the transverse direction from 1997-2004. Within the first year of service, no deterioration had been observed in load sharing among the girders. Since the truck was positioned closer to Girder 1 during the 1997 load tests, the deflection under Girder 1 is slightly larger compared to the 1998 load tests. Due to the eccentricity of load, however, the deflection under Girder 5 was less in 1997 compared to 1998 and 2004.

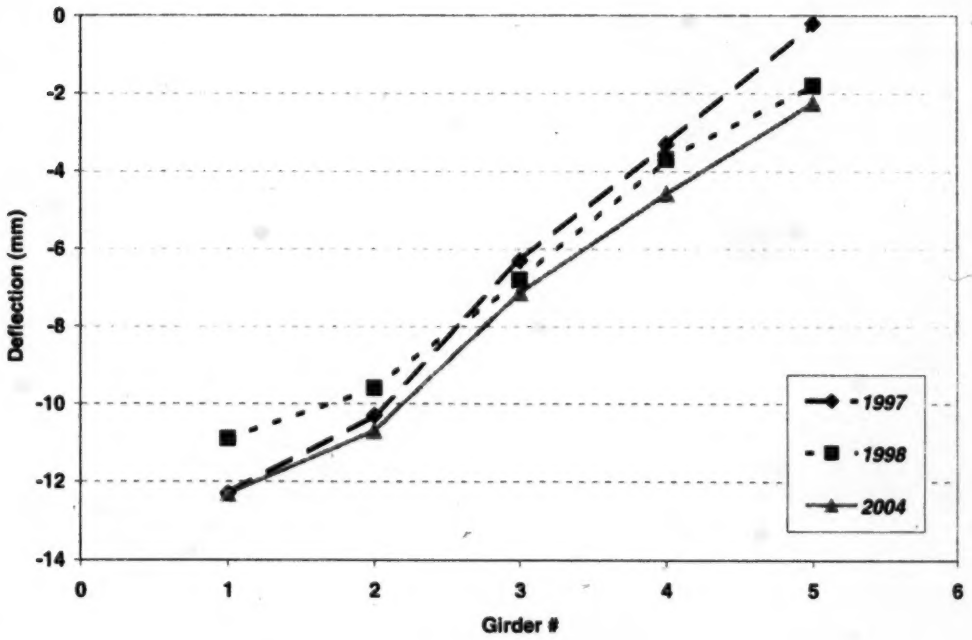

Figure 5.9 - Girder Deflection Comparisons

It is also interesting to compare the maximum deflections measured in Girder 1 during each of the load tests. The maximum downward deflections measured were 12.3 mm, 10.9 mm, and 12.3 mm for the 1997, 1998, and 2004 load tests respectively. Differences between the 1997 and 1998 deflection results can be attributed to the position of the loading truck. Deflections in Girder 1 were the same for the 1997 and 2004 test results. However, due to the position of the loading truck and eccentricity of the load in 1997, the deflections measured in the other girders are lower compared to the 2004 results. Also, the average deflection of all the girders is the highest in the 2004 results because the heaviest truck was used during these tests.

5.4.3 Comparison of Strain Distributions and Neutral Axis Location

One of the most important aspects that can be observed from the health monitoring data is the girder strain distribution. Figure 5.10 shows the strain distribution across Girder 1

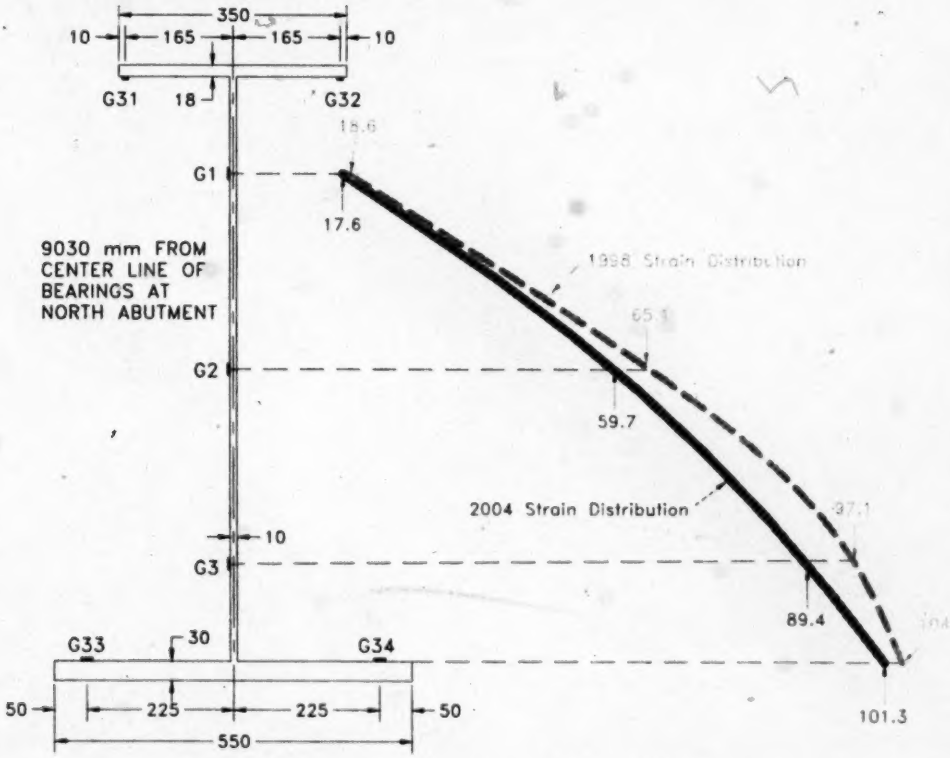

Figure 5.10 - 1998 vs. 2004 Positive Strain Region Comparison

in the positive moment region of the bridge span for 1998 and 2004 results. Results from the 1997 data are not shown as the strain values were nearly identical to the 1998 data. As seen in Figure 5.10 the strain values were relatively close between the two tests. Since strain gauges G31 and G32 were not reliable, the data obtained from the top flange is not shown. Both sets of data show that the strain distribution is consistently linear. From the 1997 & 1998 data, the neutral axis is located approximately 55 mm below the bottom face of the flange. By looking at the 2004 data, the neutral axis was found to act at approximately the same girder cross-section location. These results suggest that there

has been no change in composite action of the bridge in the positive moment region. Here the concrete deck and steel girders both resist the longitudinal moment. Overall, longitudinal composite action between the concrete deck and the steel girders has not deteriorated significantly in the positive moment region during the first seven years of service life.

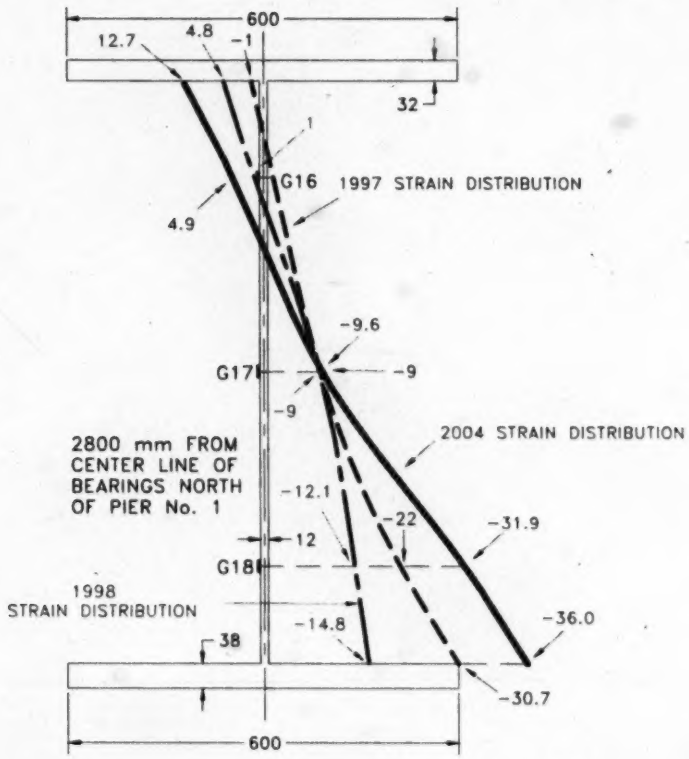

Figure 5.11 - 1998 vs. 2004 Negative Strain Region Comparison

Strain distributions were also compared in the negative moment region near the pier supports. Figure 5.11 shows the three separate strain distributions obtained from the 1997, 1998, and 2004 load tests. All strain distributions are approximately linear across the girder cross-section. Since there were no strain gauges placed on the girder flanges in the negative moment region, flange strains shown in the figure were extrapolated from the web strains. In the negative moment region, the neutral axis location has changed significantly over the last seven years. In 1997, the neutral axis was located approximately 120 mm below the bottom face of the top flange. In 1998 the neutral axis had shifted 70 mm further down to 190 mm below the bottom face of the top flange. In 2004 the neutral axis had shifted an additional 60 mm to approximately 250 mm below the bottom face of the top flange. These results suggest a steady loss in the composite action between the concrete deck and the steel girders in the negative moment region where the concrete is mostly in tension.

To estimate the approximate percentage of composite action between the concrete deck and the steel girders in the negative moment region over time, two assumptions are made: 100 % composite action occurred in 1997 and 0 % composite action would result if the neutral axis was located at 480 mm below the bottom surface of the top flange (this is the neutral axis of just the steel girder without the presence of concrete). Therefore the composite action between the steel girders and the concrete deck was approximately 80% in 1998 and 64% in 2004. As the composite action in the negative moment region has reduced over time, the girders have become the primary load-carrying structural component in the longitudinal direction. Increased girder web strains from the tests results and the changing location of the neutral axis support this conclusion. Strain results from 2004 indicate that the steel girder carries most of the longitudinal moment in the negative region.

5.5 Crack Mapping Analysis Over Service Life

5.5.1 Introduction

There are several causes of concrete cracks in the bridge deck: overloading, construction-induced, fatigue, chloride contamination, carbonation, freeze-thaw, plastic shrinkage, settlement, long-term drying shrinkage, and early thermal contraction. All concrete components that are not fully prestressed will develop cracks during the early stages of high service loading. Until crack propagation stabilizes, the behaviour of the concrete component remains inelastic. When crack development stabilizes, the structure behaves elastically. However, if crack development continues indefinitely, the structural health of the bridge is questionable. If special provisions are not made in an attempt to control cracking, cracks are typically fewer and wider. On the other hand, if special provisions are implemented to control cracks, concrete-cracking widths will generally be within serviceability limits. Therefore, a significant amount of information can be learned about the structural health of the Crowchild Trail Bridge from the crack layout and rate of crack growth within the deck.

Over the first seven years of service life, crack mapping of the underside of the Crowchild Trail Bridge deck has been inspected and recorded five times. The first complete crack mapping was documented in August 1997 immediately before the bridge was opened to traffic. The crack mapping was completed again in August 1998 after one year of operation. Crack mapping was completed three more times in June 1999, July 2002, and most recently in June 2004. As a result, the location, size, and rate of crack growth has been documented throughout the life of the bridge. Each of the bridge spans was constructed using different materials and, therefore, the crack behaviour is slightly different for each span. With the existence of longitudinal cracks in the deck in 1998, it was concluded that the contribution of concrete in transferring shear had reduced after one year of operation. Crack patterns of the south, middle, and north spans are presented in Figures 5.12, 5.13, and 5.14 respectively.

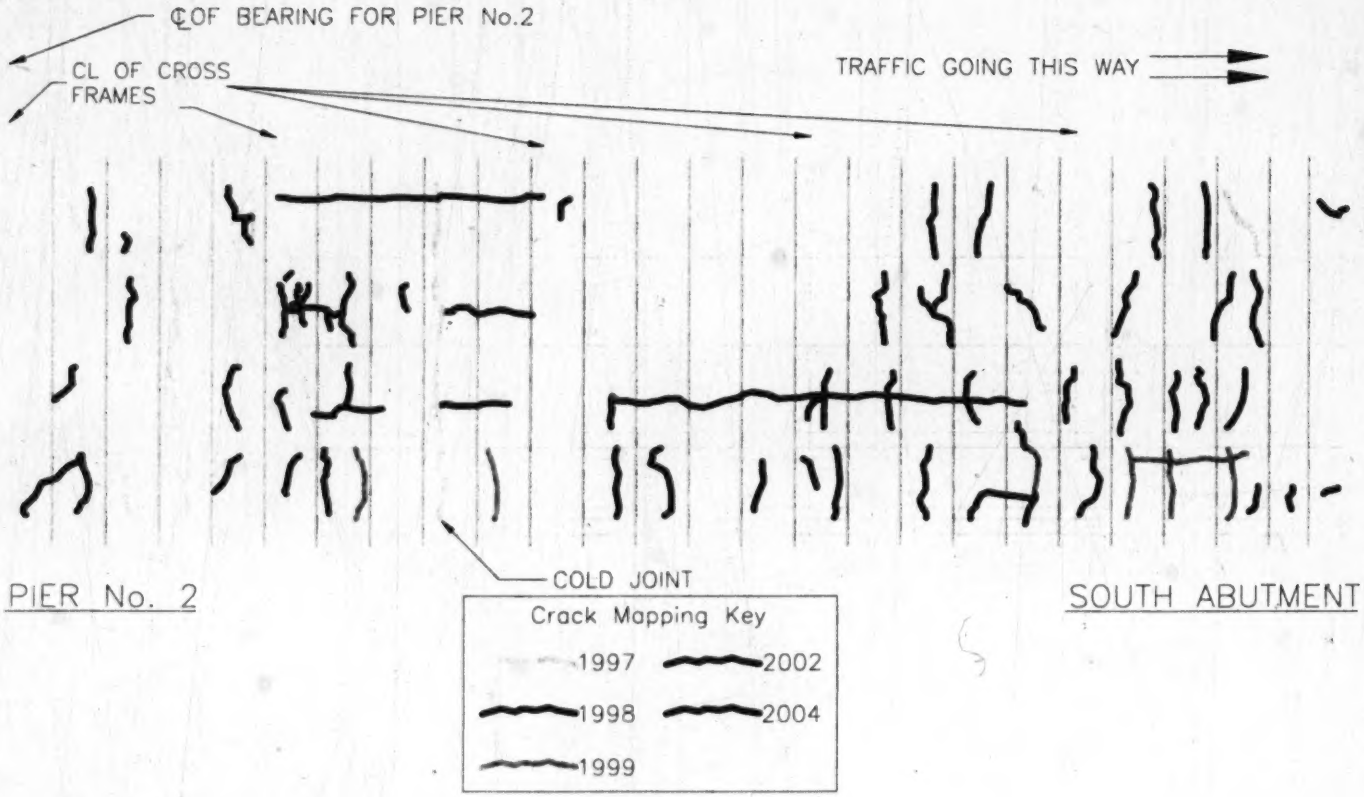

Figure 5.12 - South Span Crack Pattern

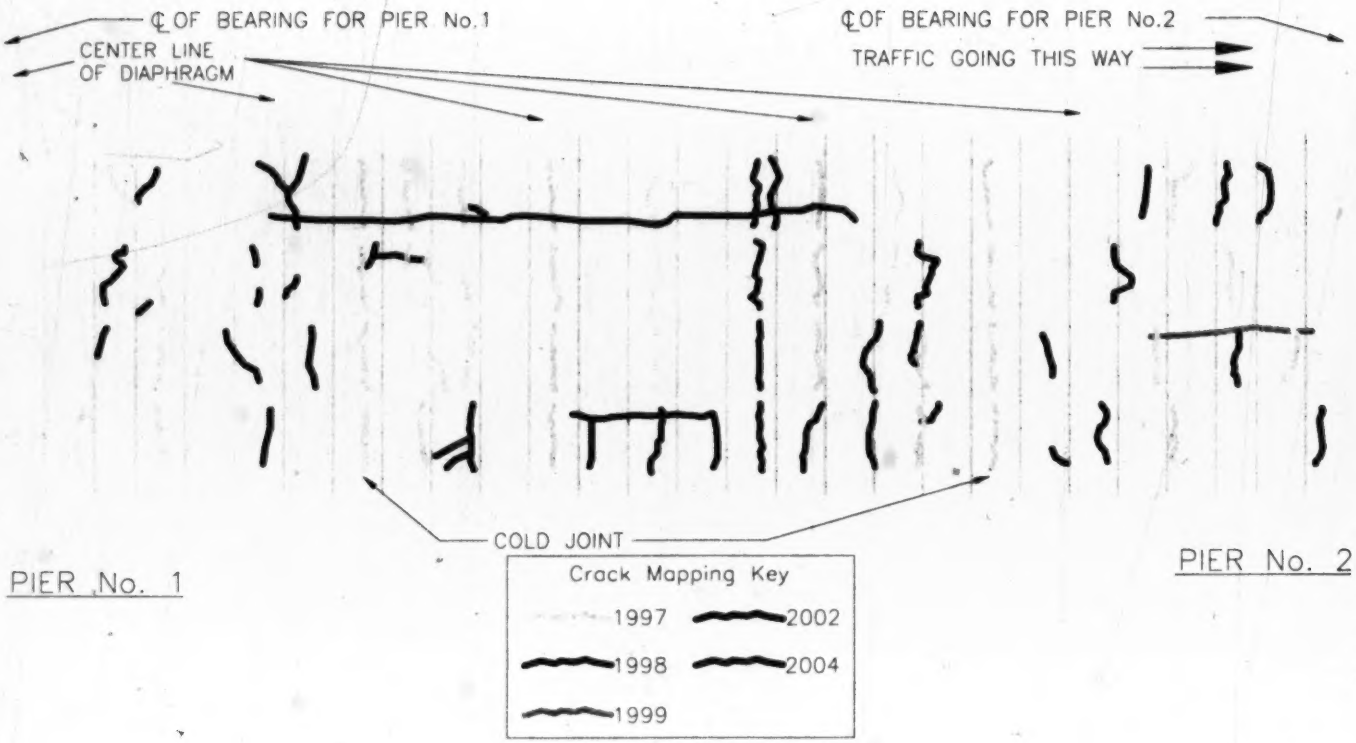

Figure 5.13 - Middle Span Crack Pattern

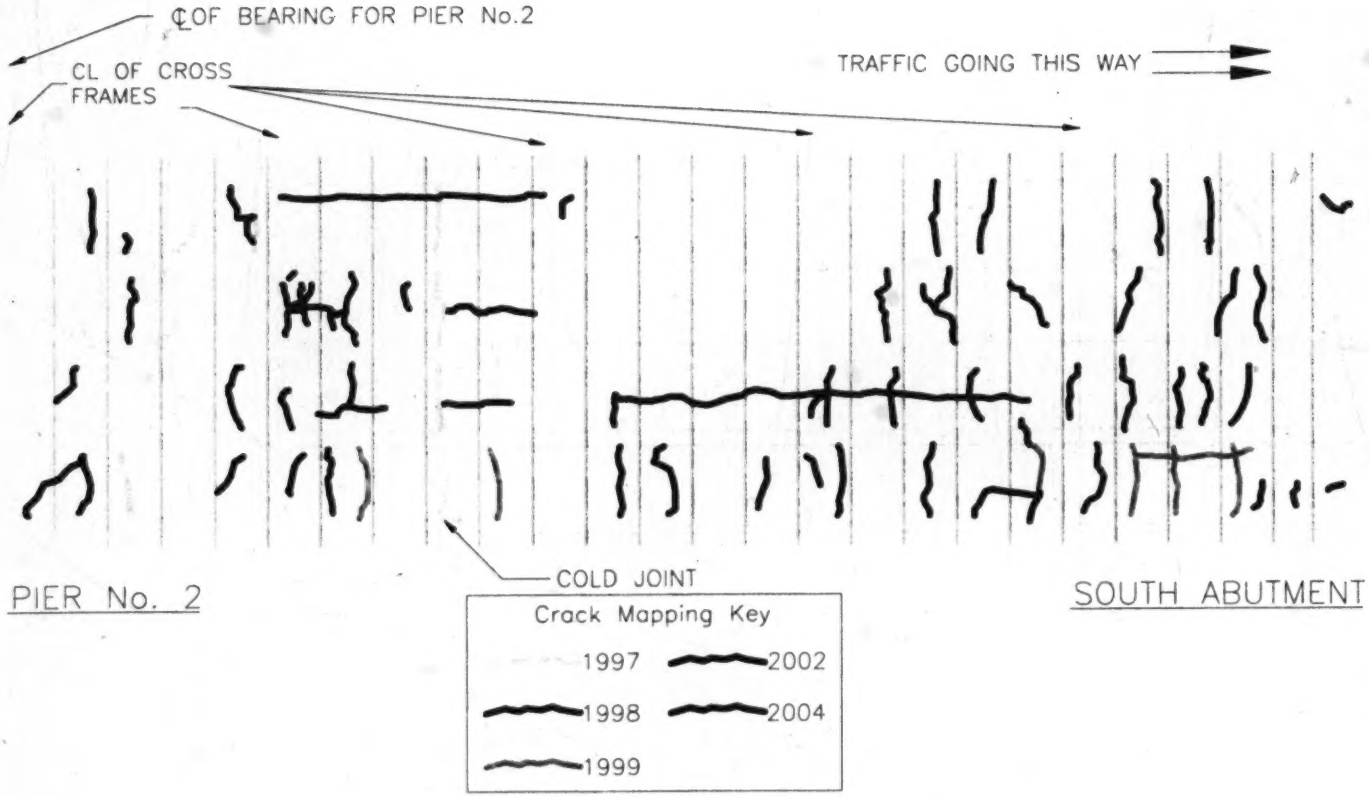

Figure 5.14 - North Span Crack Pattern

5.5.2 South Span: Crack Mapping

The south span (Figure 5.12) measures 30230 mm in length and is partially reinforced with GFRP bars. However, internal steel reinforcement was also used in this portion of the bridge deck. Very few transverse cracks were located in this span immediately after construction; the majority of cracks that had formed were located near Pier 2. Similar to the other two spans, a relatively large number of new transverse cracks had formed after a year in the south span. This span contained the least amount of longitudinal cracks compared to the other spans. However, it was the only span at this time with a longitudinal crack between two plate girders that was not adjacent to the haunched portion of the deck. In June 1999, a few new transverse cracks had formed, primarily between Girders 1 and 2. A small longitudinal crack had formed in this region as well. Several new transverse cracks had formed in July 2002. In addition, one of the longitudinal cracks had extended in this span. However, by June 2004, the rate of crack formation and crack growth in this span had significantly decreased. Only a few new transverse cracks had formed, primarily between Girders 2 and 3.

5.5.3 Middle Span: Crack Mapping

The middle span (Figure 5.13) is the longest span at 32828 mm and is reinforced with GFRP bars in the negative moment regions and transverse cantilever areas. However, no internal steel reinforcement is present. In 1997, this span had the most number of transverse cracks, however, no longitudinal cracks were detected. Most of the transverse cracks in this span were less than 0.5 mm in width. Similar to the north span in 1998, a large number of new transverse cracks had formed in the middle span within the first year of service. Existing cracks had also grown twice in width compared to the previous year. By 1998, the middle span had the largest number of transverse cracks compared to the other two spans. Only two longitudinal cracks had formed in the middle span and each crack ran approximately halfway along the length of the bridge. These cracks also ran adjacent to the haunched sections of the bridge deck. In June 1999, virtually no new cracks were identified or documented. However, this span is the most difficult to inspect as University Drive runs directly under the middle span of the Crowchild Trail Bridge.

Three years later, in July 2002, few new transverse cracks were identified. Again in June 2004, few additional transverse cracks were noted to have formed.

5.5.4 North Span: Crack Mapping

Finally, the north span (Figure 5.14) is 29830 mm long and is reinforced only in the transverse cantilever areas with GFRP reinforcement. When crack mapping was completed for the first time in 1997, there were only a few transverse cracks near Pier 1. At this time, this span had the smallest amount of cracks. In August 1998, after the first year of service, a significant number of new cracks had formed in both the transverse and longitudinal directions. Transverse cracks that had been documented the previous year expanded twice in width. Three new longitudinal cracks ran the entire length of the span and had formed adjacent to the haunched portion of the concrete deck. When crack mapping was completed again in June 1999, a fourth longitudinal crack had formed. With the addition of this crack, longitudinal cracks were present in the concrete deck between all of the plate girders. Few new transverse cracks were noted in this region. The propagation of cracks in 1999 was considerably smaller than that in previous years. In July 2002, more transverse cracks had formed after three years. Finally, in June 2004, relatively few new transverse cracks had formed and only one of the longitudinal cracks had extended further along the span.

5.5.5 Crack Mapping Summary

Overall, these inspections indicate that the rate of crack formation and crack growth had significantly decreased by 2004. Transverse cracks that had formed before the first crack mapping stage were likely due to shrinkage of the concrete. Crack growth and the formation of new cracks were likely due to cyclic traffic loading and freeze-thaw cycles throughout the year. Temperatures typically fall to –30°C in the winter and may be as high as +30°C in the summer. However, the black asphalt surface of the deck tends to absorb the sun's radiation causing the deck surface temperature to be significantly higher. Cold joints were identified at two locations in the middle span and one location in the south span. These joints had formed between separate poured sections of the concrete

deck. Cracks are noticeable because the adjacent concrete pours did not properly bond together.

Figures 5.15 and 5.16 summarize the rate of longitudinal and transverse crack formation respectively in each of the spans. The crack lengths were estimated from the crack

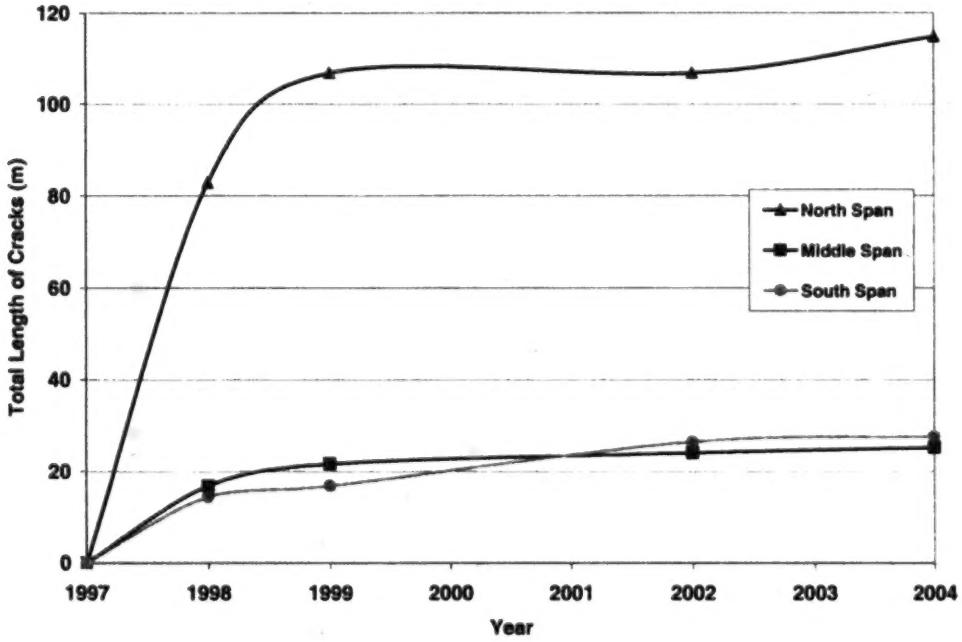

Figure 5.15 – Rate of Longitudinal Crack Formation

mapping plots. As shown in Figure 5.15, most of the longitudinal crack formation occurred within the first two years of service. During the last five years of service, relatively few new longitudinal cracks have formed. The north span contained significantly more longitudinal cracks compared to the other two spans. Approximately 25 meters of longitudinal cracks were observed in the middle and south spans by 2004. As shown in Figure 5.16, the amount of transverse cracking was relatively the same in all the spans. The north span contained the least amount of transverse cracks by 2004. However, both the middle and south spans contained approximately 100 meters of transverse cracks by 2004.

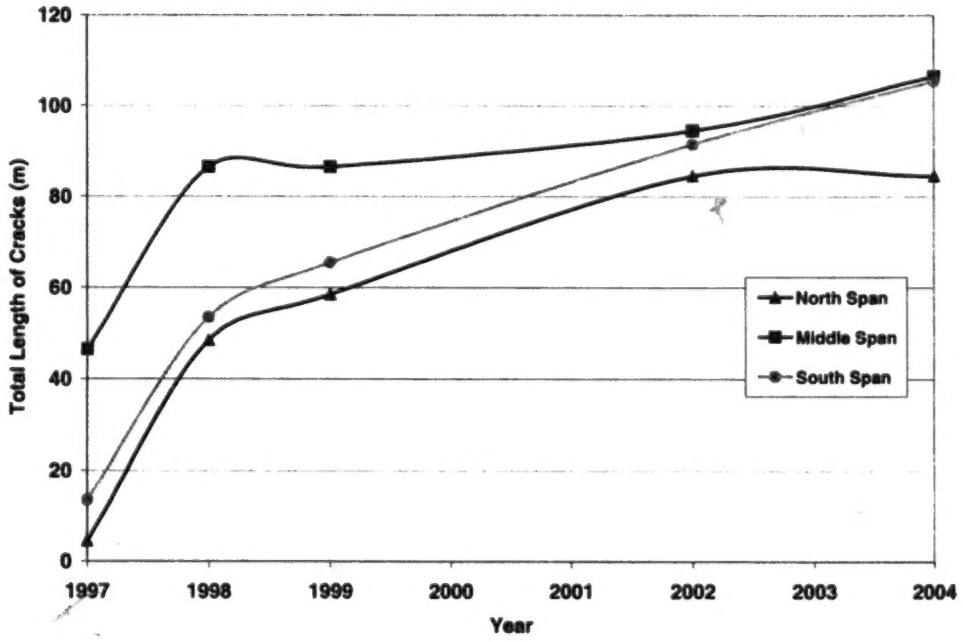

Figure 5.16 – Rate of Transverse Crack Formation

In summary, the north span, which was constructed with the least amount of internal reinforcement (reinforced only in the cantilever edge with GFRP reinforcement), contained the largest number of longitudinal cracks. However, the north span contained the least amount of transverse cracks compared to the other two spans. The middle span, which was partially reinforced with GFRP bars, contained the most amount of transverse cracks compared to the other two spans. It is interesting to note that the south span, which contained the largest amount of internal reinforcement, had the least amount of cracks after seven years of service. Overall, very few new cracks are expected to form within the entire bridge deck in the near future. Also, existing cracks are not expected to increase in size significantly.

6.0 NUMERICAL MODELS OF CROWCHILD TRAIL BRIDGE

6.1 Introduction

Numerical modelling is a powerful tool for predicting structure load response and determining the potential effects of damaged structural members. Several types of programs are available today to model a wide variety of structures, including bridges. For structural evaluation, however, the finite element approach is the most accepted type of modelling to compare measured and calculated data. According to the evaluation of the measured data, the finite element model can be improved to match as best the actual behaviour of the monitored structure. Once the finite element model has gained a certain level of completeness and validity, it provides the basis for analytical prediction and simulation. With respect to steel-free decks, numerical modelling is an effective method for parametric studies and determining overall behaviour.

Predicted natural frequencies and modes of vibration are some of the most useful parameters obtained from computer models. In combination with accurate numerical models and their predicted vibration characteristics/modal parameters, experimental modal analysis techniques can be used to identify structural damage. This type of analysis avoids traditional non-destructive techniques, such as acoustic, magnetic, thermal, and X-ray methods, which are expensive and difficult to implement for global long-term bridge monitoring. In addition, this method does not rely on visual inspection techniques that are often inadequate when the damage is invisible to human eyes.

Several numerical models of the Crowchild Trail Bridge have been constructed during the last five years. These projects include several 2-D and 3-D analytical models created at the University of British Columbia, a numerical damage detection MATLAB model created at Carleton University, and a S-Frame finite element model created at the University of Alberta. Descriptions and significant findings of each of these models will be discussed.

6.2 UBC Dynamic Computer Models

6.2.1 UBC Dynamic Model Description

Onur et al. (1999) completed a correlative study that compared the measured dynamic characteristics of the Crowchild Trail Bridge with 2-D and 3-D analytical models created by four engineering groups. Dynamic characteristics that were analyzed included natural frequencies and mode shapes. Field results were used to calibrate the 2-D and 3-D analytical computer models. The effects of various modeling assumptions on the computed dynamic characteristics of the bridge were investigated. Table 6.1 lists the software programs and the various material properties that were assumed by the four engineering teams involved in the study. Poisson ratios for the various materials are also summarized. All of the engineering groups were required to build one 2-D model and one 3-D model.

Table 6-1 – UBC Models: Material Characteristic Assumptions

Engineering Group	Modelling Program	Material Characteristic Assumptions			
		Poisson Ratio	$E_{DECK\ CONRETE}$	$E_{PIER\ CONCRETE}$	E_{STEEL}
Engineering Group 1	SAP 90	0.2	28,288 MPa	14,790 MPa	200,000 MPa
Engineering Group 2	SAP 2000	0.2 , 0.3	35,355 MPa	35,355 MPa	200,000 MPa
Engineering Group 3	SAP 90	0.25	42,000 MPa	27,400 MPa	200,000 MPa
Engineering Group 4	ANSYS 5.3	0.2 , 0.3	35,000 MPa	35,000 MPa	200,000 MPa

For the 2-D models, the engineering groups assumed the various material properties summarized in Table 6.1. Engineering Groups 1 and 3 created a 2-D model with beam elements and lumped mass at 18 nodes. However, the 2-D models created by Engineering Groups 2, 3, and 4 used beam elements with a distributed mass.

In all of the 3-D models, shell elements were used to model the steel-free deck and piers while beam elements were used to model the steel girders. Engineering Group 1 assumed a slab thickness of 150 mm and composite action was assumed between the deck and the girders. Also, abutments were modelled as pinned supports and the pier footings were modelled as fixed supports. Engineering Group 2 calculated an equivalent slab thickness for the haunched slab of 240 mm. Composite action was assumed between the deck and the girders. Abutments were modelled as roller supports and the pier footings were modelled as pinned supports. Engineering Group 3 used a slab thickness of 185 mm. No composite action was assumed between the deck and the girders. The north abutment and pier footings were modelled as fixed supports. However, the south abutment was modelled as a pin support. Engineering Group 4 used a uniform slab thickness of 185 mm. No composite action was assumed between the deck and the girders. The abutments and piers were both modelled as pinned supports.

6.2.2 UBC Computer Model Results and Conclusions

Natural frequencies values and modal shapes predicted by the analytical models were compared with measured field properties. The Modal Assurance Criterion (MAC), the Coordinate Modal Assurance Criterion (COMAC), and the Modal Scaling Factor (MSF) methods were used to compare the analytical and measured modal shapes.

The 2-D models could not show torsional modes. In addition, other natural frequencies did not exhibit good correlation with the measured frequencies. Overall it was found that the 3-D models were far more accurate in predicting the dynamic properties of the actual bridge. Vertical modes were the easiest to predict using the models. Transverse mode shapes had the poorest match with the measured results. Higher natural frequencies were difficult to capture through field measurements and were not compared with the models.

When considering only the natural frequencies, the 3-D model created by Group 2 exhibited the best correlation of dynamic properties with the measured results. However, based on the MAC results, the model's correlation decreased in the higher modes after good correlation shown in only the first three mode shapes. MAC results for the 3-D

model created by Group 3 exhibit better correlation with the measured mode shapes. As summarized earlier, Group 3 modelled the north abutment and pier footings as fixed supports, the south abutment as a pin support, and assumed a uniform deck thickness of 185 mm. Therefore, the support and material assumptions of Group 3 were the most accurate for dynamic modelling of the Crowchild Trail Bridge.

It was concluded that the use of a mode shape correlation technique in addition to the comparison of natural frequencies is essential in the calibration of analytical models with experimental data. Results of the study provide some guidelines to properly calibrate bridge computer models for structural dynamic analysis. First, a good match of the experimental and analytical natural frequencies of the bridge is necessary. In some cases, a good match in frequencies between the experimental and analytical results does not necessarily correspond to good agreement with the measured mode shapes. If the two conditions are not met, inaccurate conclusions about the real behaviour of the bridge will be obtained from a numerical model.

6.3 Carleton University Damage Identification Models

6.3.1 Carleton University Model Descriptions

Bagchi et al (2004) investigated the application of vibration based damage identification (VBDI) techniques in health monitoring of the Crowchild Trail Bridge. Vibration based damage identification techniques can determine the location and severity of damage based on the differences in vibration characteristics of a healthy and a damaged structure. Although there are several techniques available for vibration based damage identification, the modal strain energy and matrix updates methods were selected because of their relative advantages. The modal strain energy method compares modal strain energy in members before and after damage occurs. Matrix update methods are based on the determination of perturbations in the property matrices. Damage in the structure may change both the stiffness and the mass matrices, altering the frequencies as well as the mode shapes.

Two types of Crowchild Trail Bridge models were developed. First, a detailed finite element model was created using a MATLAB based program. Three-dimensional beam elements were selected to model the piers, girders, diaphragms, cross-frames, and steel straps. Shell elements were chosen to model the deck and side barriers. Deck elements were connected to the girder elements by rigid beam elements. The density of steel was assumed to be 76 kN/m^3 and the concrete density was assumed to be 24 kN/m^3. In total, the finite element model contained 351 elements and 247 nodes. Piers were assumed fixed at their base, while roller and pin supports were assumed to exist at the north and south abutments respectively.

In addition, an equivalent continuous beam model was constructed and correlated with the first number of flexural modes. This model was greatly simplified compared to the detailed finite element model. The simplified beam model was constructed using three types of equivalent steel beam sections and used only 15 elements in total. Equivalent section properties were calculated based on the actual girder and deck properties.

6.3.2 Model Calibration with Field Results

Two MATLAB finite element models, CC-97 and CC-99, were correlated with 1997 and 1998-1999 field data so that their behaviour would closely resemble that of the actual bridge for the given year. It is important to note that only the dynamic characteristics of the models were compared to the field results. In both models, the stiffness of individual elements was modified using model update and correlation methods. These methods optimized the stiffness values to obtain the best match of modal frequencies of the system. Table 6.2 shows the field and model natural frequencies

As shown in Table 6.2, the CC-97 was used as the base model for the undamaged structure and assumed the concrete was uncracked. The model natural frequency results closely match the 1997 field results. Individual member properties were modified for the CC-99 model to simulate the cracking of concrete and the overall changed behaviour of the bridge. With the correlation methods, the model natural frequencies exactly matched the 1998-1999 field results.

Table 6.2 – Carleton University Results: Natural Frequencies

Bridge Model	Mode	Natural Frequencies (Hz)	
		Field Results	Model Results
CC-97 • concrete uncracked • undamaged base model	1	2.78	2.78
	2	3.13	3.13
	3	3.76	3.72
	4	4.05	4.03
CC-99 • 10% reduced deck stiffness (POS) • 30% reduced deck stiffness (NEG) • 20% reduced barrier stiff. (POS) • 30% reduced barrier stiff. (NEG) • 10% reduced pier stiffness	1	2.60	2.60
	2	2.90	2.90
	3	3.63	3.63
	4	3.85	3.85

For the simplified beam model, several iterations were performed in order to achieve good correlation between the analytical and experimental frequencies of the first three flexural modes. Section properties were manually modified in order to properly model the minor concrete cracking in the positive moment region and the large amount of concrete cracking in the negative moment region.

6.3.3 Vibration Based Damage Identification Testing and Results

The applicability of VBDI techniques to the large and complex Crowchild Trail Bridge structure was considered. Two damage cases were considered to evaluate the effectiveness of vibration based damage identification techniques. The first case simulated damage by reducing the stiffness in some sections of the longitudinal girders by 30%. The second case simulated damage by reducing the stiffness in a section of the concrete deck by 30%. For the CC-97 model, the first four natural frequencies decreased slightly as a result of the damage cases considered. Similarly, for the CC-99 model, the natural frequencies decreased for the damaged girder scenario.

Next, the modified damage index was used for damage localization and the matrix update method was used to estimate the severity of the damage. The damage index method was found to successfully identify the correct damage locations. In addition, the matrix update method also gave a very good measure of the damage extent. However, it was determined that measurement noise, incomplete modes, combined with the complexity of a detailed finite element model affected the performance of the VBDI techniques used. In the simplified beam model, it was found that VBDI techniques could give a reasonable estimate of both the location and severity of the damage.

In summary, it was found that only realistic adjustments in the element stiffness had to be made in combination with fine-tuning of physical properties in order to properly correlate the model with field results. However, the models did not reflect changes in environmental factors, temperature changes, changes in boundary conditions, and nonlinearities caused by cracking. Overall, VBDI methods were successful in identifying the location of damage in the Crowchild Trail Bridge models if the damage was relatively large and the modal strain energy contribution of the element was significant. However, due to the large number of degrees of freedom and complexity of the Crowchild Trail Bridge finite element model, VBDI techniques were not always successful in determining damage. VBDI techniques were found to be more successful in the simpler equivalent beam model despite incomplete and noisy modes of the damaged structure.

6.4 U of A S-Frame Finite Element Model

6.4.1 U of A FEM Description

A three-dimensional finite element model (FEM) was created at the University of Alberta by Afhami et al. (1998). The FEM model was constructed using the software analysis program S-Frame and could accurately resemble the static and dynamic behaviour of the Crowchild Trail Bridge superstructure. Two versions of the model were initially created to match both the 1997 and 1998 field results. The model locations of the interior pier supports and truck loading were slightly modified in 2004 to more accurately reflect the bridge. These changes were found to improve the 1998 model correlation with the measured field results. The model was further modified to reflect the 2004 measured

field data. In each model version, the supports and truck loading configurations were slightly modified to more accurately reflect the actual behaviour of the Crowchild Trail Bridge. In the following section, the S-Frame bridge model is compared to 1997, 1998, and 2004 field results. Similar to the Carleton Crowchild Trail Bridge Model, dynamic characteristics of the S-Frame FEM are compared to the field results. In addition, S-Frame FEM deflections are also compared to the static field results.

Dimensions and model elements selected were the same in each version in the model. The overall model dimensions were chosen to match the exact field dimensions. The substructure of the bridge, including the piers and abutments, was not included in the model. Alternatively, a variety of pinned and fixed-type supports were chosen to accurately model the effects of the supports at the pier and abutment locations.

One-dimensional beam elements were used to model the steel girders, steel diaphragms, cross frames, and steel straps. Two-dimensional shell elements were used to model the concrete deck and barriers. A series of one-dimensional rigid elements were selected to connect the steel girder elements to the concrete deck elements. These rigid elements did not represent a particular component of the bridge, however, they were necessary in order to accurately model the physical space between the girders and the concrete deck. In this way, the composite bending and overall behaviour of the bridge could be more accurately modelled.

Several types of materials were used to accurately model the bridge. Steel, with E = 200,000 MPa and weight of 76 kN/m^3, was used to model the straps, girders, diaphragms, and cross-frames. Steel rigid elements, with E=200,000 MPa and weight of 0.01 kN/m^3, were used to model the connectors between the concrete deck and the girders. Finally, several different types of concrete were incorporated depending on the model and the region of the concrete. Concrete material was used in the deck and side barriers of the bridge model. In all of the models the concrete weight was assumed to be 24 kN/m^3. Assuming a concrete compressive strength of $f'c$ = 35 MPa, the full modulus of elasticity of the concrete (E_c) was estimated to be 26.6 GPa.

Several steel and concrete sections were used in the construction of the finite element models. Table 6.3 lists the seven steel section types, location, moment of inertia properties, and cross-sectional area. The concrete shell elements varied in thickness depending on the location of the material. For the concrete deck, a 700 mm wide sections centred over the girders were modelled using 265 mm thick concrete shell elements. These thicker areas resembled the haunched portions of the concrete deck. 185 mm thick concrete shell elements were used to model the remaining flat sections of the deck. The concrete barriers were modelled using 320 mm thick concrete shell elements that were 855 mm high. All of the deck and barrier shell elements were approximately 1030 mm long.

Truck wheel loads were modelled using a series of point loads applied at various locations on the bridge deck. Since S-Frame does not allow the application of point loads within a shell element area, equivalent point loads were calculated and positioned at the four corners of the respective shell element where the wheel load was applied. Applied loads in each of the models reflect the differences of the 1997, 1998, and 2004 truckloads.

Table 6.3 – S-Frame FEM Steel Section Properties

Section	Description	Inertia Properties (mm^4)	Section Area (mm^2)
1	Steel Girder (+ ve region) N. & S. Spans	T_c = 5,930,400 I_y = 4,785,167,000 I_z = 480,325,000	31,800
2	Steel Girder (- ve region) Over Piers	T_c = 18,046,400 I_y = 9,860,151,000 I_z = 1,260,130,000	52,800
3	Steel Girder (+ ve region) Middle Span	T_c = 3,584,566 I_y = 4,309,098,000 I_z = 324,804,200	27,800
4	Steel Diaphragm Piers and Abutments	I_y = 12,021,060,000 I_z = 1,832,407,000	76,080
5	Steel Cross-Frame (Spaced every 6 m)	I_y = 396,500,000	5,440
6	Rigid Element Connector	I_y = 360,630,600,000 I_z = 54,972,210,000	2,282,400
7	Steel Deck Straps (Spaced every 1030 mm)	I_y = 50,688 I_z = 170,368	1056

6.4.2 Differences in 1997, 1998, 2004 Model Construction

In order to match the measured field results for each year, material properties and support conditions were slightly changed for the 1997, 1998, and 2004 bridge models. The concrete modulus of elasticity was changed in each model to reflect the effects of cracking and reduced deck stiffness. In order to match the measured deflection and natural frequency results, the concrete stiffness in the negative moment region was reduced each year. The concrete stiffness in the positive moment region was only

reduced in the 2004 model. The concrete stiffness values assumed for each year are as summarized as follows:

- 1997 Crowchild Trail Bridge FEM: E_C = 80% of 26.6 GPa in positive moment region where concrete is in compression; E_C = 60% of 26.6 GPa in negative moment region to account for 1997 cracks
- 1998 Crowchild Trail Bridge FEM: E_C = 80% of 26.6 GPa in positive moment region where concrete is in compression; E_C = 20 % of 26.6 GPa in negative moment region to account for 1998 cracks
- 2004 Crowchild Trail Bridge FEM: E_C = 60% of 26.6 GPa in positive moment region where concrete is in compression; E_C = 10 % of 26.6 GPa in negative moment region to account for 1998 cracks

In previous research, summarized briefly in Chapter 5, temperature has been shown to influence material properties and, subsequently, the overall dynamic behaviour of the bridge. Unfortunately, the effects of temperature could not be modelled in the S-Frame program. Therefore changes in the measured results between the 1998 and 2004 field tests had to be modelled by changes in the support conditions in addition to changes in the concrete stiffness. Support boundary conditions in the Crowchild Trail Bridge may changed over time as a result of pier and abutment settlement, vehicle overloading, fatigue, nearby construction, and a variety of other influences.

Supports were modelled at the end of each girder by the abutments and by the interior piers. In the 1997 and 1998 bridge models, the north abutment girder pin supports are modelled to prevent movement in the vertical direction only. At the south abutment, the girder pin supports are modelled to prevent movement in the vertical and longitudinal directions. At both interior pier locations, one pin support is modelled to prevent movement in the vertical direction, and the other pin support is modelled to prevent movement in the vertical and transverse directions. For the 2004 bridge model, the north and south abutment supports were slightly modified in order to obtain the desired bridge behaviour.

6.4.3 U of A FEM Natural Frequency Results

Table 6.4 shows the natural frequencies of the first six mode shapes determined from the 1997, 1998, and 2004 bridge models. Measured bridge frequencies obtained by UBC in 1997 and the U of A in 1998 and 2004 are also presented for comparison. Corresponding dynamic mode shapes are presented on the following page in Figure 6.1. The 1997 model results were obtained from the original S-Frame FEM created by Afami and Khattak. The 1998 and 2004 model results were obtained from the S-Frame FEM modified by Van Zwol.

Table 6.4 – S-Frame FEM and Measured Natural Frequencies

Mode Shape	1997		1998		2004	
	S-Frame Model	Field Results	S-Frame Model	Field Results	S-Frame Model	Field Results
1	2.63	2.78	2.69	2.60	2.71	2.80
2	3.08	3.13	2.96	2.90	2.93	3.16
3	3.76	3.76	3.73	3.63	3.99	3.79
4	4.17	4.05	3.99	3.85	4.40	4.19
5	4.77	4.64	4.49	4.43	4.74	4.66
6	5.16	5.18	4.77	5.00	4.88	5.36

Overall, the 1997, 1998 and 2004 models accurately reflect the measured dynamic results for those years. Considering the ambient vibration results, the 1997 S-Frame model exhibits the best correlation with the measured field results while the 2004 S-Frame model exhibits the worst correlation with the measured field results. 1998 natural frequencies for the first six mode shapes were consistently lower than the 1997 results for both the field and model results. This resulted from the lower concrete stiffness assumed for the negative moment regions; 60 % E_c for 1997 versus 20 % E_c for 1998. Similar to the measured results, the 2004 model natural frequencies for the first six mode shapes were consistently higher than the 1998 results. This was a result of changes in the concrete material properties and support conditions. All of the model mode shapes shown in Figure 6.1 match the measured mode shapes.

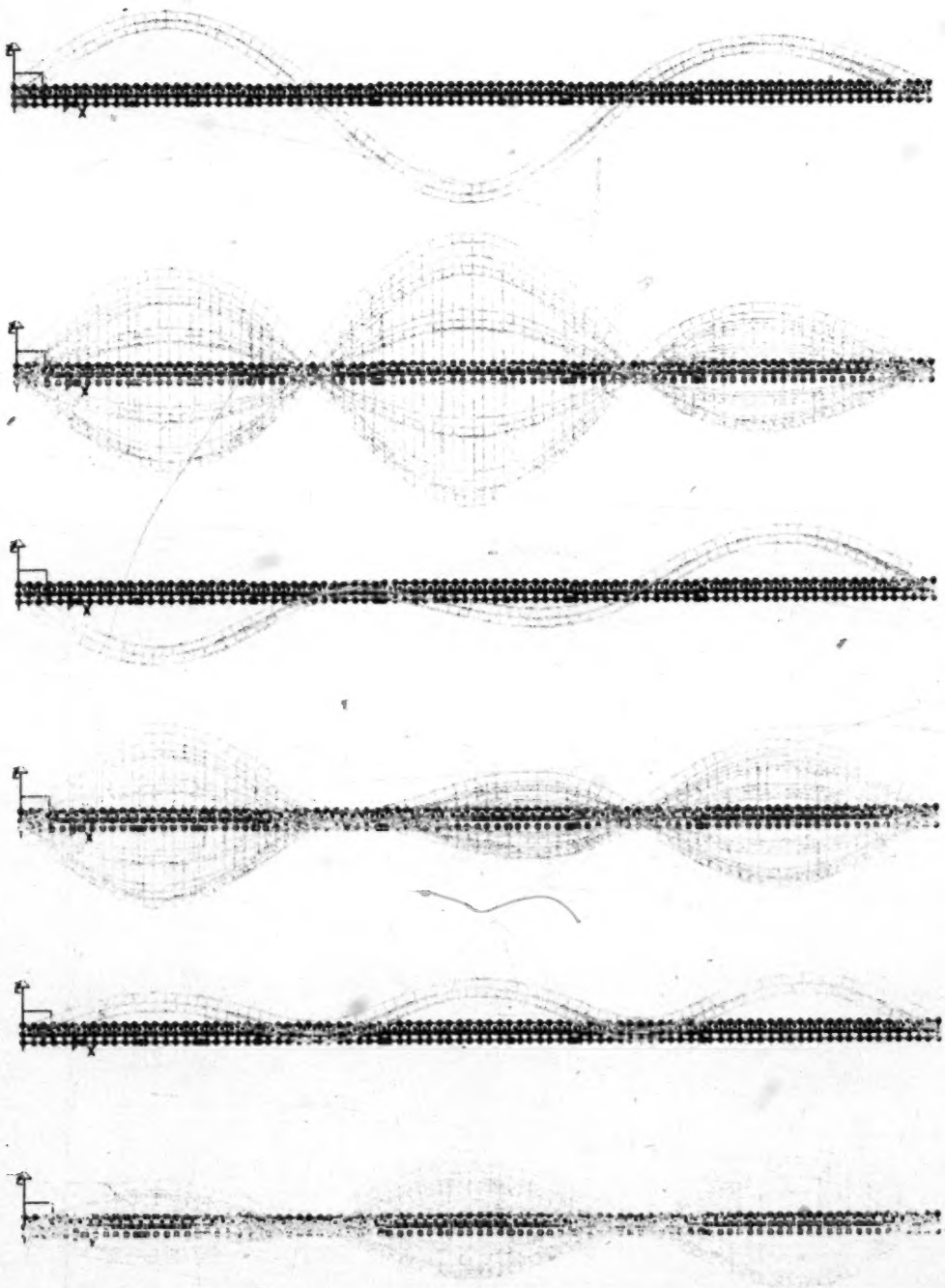

Figure 6.1 – FEM Modal Shapes of First Six Natural Frequencies (from top to bottom)

It is interesting to note that the S-Frame FEM had similar success compared to the UBC Group 2 3-D model in predicting the 1997 natural frequencies of the bridge. Although the MATLAB FEM created by Carleton University exhibited better correlation with the measured natural frequencies, no comparison was made with the measured girder deflections. The U of A S-Frame FEM exhibits satisfactory correlation with both measured natural frequencies and measured girder deflections, as will be shown in the next section.

6.4.4 U of A FEM Deflection Results

Deflections of the three S-Frame models were also compared to measured field results. Table 6.5 shows the 1997, 1998, and 2004 deflections due to truckloads determined from both the model analysis and from the measured field results. Again, the 1997 model results shown were obtained from the original S-Frame FEM created by Afami and Khattak. The 1998 and 2004 model results were obtained from the S-Frame FEM modified by Van Zwol.

Table 6.5 – S-Frame FEM and Measured Deflections

Girders	1997 Deflections		1998 Deflections		2004 Deflections	
	S-Frame Model	Field Results	S-Frame Model	Field Results	S-Frame Model	Field Results
1	8.4	12.3	10.9	10.9	9.3	12.3
2	7.4	10.3	9.5	9.6	8.3	10.7
3	5.9	6.3	7.6	6.8	6.8	7.1
4	4.3	3.3	5.4	3.7	4.7	4.6
5	2.6	0.2	3.2	1.8	2.6	2.2
Average	*5.7*	*6.5*	*7.3*	*6.6*	*6.3*	*7.4*

Since the deflections during the 1997 static test were measured using surveying equipment, these results are not as accurate or reliable compared to the 1998 and 2004 measured deflections that were obtained using cable transducers. As seen in Table 6.5,

the measured and model predicted deflection results are relatively the same. For the 1997 and 2004 models, the average model deflections are lower than the field measured deflections. For the 1998 results, the average model deflection is higher than the field measured deflections. Here the deflections of Girders 1 and 2 are identical and the deflections in the other girders are higher than the measured results. However, in the 2004 model, the deflections of Girders 3, 4, and 5 are more accurate than deflection of Girders 1 and 2. All of the models exhibit superior load sharing characteristics compared to the actual bridge.

6.5 Numerical Modeling Conclusions

All of the models presented were accurate in predicting the natural frequencies and mode shapes of the Crowchild Trail Bridge. In addition, the models were useful in determining the actual material properties of the bridge components and the effects of damage and changing boundary conditions on the overall behaviour of the bridge.

From the UBC model study, it was concluded that the use of a mode shape correlation technique in addition to comparison of natural frequencies is essential in the calibration of analytical models with experimental data. Both 2-D and 3-D models could successfully imitate the dynamic behaviour of the Crowchild Trail Bridge. MATLAB FEMs created at Carleton University exhibited the best correlation with measured dynamic results. However, static deflection results were not compared in their research, allowing for the accurate correlation of only the dynamic results. VBDI techniques were successful in locating simulated damage of the bridge. S-Frame FEMs constructed at the U of A showed satisfactory correlation with both measured dynamic and static results. The models showed that the stiffness of the bridge decreased since it first opened. In addition, slight changes in boundary conditions and concrete material properties were shown to affect the behaviour of the 2004 bridge model.

7.0 SUMMARY, CONCLUSIONS AND RECOMMENDATIONS

7.1 Summary

A large majority of Canadian bridge infrastructure consists of bridges constructed with reinforced concrete decks on steel girders. Corrosion of internal steel reinforcement leads to a variety of maintenance issues including the deterioration of the surrounding deck concrete and may significantly reduce the bridge service life. Steel-free deck designs incorporating innovative materials eliminate the probability of internal steel corrosion. In addition, these types of designs require minimal maintenance and claim to have a long service life. Several steel-free bridge decks were constructed during the 1990s in Canada. Despite some serviceability issues with regard to crack widths and fatigue resistance, these bridges are still in service today.

Over the past decade steel-free deck research has looked at several aspects including deck load capacity, simple bridge span applications, continuous bridge span applications, transverse confinement systems, bridge code requirements, fatigue resistance, and cracking resistance. Current research has led to the development of second-generation steel-free decks. These decks improve on the first-generation design with a crack-control mesh/grid of GFRP reinforcement to reduce severe cracking. Through research efforts, including laboratory tests and field monitoring, the satisfactory short-term behaviour of steel-free decks has been well established. However, before this type of design gains wider acceptance by bridge owners, significant research needs to be completed based on the long-term performance. Insight gained from the long-term monitoring of the performance of steel-free bridges will lead to improved and more cost-effective designs. Research proving the long-term satisfactory performance of steel-free bridge decks will convince governing bodies to incorporate these designs.

The Crowchild Trail Bridge in Calgary, Alberta was the first continuous steel-free deck in the world when constructed in 1997. It is located on Crowchild Trail southbound, which is one of the main traffic arteries leading into the downtown business district. Covering three - 30 m long spans, the bridge consists of a concrete steel-free deck with

polypropylene fibres above five steel-plate girders. Steel straps located directly below the bridge deck carry tensile forces in the transverse directions between neighbouring girders. Extensive instrumentation was built into the bridge to collect data for periodical health monitoring. Despite some serviceability issues over the last seven years, the Crowchild Trail Bridge is still in service today and remains in satisfactory condition.

Over the last seven years of service life, static and dynamic load tests, ambient vibration tests, and cracking patterns have been thoroughly documented for the Crowchild Trail Bridge. Strains and deflections of the significant structural components have been measured while under static truckloads, dynamic truckloads, and random dynamic traffic loads. From this data, maximum load effects could be determined in addition to girder strain profiles, load sharing characteristics, and dynamic characteristics. Natural frequencies and mode shapes have been measured three times. Changes in these bridge characteristics can be used to determine the overall health of the structure or locations of damage.

Overall, the behaviour of the Crowchild Trail Bridge has remained the same during seven years of service despite harsh ambient conditions and millions of traffic loading cycles. Maximum bridge deflections and strains are relatively the same in all of the bridge tests. Girder load sharing characteristics have also remained the same, indicating satisfactory deck stiffness in the transverse direction. In the positive moment region, the neutral axis has remained near the same location indicating satisfactory composite action between the girders and the concrete deck. However, in the negative moment region, the neutral axis has shifted downward indicating continual loss of composite action. This is a result of significant concrete deck cracking and loss of deck stiffness in the negative moment regions.

A significant amount of information can be learned about the structural health of the bridge deck from the crack layout and rate of crack growth. Longitudinal cracks exist between most of the girders in addition to transverse cracks. However, most of these cracks formed within the first couple years of operation and the rate of crack growth

within the last couple of years has decreased significantly. With the exception of the higher modes, the mode shapes have remained relatively the same over seven years. In 1998, natural frequencies had decreased by approximately 0.20 Hz for most of the modes compared to 1997 results. This was attributed to a loss of stiffness in the concrete deck. In 2004, natural frequencies had increased slightly for most of the modes. Even with a slight decrease in assumed bridge stiffness, these results seemed reasonable considering environmental effects of temperature and relative humidity during testing or slight changes in the boundary support conditions.

Several numerical models of the Crowchild Trail Bridge have been constructed in the past several years. From a UBC model study, it was concluded that the use of a mode shape correlation technique in addition to comparison of natural frequencies is essential in the calibration of analytical models with experimental data. Both 2-D and 3-D models could successfully imitate the dynamic behaviour of the Crowchild Trail Bridge. MATLAB FEMs created at Carleton University exhibited the best correlation with measured dynamic results. However, static deflection results were not compared in their research, allowing for the accurate correlation of only the dynamic results. VBDI techniques used were successful in locating simulated damage of the bridge. S-Frame FEMs constructed at the U of A showed satisfactory correlation with both measured dynamic and static results. By comparing natural frequencies, the models showed that the stiffness of the bridge decreased since it first opened. In addition, slight changes in temperature or boundary conditions were shown to affect the behaviour of the 2004 bridge model.

7.2 Conclusions

The following conclusions and observations are based on the steel-free deck literature review, recent data obtained from Crowchild Trail Bridge, and results from the numerical models:

1. The five steel-free deck bridges constructed between 1995 and 1999 in Canada remain in service today. However, all of these slabs developed relatively wide, full-

depth longitudinal cracks midway between the girders that exceed serviceability standards. With the exception of periodical crack inspections, minimal long-term structural health monitoring has been performed for these bridges to establish their long-term performance.

2. Recent research has shown that GFRP reinforcement has the best fatigue resistance and prevents the formation of wide longitudinal cracks. In order to reduce deck cracking and improve fatigue resistance, steel-free deck designs require a nominal crack-control grid of GFRP reinforcement. This research has contributed to the development of second-generation steel-free decks with improved serviceability characteristics.

3. Based on the overall static, dynamic, and ambient vibration tests in 2004, the Crowchild Trail Bridge behaviour has not changed significantly during the first seven years of service. Despite some deck cracking and leakage serviceability concerns, the Crowchild Trail Bridge remains a safe and reliable structure. With these considerations, the steel-free deck concept has proved to be a satisfactory alternative for bridge deck construction.

4. The maximum girder deflection measured during the 2004 tests was -13.2 mm under dynamic loading due to a 415 kN truck load. This is well within the maximum serviceability requirements. Deflections measured in the other girders during static loading indicate excellent load sharing characteristics in the transverse direction of the bridge deck. Therefore, transverse stiffness of the Crowchild Trail Bridge remains satisfactory since construction.

5. Maximum measured stains during the 2004 tests for the girder, steel straps, and cross frames were 109.9 με, 79.2 με, and 63.5 με respectively. These results are well within the elastic range and capacity of these steel components. Strains in neighbouring girders also indicate satisfactory girder load sharing in the transverse

direction. Measured strains in the other concrete and reinforcement bridge components were relatively small and are not a concern.

6. Girder strain profiles obtained from the 2004 tests indicate that the location of the neutral axis has not changed in the positive moment region. However, the location of the neutral axis, relative to the top flange, has shifted downward in the negative moment region: 1997 - neutral axis located at 120 mm, 1998 - neutral axis located at 190 mm, 2004 - neutral axis located at 250 mm. These results suggest a steady loss in the composite action between the concrete deck and the steel girders in the negative moment region. The girders have become the primary load-carrying structural component in the longitudinal direction within the negative moment region. Overall, the Crowchild Trail Bridge static load-carrying characteristics are not expected to change significantly over the next ten years of service life.

7. With the exception of a few higher modes, most of the mode shapes remain unchanged. In 1998, the first eight natural frequencies of the Crowchild Trail Bridge were approximately 0.20 Hz lower compared to 1997 results. This was attributed to a loss in concrete deck stiffness due to cracking. In 2004, the first eight natural frequencies were approximately 0.20 Hz higher compared to the 1998 results. Even with a slight decrease in deck stiffness, these results may be attributed to changes in the boundary conditions or ambient conditions. In general, however, the ambient vibration test results indicate that the dynamic characteristics of the Crowchild Trail Bridge have remained relatively the same over seven years. Significant bridge damage was not indicated by the ambient vibration test results. Based on the 2004 ambient vibration results, the vibration characteristics of the Crowchild Trail Bridge are not expected to change significantly within the next 5-10 years.

8. Crack mapping has been thoroughly documented five times since the bridge was constructed. In the last couple of years, the number of new cracks has decreased significantly. Currently, the north span, which was constructed with the least amount of internal reinforcement (reinforced only in the cantilever edges and south end pier

with GFRP reinforcement), contained the largest number of longitudinal cracks. However, the north span contained the least amount of transverse cracks compared to the other two spans. The middle span, which was partially reinforced with GFRP bars in the cantilever edges and both ends at pier locations, contained the most amount of transverse cracks compared to the other two spans. It is interesting to note that the south span, which contained the minimum temperature steel reinforcement, contained the least amount of cracks after seven years of service. Therefore a minimal amount of reinforcement is required for any deck design in order to control cracking. Water was observed to leak through the concrete bridge deck in several locations. Cracks in the bridge barriers are more visible compared to the deck cracks. Overall, very few new cracks are expected to form within the bridge concrete sections in the future and existing cracks are not expected to increase in size significantly.

9. The behaviour of the Crowchild Trail Bridge is very similar to the behaviour of other steel-free bridge decks constructed in the same time period. Short-term measured deflections and strains of the steel-free decks are satisfactory and are well within elastic ranges of the respective construction materials. Longitudinal and transverse cracking observed in the Crowchild Trail Bridge was also evident in the other steel-free deck bridges. Most of the cracking was noted to occur primarily within the first year or two of service. After this initial period, further deck cracking in all steel-free deck bridges was minimal. The lack of long-term monitoring data of other steel-free deck bridges prevents further comparisons with long-term monitoring data from the Crowchild Trail Bridge.

10. S-Frame FEMs constructed at the U of A showed satisfactory correlation with both measured dynamic and static results. The models showed that the stiffness of the bridge decreased since it first opened. In addition, slight changes in concrete material properties and boundary conditions were shown to affect the behaviour of the bridge between 1998 and 2004.

7.3 Recommendations

Thorough load and ambient vibration tests of other steel-free bridge decks constructed in the 1990s should be completed and compared to previous tests results. These results, in addition to deck cracking observations, would provide a more accurate analysis of the long-term performance of steel-free decks. This type of deck design will gain wider acceptance if satisfactory long-term structural performance is well established. Furthermore, long-term monitoring will lead to additional improvements in steel-free deck designs.

Future field tests are recommended for the Crowchild Trail Bridge. Based on the results of the 2004 test results, it is recommended that similar load and ambient vibration tests be completed every five years. After future load tests, analysis of the concrete strains may contribute to a better understanding of the behaviour of the compression struts within the concrete deck. In addition, thorough visual inspections should be completed once a year to ensure that no significant structural damage has occurred. Careful inspection of the top concrete deck surface is recommended to locate any through-thickness cracks. In order to increase the effectiveness of damage detection using VBDI techniques, the effects of temperature and boundary conditions on the dynamic behaviour of the Crowchild Trail Bridge should be isolated and examined in more detail. These steps taken during field tests would contribute to a better understanding of the long-term structural behaviour of steel-free decks.

A more detailed finite element model of the Crowchild Trail Bridge would be advantageous in simulating actual field conditions. Future bridge models should exhibit increased detail in the deck transverse direction and in the concrete deck thickness. With these model improvements, internal deck stresses could be estimated and transverse deck behaviour would be more accurate. Cracking conditions could also be modelled instead of assuming a reduced concrete stiffness value for the entire deck. Modelled deck stresses due to temperature changes would also help in determining any changes in the bridge dynamic behaviour.

It is expected that the behaviour of the Crowchild Trail Bridge will remain relatively the same during the next five to ten years unless leakage through the concrete deck increases significantly. Deterioration of the concrete deck and structural steel components could result if deck leakage increases. Maintenance should be performed to minimize the visual impact of the barrier cracks and minimize leakage through deck cracks. For example, epoxy grout could be used to fill in these cracks so that they are not as noticeable. However, an investigation should be completed to determine the most efficient and cost-effective repair solution.

Based on the 2004 Crowchild Trail Bridge test results, several improvements can be incorporated into future steel-free deck designs. The strains measured in the tension straps are well within the elastic range and the spacing of the tension straps is conservative. Future designs could utilize fewer steel straps and still achieve satisfactory transverse confinement. In the spans where GFRP reinforcement was minimal, there are significant amounts of cracks. Future steel-free decks must have better cracking resistance compared to the Crowchild Trail Bridge and other first-generation steel-free decks. Water leakage through the deck should also be minimized in future steel-free design as this can be visually unappealing and could lead to further deterioration of other bridge structural components. Second-generation steel-free decks are designed to have improved cracking resistance because of a secondary reinforcement layer of GFRP.

REFERENCES

1. Afhami, S., Alexander, S.D.B., and Cheng, J.J.R., "Field Instrumentation and Monitoring Crowchild Bridge in Calgary, Alberta", 1st Annual Report, University of Alberta, Civil and Environmental Engineering, 1998.

2. Bagchi, A., Humar, J., Xu, H. "Vibration Based Damage Identification for the Crowchild Bridge, an Innovative Steel Free Deck Bridge Located in Canada". Draft Manuscript for the Structural Health Monitoring Journal, 2004.

3. Bakht, B., Mufti, A.A., "FRC Deck Slabs Without Tensile Reinforcement." Concrete International 2. (1996): 50-55.

4. Bakht, B., Mufti, A.A., "Five Steel-Free Bridge Deck Slabs in Canada." Structural Engineering International 8 (1998): 196-200.

5. Bakht, B., Al-Bazi, G., Banthia, N., Cheung, M., Erki, M.A., Faoro, M., Machida, A., Mufti, A.A., Neale, K., Tadros, G. "Candian Bridge Design Code Provisions for Fibre-Reinforced Structures." Journal of Composites for Construction 2 (2000): 3-15.

6. Bakht, B., Lam, C. "Behaviour of Transverse Confining Systems for Steel-Free Deck Slabs." Journal of Bridge Engineering May (2000): 139-147.

7. Bakht, B., Lam, C. "Closure to "Behaviour of Transverse Confining Systems for Steel-Free Deck Slabs." Journal of Bridge Engineering Jan. (2002): 68-70.

8. Bakht, B., Mufti, A.A., Tadros, G. "Discussion of "An Experimental Investigation of Steel-free Deck Slabs." Canadian Journal of Civil Engineering 30 (2003): 787-789.

9. Bakht, B. "Extracting Cores from GFRP-Reinforced Barrier Walls of the Chatham Bridge in Ontario." Preliminary Field Report. October 2004.

10. Benmokrane, B., Rahman, H., Mukhopadhyaya, P., Masmoudi, R., Chekired, M., Nicole, J., El-Safty, A. "Use of Fibre Reinforced Polymer Reinforcement Integrated With Fibre Optic Sensors for Concrete Bridge Deck Slab Construction." Canadian Journal of Civil Engineering 27 (2000): 928-940.

11. Bergmeister, K., Santa, U. "Global Monitoring Concepts for Bridges." Structural Concrete. 2 (2001): 29-39.

12. Chajes, M.J., Shenton, H.W., Finch, W.W. "Performance of Glass Fibre-Reinforced Polymer Deck on Steel Girder Bridge." Transportation Research Record. n1770. 105-112.

13. Cheng, J.J.R., Afhami, S., 1999. "Field Instrumentation and Monitoring of Crowchild Trail Bridge in Calgary, Alberta". University of Alberta report for the City of Calgary, July.

14. Cunha, A., Caetano, E., Calcada, R., De Roeck, G., Peeters, B. "Dynamic Measurements on Bridges: Design, Rehabilitation and Monitoring." Bridge Engineering 156. Issue BE3, (2003): 135 – 148.

15. Desjardins, S.L., Londono, N.A., Lau, D.T. "Implications on the Use of Continuous Dynamic Monitoring Data for Structural Evaluation." Ottawa-Carleton Bridge Research Institute, Carleton University, Ottawa, Canada.

16. Dorey, A.B., Newhook, J.P., and Mufti, A.A. "The Behaviour of a Reinforcing Steel-Free Bridge Deck Under Negative Moment." Concrete International 18(6), (1996): 50-55.

17. Dorton, R.A., Holowka, M., King, J.P.C. "The Conestoga River Bridge – Design and Testing." The Canadian Journal of Civil Engineering. 4 (1977): 18-39.

18. Emmons, Peter H. Concrete Repair and Maintenance Illustrated. Kingston: RS Means Company, 1993.

19. Farrar, C.R. and Doebling, S.W., "DAMAGE DETECTION II: Field Applications to Large Structures." Modal Analysis and Testing, Nato Science Series, Kluwer Academic Publishers, Dordrecht, Netherlands, 1999.

20. Hassan, A., Kawakami, M., Niitani, K., Yoshioka, T. "An Experimental Investigation or Steel-free Deck Slabs." Canadian Journal of Civil Engineering 29 (2002): 831-841.

21. Hassan, A., Kawakami, M. "Reply to the discussion by Bakht et. al. on "An Experimental Investigation of Steel-Free Deck Slabs." Canadian Journal of Civil Engineering 30 (2003): 790-791.

22. ISIS Canada Design Manual. 1st ed. CD-ROM. ISIS Canada, 2001.

23. Klowak, C., Eden, R., Mufti, A., Tadros, G., Bakht, B. "First Application of Second-Generation Steel-Free Deck Slabs for Bridge Rehavilitation". Proceedings of The International Society for Optical Engineering Volume 5393. California, USA, 2004.

24. Marshe, S., Green, M.F. "Punching Behaviour of Composite Bridge Decks Transversely Prestressed with Carbon Fibre Reinforced Polymer Tendons." Canadian Journal of Civil Engineering 26 (1999): 618-630.

25. Memon, A.H., Mufti, A.A., (2004), "Fatigue Behaviour of Concrete Bridge Deck Slabs Reinforced With FRP and Steel Straps", Proceedings of the 5th Structural

Specialty Conference of the Canadian Society of Civil Engineering, Saskatoon, SK, Canada, ST-229 pp.1-10.

26. Mufti, A.A., Jaeger, L.G., Bakht, B., Wegner, L. D. "Experimental Investigation of Fibre-reinforced Concrete Deck Slabs Without Internal Steel Reinforcement." Canadian Journal of Civil Engineering 20 (1993): 398-406.

27. Mufti, A.A., Newhook, J.P. "On the Use of Steel-Free Concrete Bridge Decks in Continuous Span Bridges." Canadian Journal of Civil Engineering 6 (1999): 667-672.

28. Mufti, A.A., Labossiere, P., Neale, K. "Recent Bridge Applications of FRPs in Canada." Structural Engineering International. 2 (2002): 96-98.

29. Mufti, A.A., "Structural Health Monitoring of Innovative Canadian Civil Engineering Structures." Structural Health Monitoring Journal 1 (2002): 89-103.

30. Mufti, A.A., Memon, A.H., Bakht, B., and Banthia, N., 2002, "Fatigue Investigation of the Steel-Free Bridge Deck Slabs," ACI International, SP-206: 61-70.

31. Mufti, A.A., Bakht, B., Newhook, J.P. "Precast Concrete Decks for Slab-on-Girder Systems: A New Approach." ACI Structural Journal. 101(2004): 395-402.

32. Newhook, J.P., Mufti, A.A., "A Reinforcing Steel-Free Concrete Deck Slab for the Salmon River Bridge." Concrete International 6 (1996): 30–34.

33. Onur, T., Ventura, C.E., Black, C., Tsai, P.-C. "Correlative Study of Experimental and Analytical Dynamic Properties of a Three-Span Bridge". Proceedings of 27th Annual CSCE Conference. Regina, SK, 1999.

34. Peeters, B., De Roeck, G. "One-year Monitoring of the Z24-Bridge:Environmental Effects Versus Damage Events." Earthquake Engineering and Structural Dynamics. v30 n2, (2001): 149 – 171.

35. Ren, W.-X., De Roeck, G. "Structural Damage Identification Using Modal Data. I: Simulation Verification." Journal of Structural Engineering Jan. (2002): 87-95.

36. Rizkalla, S., Shehata, E., Abdelrahman, A., Tadros, G. "Design and Construction of a Highway Bridge with CFRP: The New Generation." Concrete International 7 (1998): 35-38.

37. Salem, A.H., El-Aghoury, M.A., Sayed-Ahmed, E.Y., Moustafa, T.S. "Composite Steel Free Deck Bridges: Numerical Modelling and Pilot Parametric Study." Canadian Journal of Civil Engineering 29 (2002): 662-678.

38. Solutions for Structural Health Monitoring. 2004. 15 Oct. 2004 <http://www.shmsystems.com/structures/structures_home.html>

39. Tadros, G., Tromposch, E., Muft, A.A. 1998. "Superstructure Replacement of Crowchild Trail Bridge Calgary, Canada". Proceedings of the Fifth International Conference on Short and Medium Span Bridges, Calgary, Alta. Canadian Society for Civil Engineering, Montreal, Que., CD-ROM.

40. Taing, K.K., (2000), "Field Assessment of Crowchild Trail Bridge in Calgary, Alberta", M.Sc. Thesis, Department of Civil Engineering, University of Alberta.

41. Ventura, C.E., Black, C. and Tsai, P.-C, "Ambient Vibration Measurements of the University Drive / Crowchild Trail Bridge in Calgary, Alberta." U.B.C. Earthquake Engineering Research, Project number EQ 97-005, 1997.

42. Ventura, C.E., Cook, S.E. "Testing of a Steel-Free Concrete Bridge." Experimental Techniques 11 (1998): 39-42.

43. Ventura, C.E., Onur, T. and Tsai, P.-C. "Dynamic characteristics of the Crowchild Trail Bridge." Canadian Journal of Civil Engineering. 27 (2000): 1046-1056.

44. Ward, H. "Traffic Generated Vibrations and Bridge Integrity." Journal of Structural Engineering. v110 n10 (1984): 2487-2498.

45. Xiaotong W., Chang, C.C., Fan, L. "Nondestructive Damage Detection of Bridges: A Status Review." Advances in Structural Engineering v4 n2 (2001): 75-91.

46. Yang, C., Limaye, V., Newhook, J., (2004), "Experimental Evaluation of Load Distribution in Steel-Free Bridge Decks", Proceedings of the 5th Structural Specialty Conference of the Canadian Society of Civil Engineering, Saskatoon, SK, Canada, ST-86 pp.1-10.

Appendix A – Location of Bridge Instrumentation

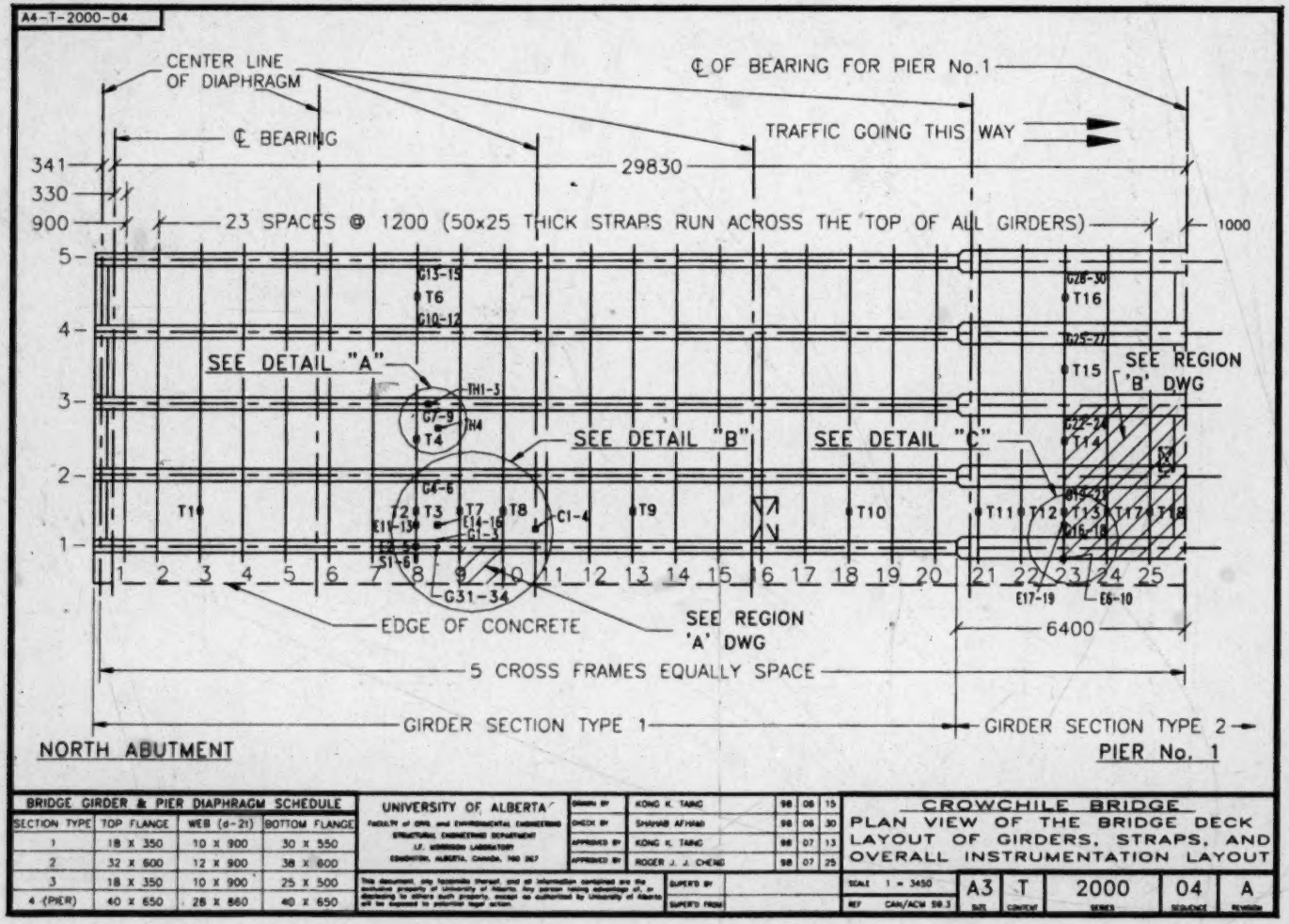

BRIDGE GIRDER & PIER DIAPHRAGM SCHEDULE			
SECTION TYPE	TOP FLANGE	WEB (d-21)	BOTTOM FLANGE
1	18 X 350	10 X 900	30 X 550
2	32 X 600	12 X 900	38 X 600
3	18 X 350	10 X 900	25 X 500
4 (PIER)	40 X 650	28 X 860	40 X 650

UNIVERSITY OF ALBERTA
FACULTY OF CIVIL and ENVIRONMENTAL ENGINEERING
STRUCTURAL ENGINEERING DEPARTMENT
J.F. KEARNEY LABORATORY
EDMONTON, ALBERTA, CANADA, T6G 2G7

DRAWN BY	KONG K. TANG	98	06	15
CHECK BY	SHAHAB AFHAMI	98	06	30
APPROVED BY	KONG K. TANG	98	07	13
APPROVED BY	ROGER J. J. CHENG	98	07	25
SUPERV BY				
SUPERV FROM				

CROWCHILE BRIDGE
PLAN VIEW OF THE BRIDGE DECK LAYOUT OF GIRDERS, STRAPS, AND OVERALL INSTRUMENTATION LAYOUT

SCALE	1 = 3450	A3	T	2000	04	A
REF	CAN/ACM 98.3	SIZE	CONTENT	SERIES	SEQUENCE	REVISION

This document, any facsimile thereof, and all information contained are the exclusive property of University of Alberta. Any person making reproduction of, or disclosing to others such property, except as authorized by University of Alberta, will be prosecuted to extreme legal extent.

Figure A.1 – Overall Instrumentation Layout

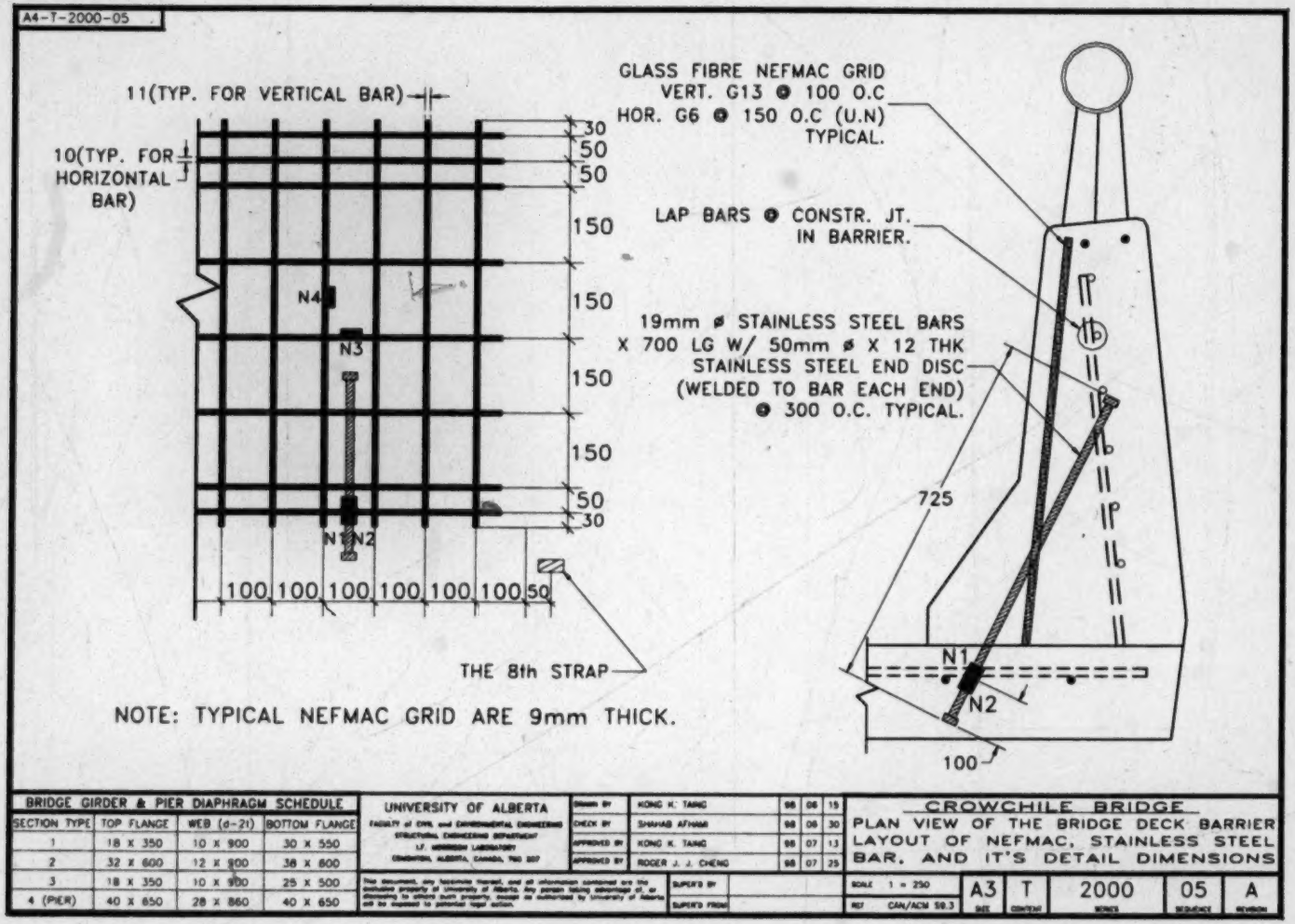

BRIDGE GIRDER & PIER DIAPHRAGM SCHEDULE			
SECTION TYPE	TOP FLANGE	WEB (d-21)	BOTTOM FLANGE
1	18 X 350	10 X 900	30 X 550
2	32 X 600	12 X 900	38 X 600
3	18 X 350	10 X 900	25 X 500
4 (PIER)	40 X 850	28 X 860	40 X 650

UNIVERSITY OF ALBERTA
FACULTY of CIVIL and ENVIRONMENTAL ENGINEERING
STRUCTURAL ENGINEERING DEPARTMENT
I.F. MORRISON LABORATORY
EDMONTON, ALBERTA, CANADA, T6G 2G7

This document, any facsimile thereof, and all information contained are the exclusive property of University of Alberta. Any person taking advantage of, or disclosing to others such property, except as authorized by University of Alberta will be exposed to potential legal action.

Drawn BY	KONG K. TANG	98	06	15
CHECK BY	SHAHAB AFHAMI	98	06	30
APPROVED BY	KONG K. TANG	98	07	13
APPROVED BY	ROGER J. J. CHENG	98	07	25
SUPER'D BY				
SUPER'D FROM				

CROWCHILE BRIDGE
PLAN VIEW OF THE BRIDGE DECK BARRIER LAYOUT OF NEFMAC, STAINLESS STEEL BAR, AND IT'S DETAIL DIMENSIONS

SCALE	1 = 250					
REF	CAN/ACM S9.3	A3 SIZE	T CONTENT	2000 SERIES	05 SEQUENCE	A REVISION

Figure A.2 – NEFMAC Bridge Barrier Gauges

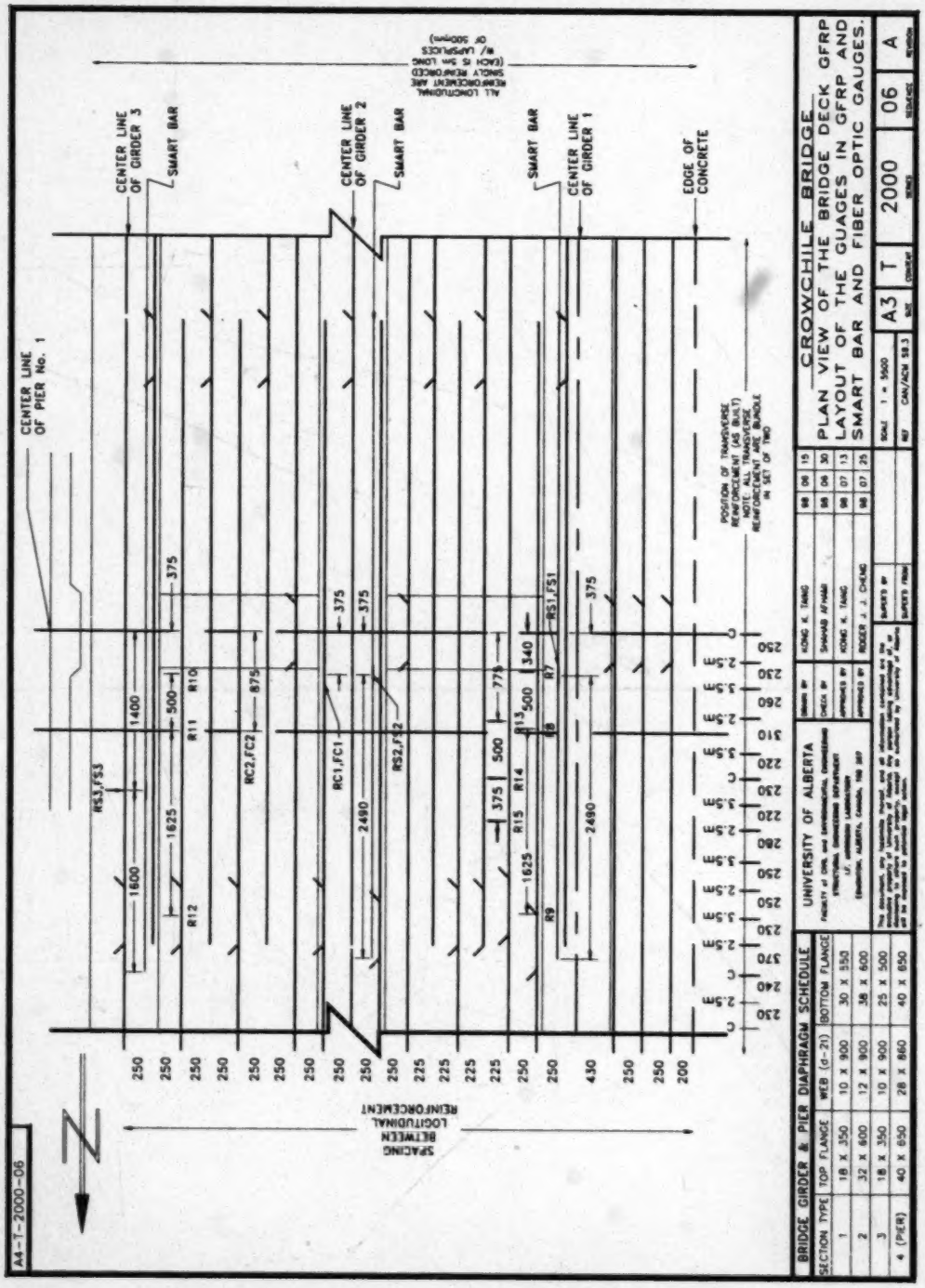
CROWCHILE BRIDGE
PLAN VIEW OF THE BRIDGE DECK GFRP
LAYOUT OF THE GUAGES IN GFRP AND
SMART BAR AND FIBER OPTIC GAUGES.
CENTER LINE OF PIER No. 1
CENTER LINE OF GIRDER 3
CENTER LINE OF GIRDER 2
CENTER LINE OF GIRDER 1
SMART BAR
EDGE OF CONCRETE
SPACING BETWEEN LONGITUDINAL REINFORCEMENT
UNIVERSITY OF ALBERTA
BRIDGE GIRDER & PIER DIAPHRAGM SCHEDULE
A4-T-2000-06

Figure A.3 – Location of Reinforcement Bar Gauges

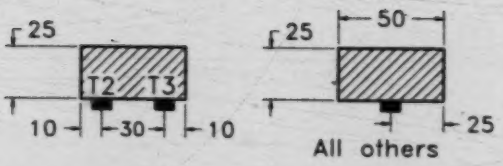

Figure A.4 – Tension Strap Gauges

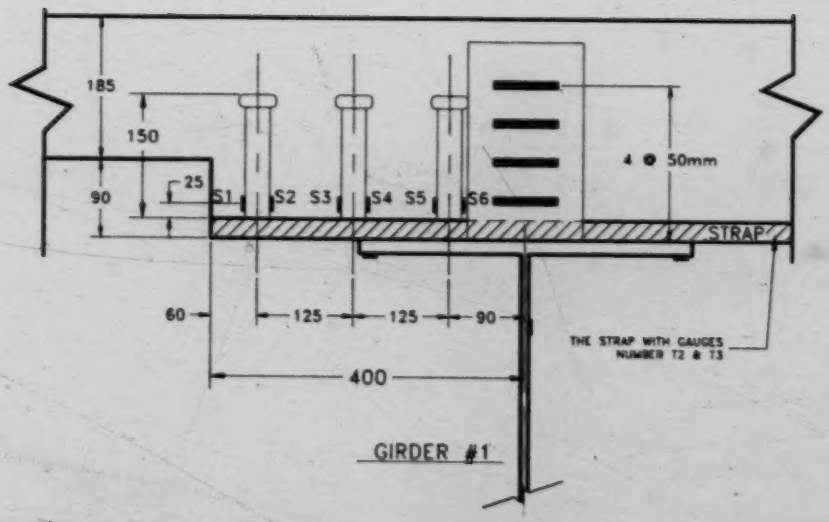

Figure A.5 – Shear Stud Gauges

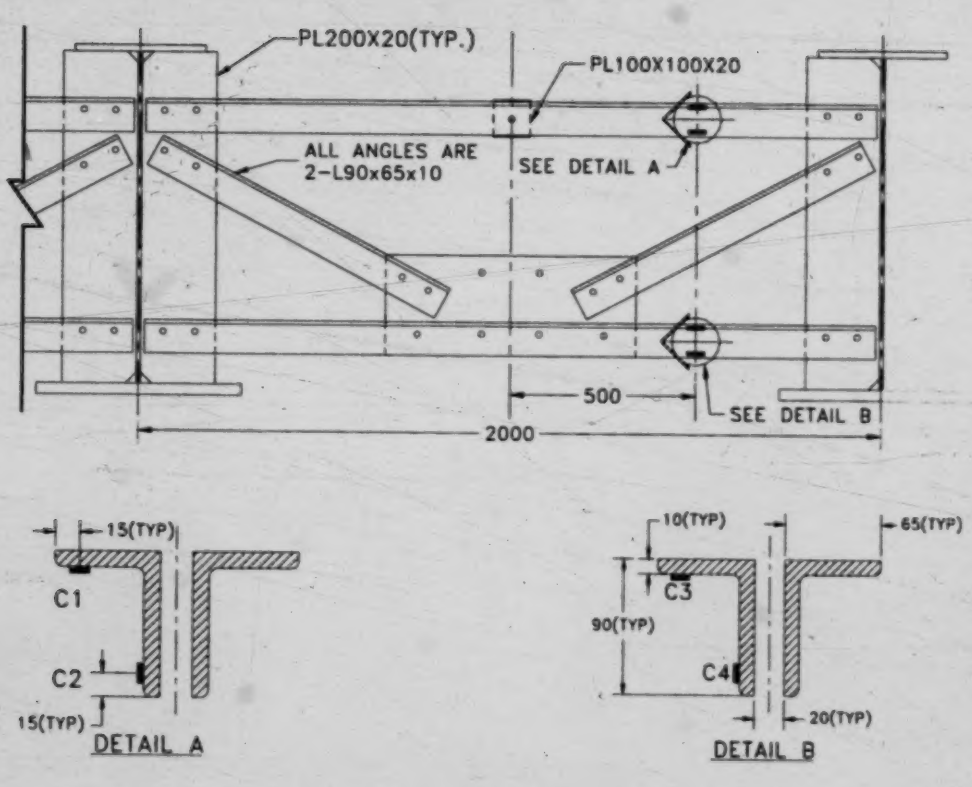

Figure A.6 – Cross-Frame Gauges

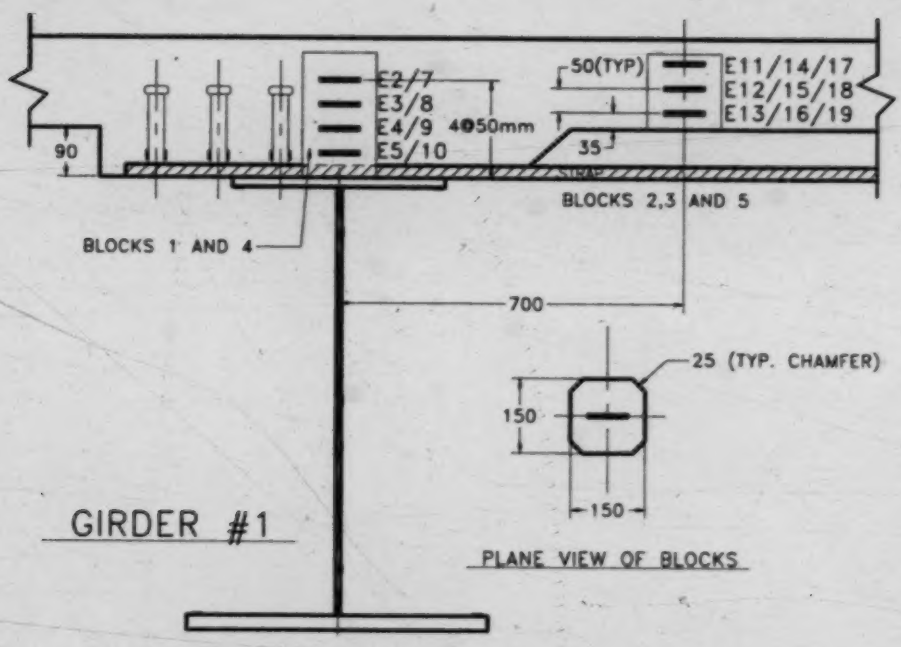

Figure A.7 – Embedded Concrete Gauges

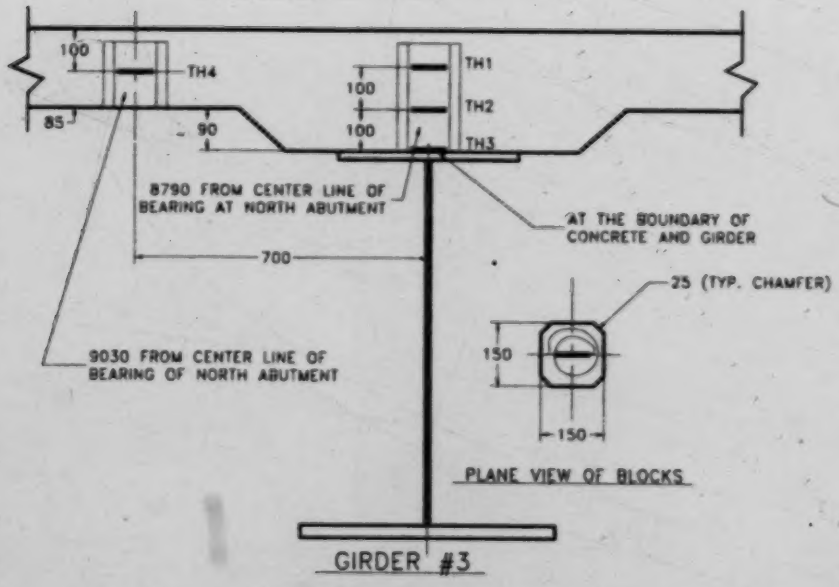

Figure A.8 – Embedded Thermistors.

Appendix B – 2004 Static Load Test Raw Data

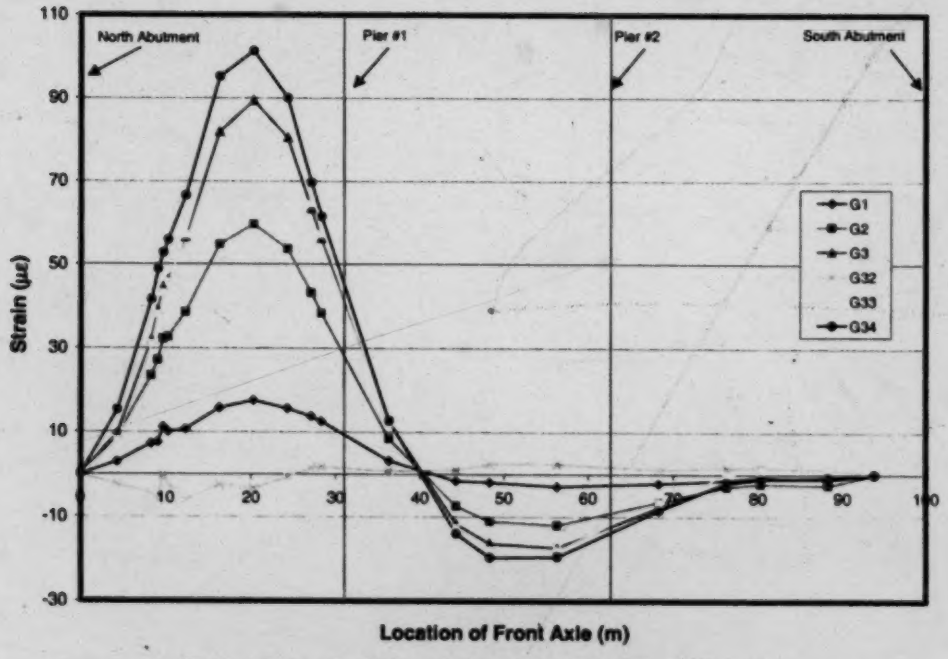

Figure B.1 – Static Load Raw Data: G1-G3, G32-G34

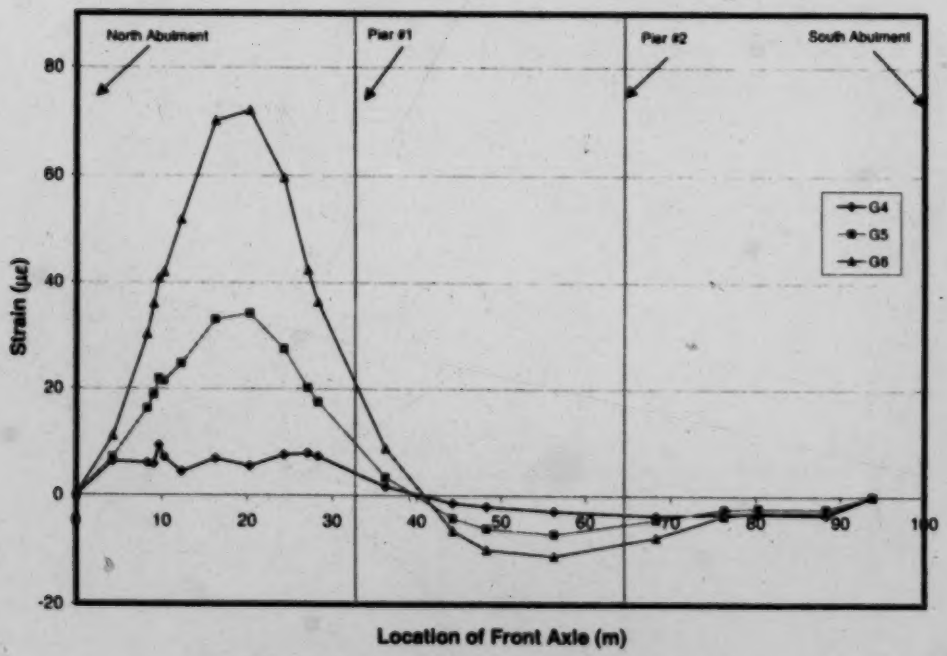

Figure B.2 – Static Load Raw Data: G4-G6

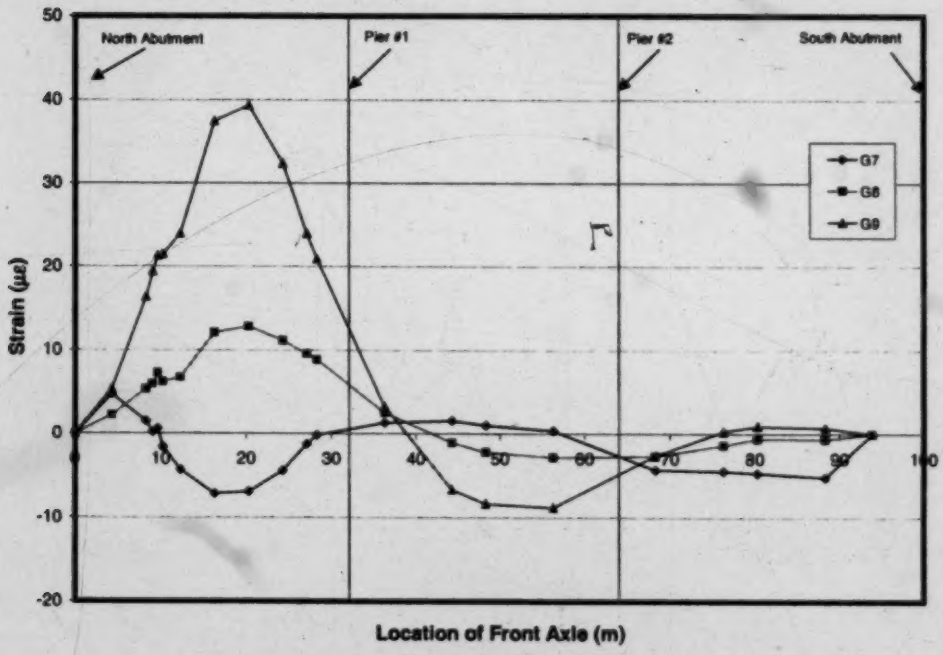

Figure B.3 – Static Load Raw Data: G7-G9

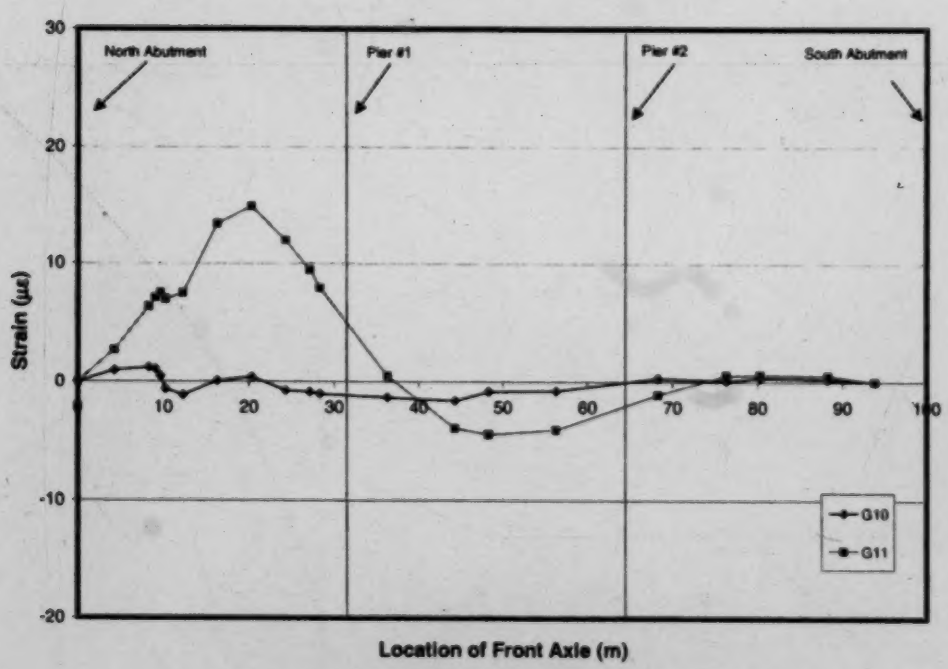

Figure B.4 – Static Load Raw Data: G10-G11

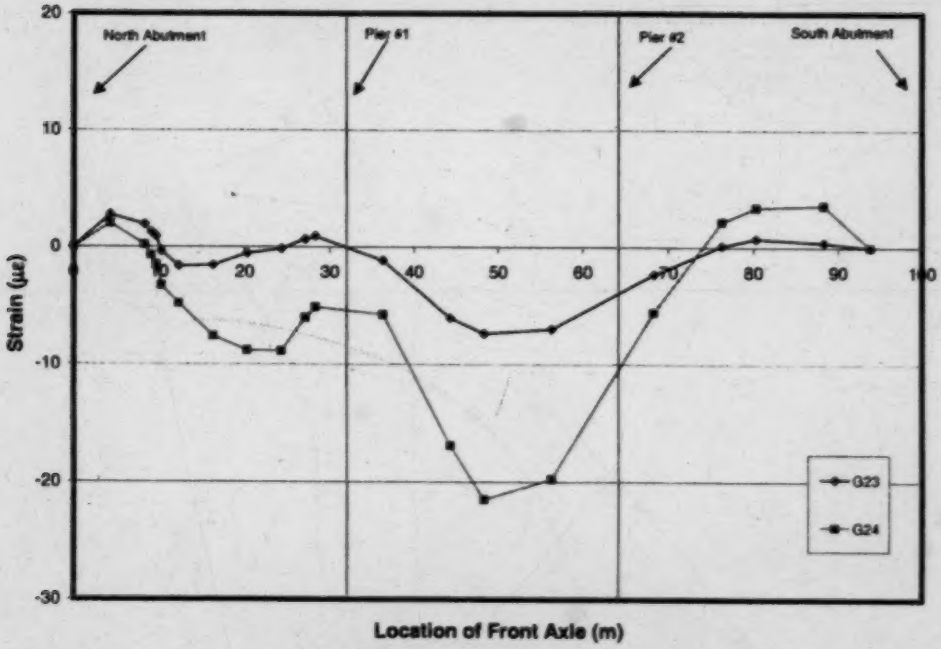

Figure B.5 – Static Load Raw Data: G23-G24

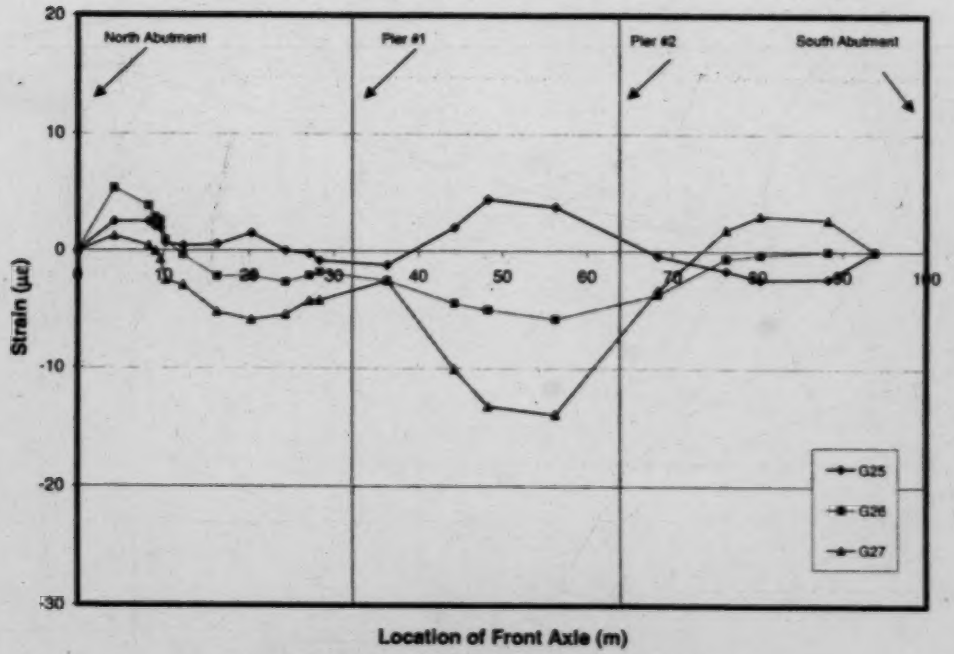

Figure B.6 – Static Load Raw Data: G25-G27

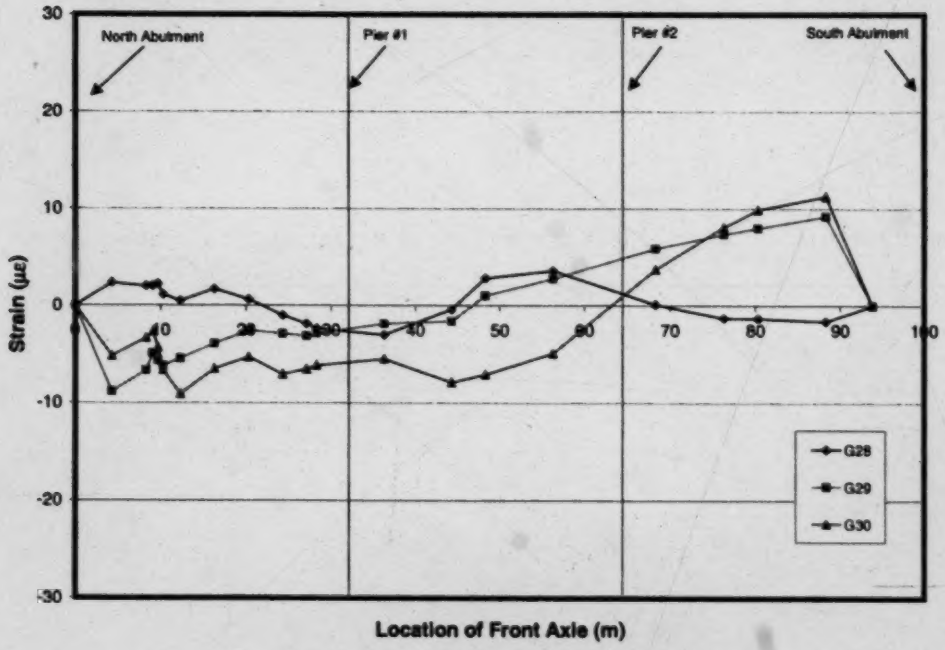

Figure B.7 – Static Load Raw Data: G28-G30

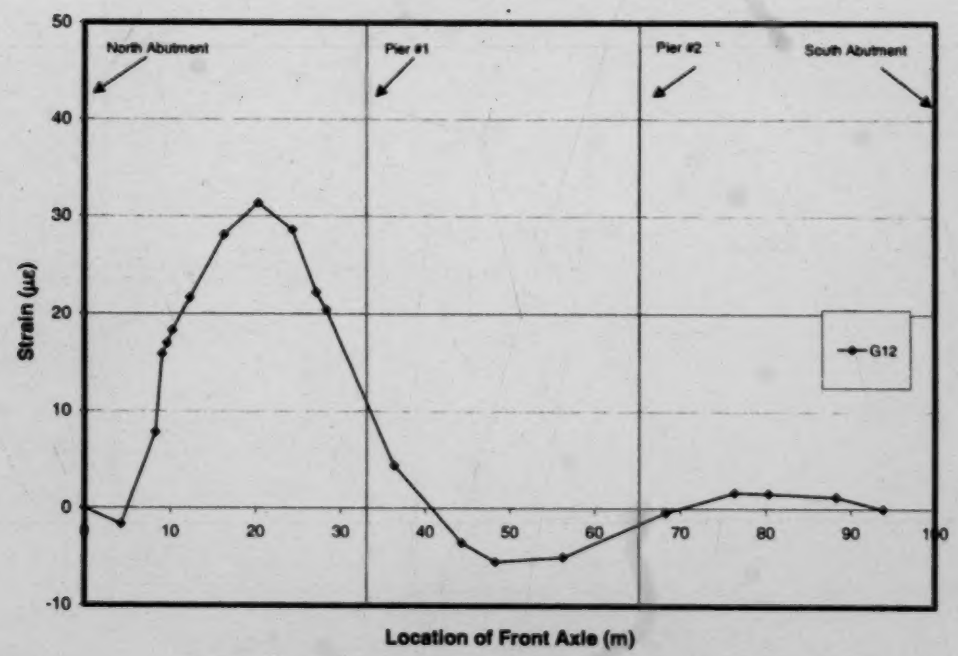

Figure B.8 – Static Load Raw Data: G12

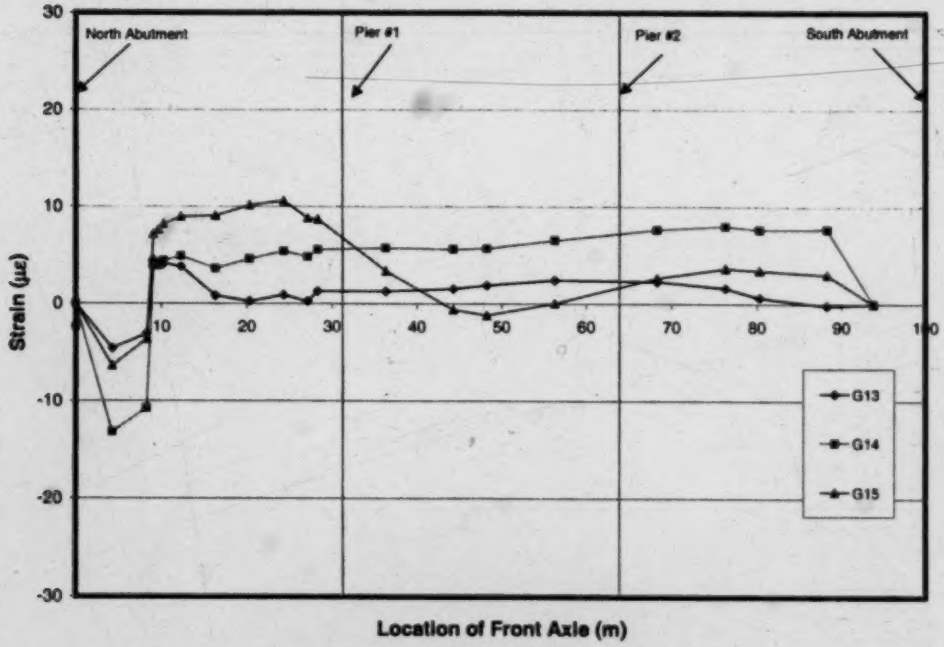

Figure B.9 – Static Load Raw Data: G13-G15

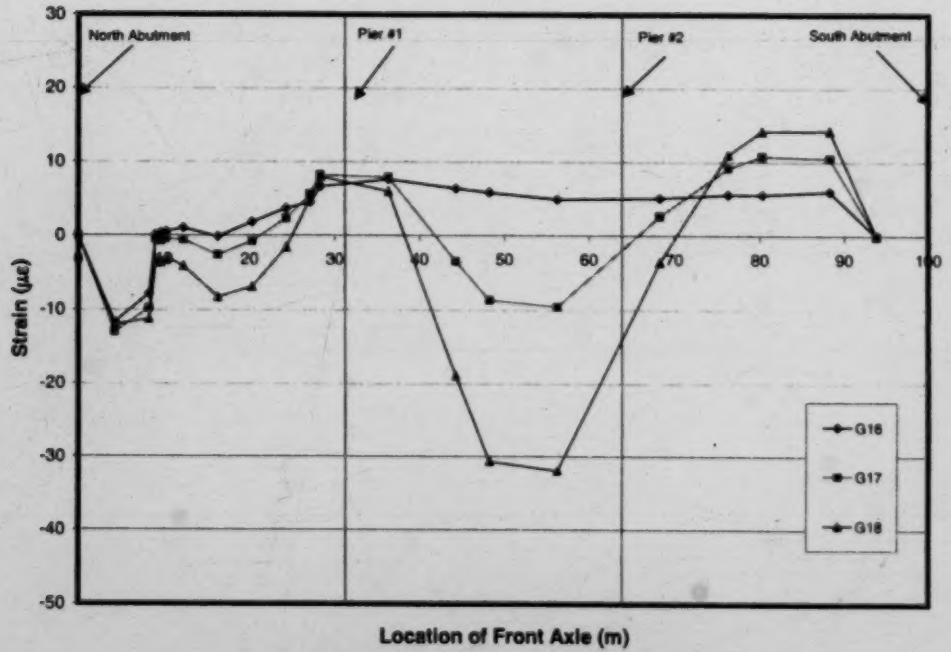

Figure B.10 – Static Load Raw Data: G16-G18

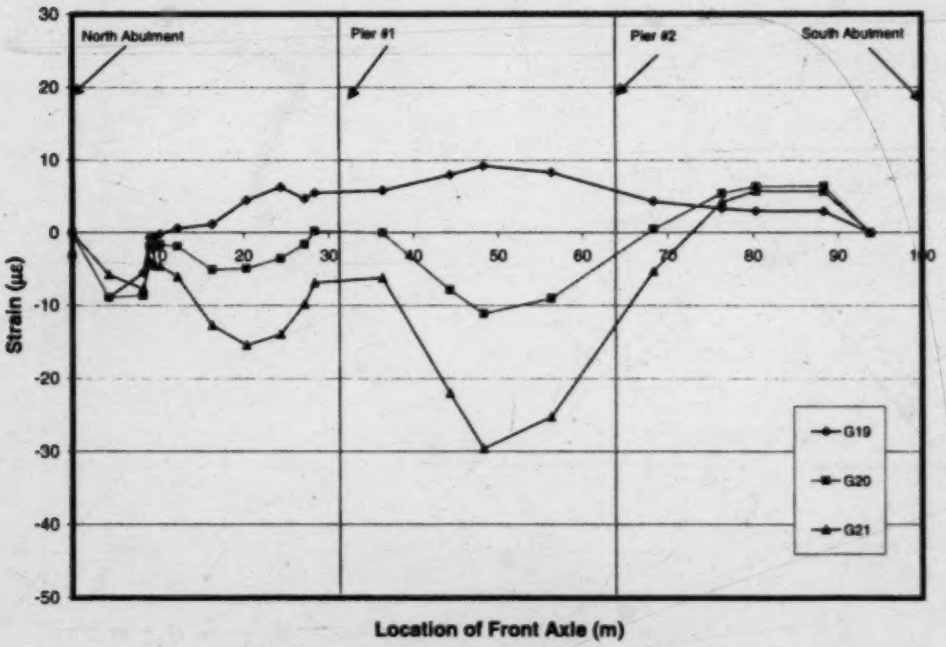

Figure B.11 – Static Load Raw Data: G19-G21

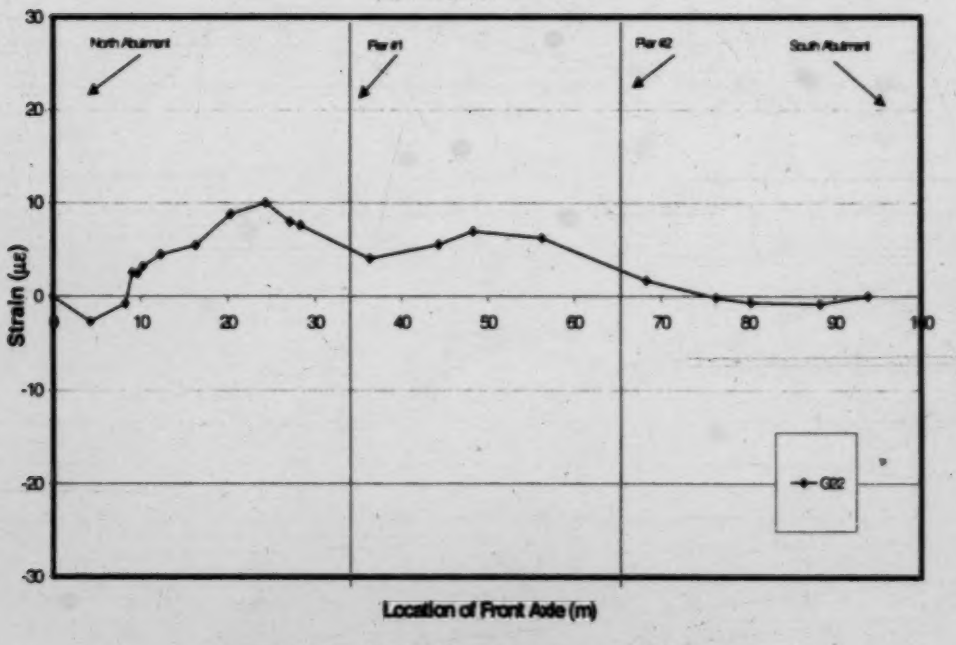

Figure B.12 – Static Load Raw Data: RC1-RC2

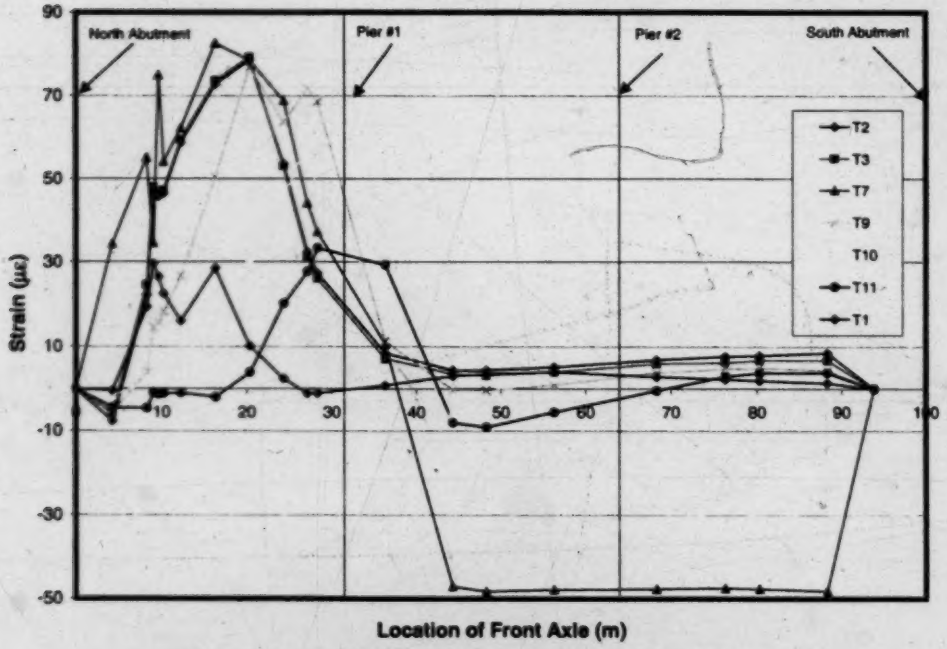

Figure B.13 – Static Load Raw Data: T1-T3,T7,T9-T11

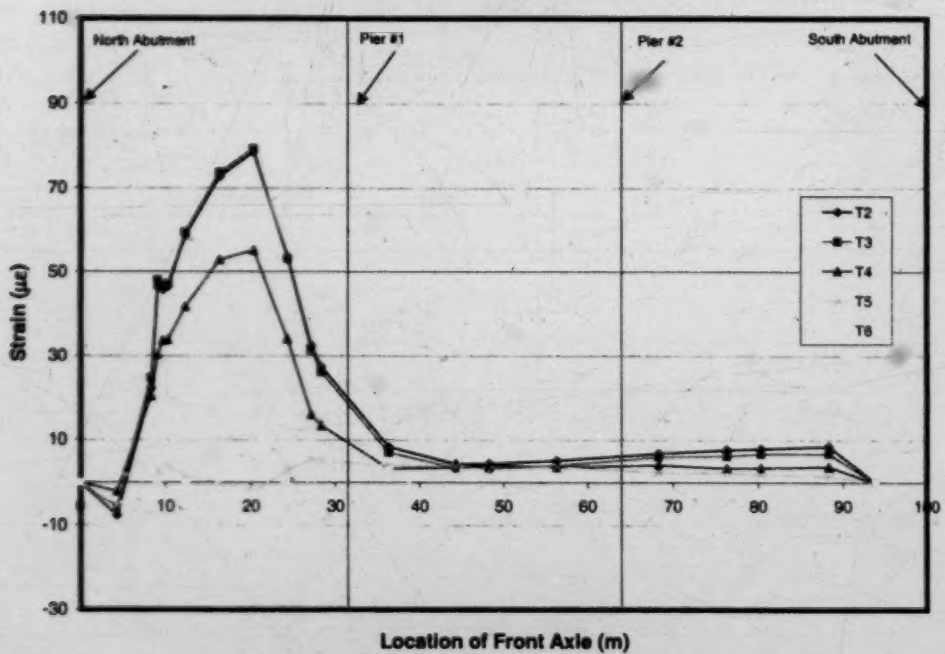

Figure B.14 – Static Load Raw Data: T2-T6

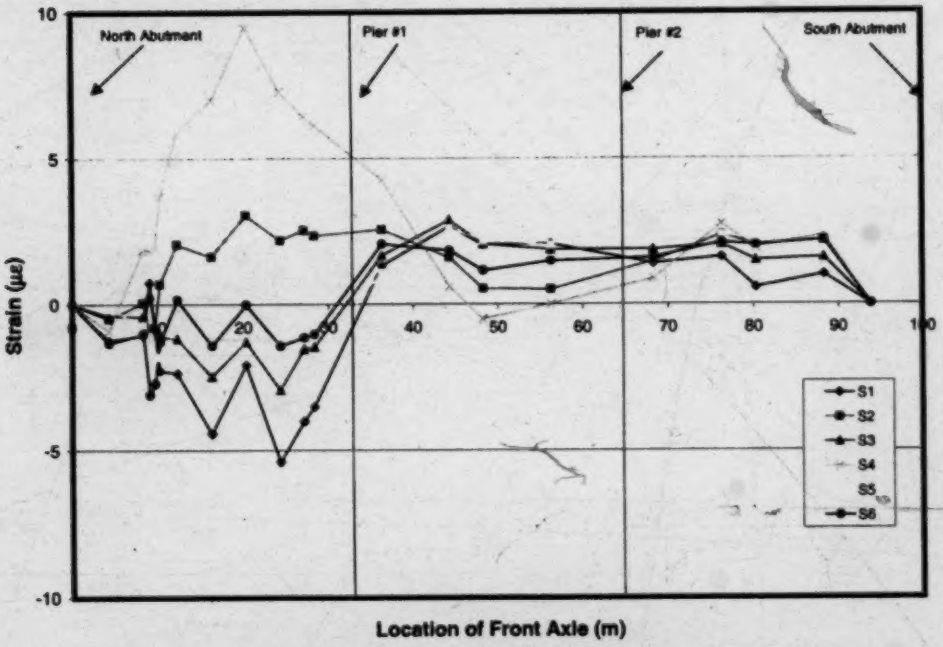

Figure B.15 – Static Load Raw Data: S1-S6

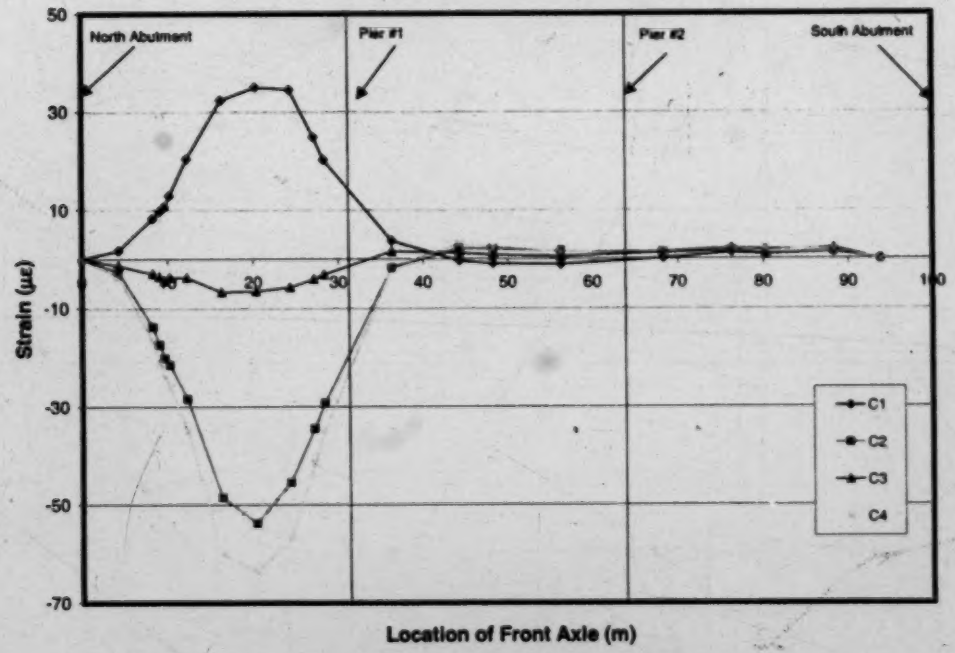

Figure B.16 – Static Load Raw Data: C1-C4

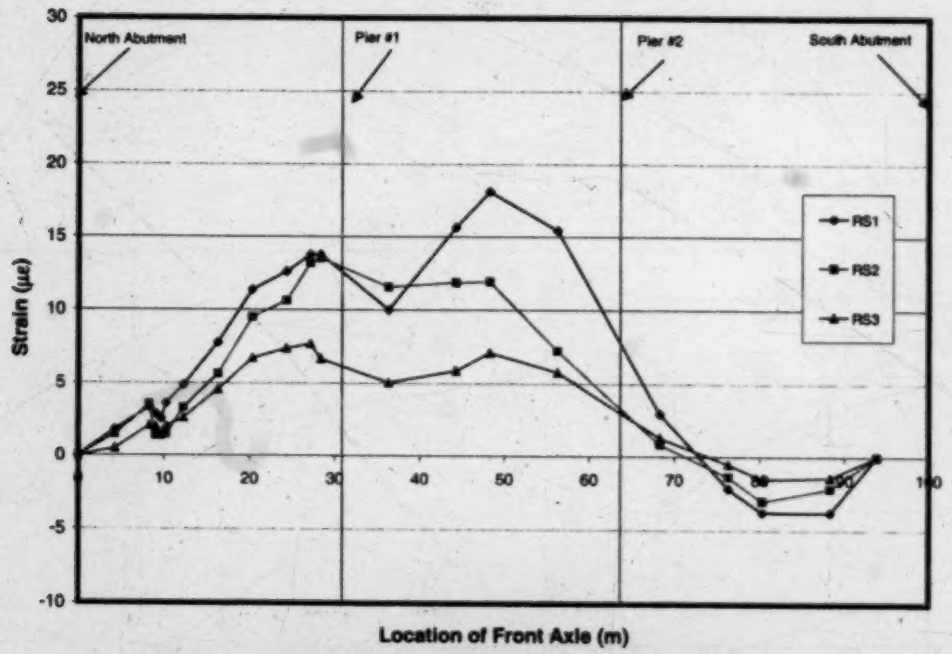

Figure B.17 – Static Load Raw Data: RS1-RS3

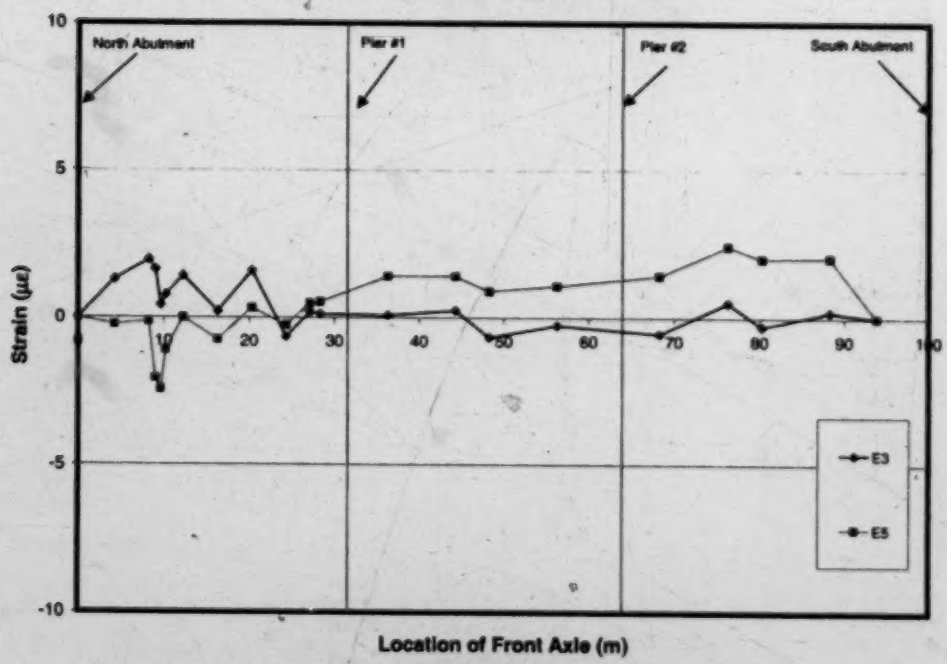

Figure B.18 – Static Load Raw Data: E3, E5

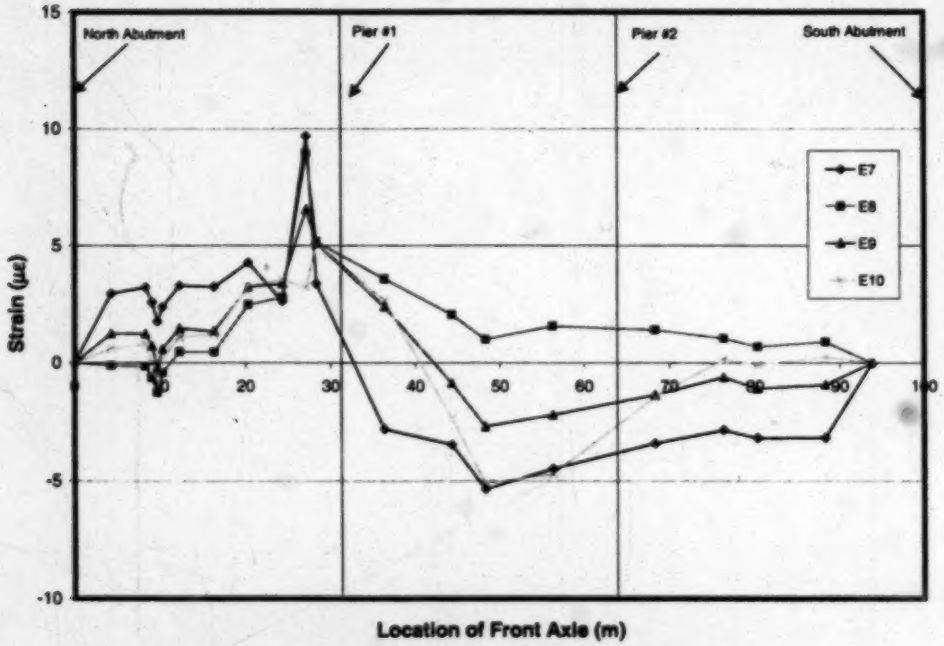

Figure B.19 – Static Load Raw Data: E7-E10

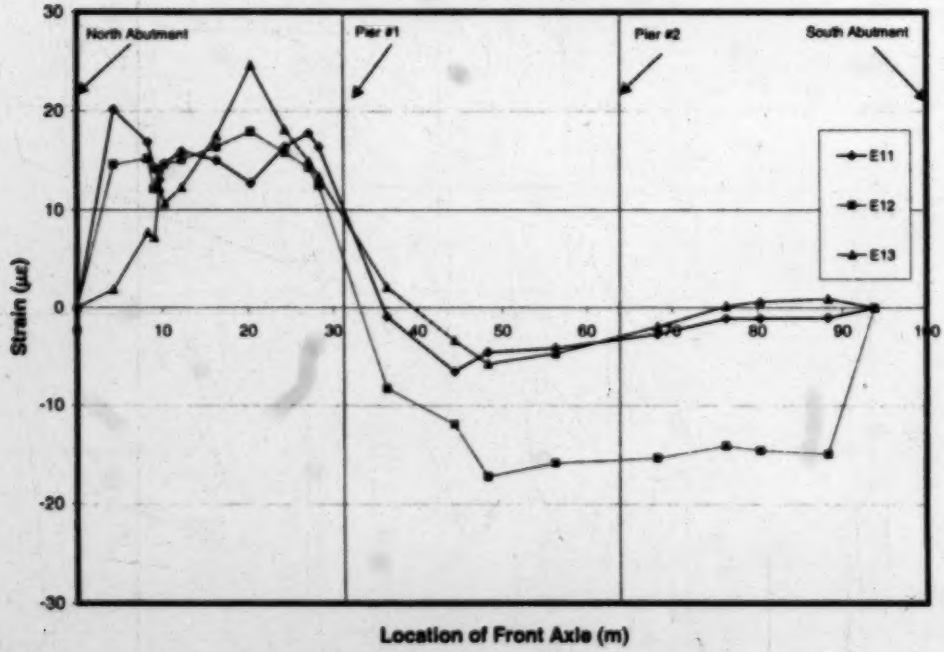

Figure B.20 – Static Load Raw Data: E11-E13